Title
Nanomagnetic Logic

Author
Carlton, David

Publication Date
2012

Peer reviewed|Thesis/dissertation

Nanomagnetic Logic

by

David Bryan Carlton

A dissertation submitted in partial satisfaction of the

requirements for the degree of

Doctor of Philosophy

in

Engineering - Electrical Engineering & Computer Science

and the Designated Emphasis

in

Nanoscale Science and Engineering

in the

Graduate Division

of the

University of California, Berkeley

Committee in charge:

Professor Jeffrey Bokor, Chair
Professor Sayeef Salahuddin
Professor Yuri Suzuki

Spring 2012

Nanomagnetic Logic

David Bryan Carlton

Abstract

Nanomagnetic Logic

by

David Bryan Carlton

Doctor of Philosophy in Engineering - Electrical Engineering & Computer Science and the Designated Emphasis in Nanoscale Science and Engineering

University of California, Berkeley

Professor Jeffrey Bokor, Chair

The exponential improvements in speed, energy efficiency, and cost that the computer industry has relied on for growth during the last 50 years are in danger of ending within the decade. These improvements all have relied on scaling the size of the silicon-based transistor that is at the heart of every modern CPU down to smaller and smaller length scales. However, as the size of the transistor reaches scales that are measured in the number of atoms that make it up, it is clear that this scaling cannot continue forever.

As a result of this, there has been a great deal of research effort directed at the search for the next device that will continue to power the growth of the computer industry. However, due to the billions of dollars of investment that conventional silicon transistors have received over the years, it is unlikely that a technology will emerge that will be able to beat it outright in every performance category. More likely, different devices will possess advantages over conventional transistors for certain applications and uses.

One of these emerging computing platforms is nanomagnetic logic (NML). NML-based circuits process information by manipulating the magnetization states of single-domain nanomagnets coupled to their nearest neighbors through magnetic dipole interactions. The state variable is magnetization direction and computations can take place without passing an electric current. This makes them extremely attractive as a replacement for conventional transistor-based computing architectures for certain ultra-low power applications.

In most work to date, nanomagnetic logic circuits have used an external magnetic clocking field to reset the system between computations. The clocking field is then subsequently removed very slowly relative to the magnetization dynamics, guiding the nanomagnetic logic circuit adiabatically into its magnetic ground state. In this dissertation, I will discuss the dynamics behind this process and show that it is greatly influenced by thermal fluctuations. The magnetic ground state containing the answer to the computation is reached by a stochastic process very similar to the thermal annealing of crystalline materials. We will discuss how these dynamics affect the expected reliability, speed, and energy dissipation of NML systems operating under these conditions.

Next I will show how a slight change in the properties of the nanomagnets that make up a NML circuit can completely alter the dynamics by which computations take place. The addition of biaxial anisotropy to the magnetic energy landscape creates a metastable state

along the hard axis of the nanomagnet. This metastability can be used to remove the stochastic nature of the computation and has large implications for reliability, speed, and energy dissipation which will all be discussed.

The changes to NML operation by the addition of biaxial anisotropy introduce new challenges to realizing a commercially viable logic architecture. In the final chapter, I will discuss these challenges and talk about the architectural changes that are necessary to make a working NML circuit based on nanomagnets with biaxial anisotropy.

This work is dedicated to my parents and to my advisor Jeff Bokor

Contents

Chapter 1

Introduction

Contents

This dissertation will present work directed towards the realization of a logic device capable of performing universal computations with power usage approaching the ultimate limits in efficiency. The device is based on nearest-neighbor interacting single domain nanomagnets and is able to function without passing an electric current.

Before discussing the details of this architecture, I will begin with an introduction to motivate the need for such an architecture and briefly discuss the history of magnetism and the computer industry.

1.1 The end of Moore's Law

The multibillion dollar semiconductor industry's vast growth over the last 40 years has been powered by the exponential improvements in speed, cost, and energy efficiency described by Gordon Moore's famous law [1]. Moore observed that transistors were shrinking at a rate that

allowed twice as many transistors to be fit on a single chip every 2 years. As transistors scale, they get faster, consume less energy, and cost less to produce. This has led to a virtuous circle between consumers and industry and has produced the vast improvements we look forward to every year in the usefulness and cost of our computers.

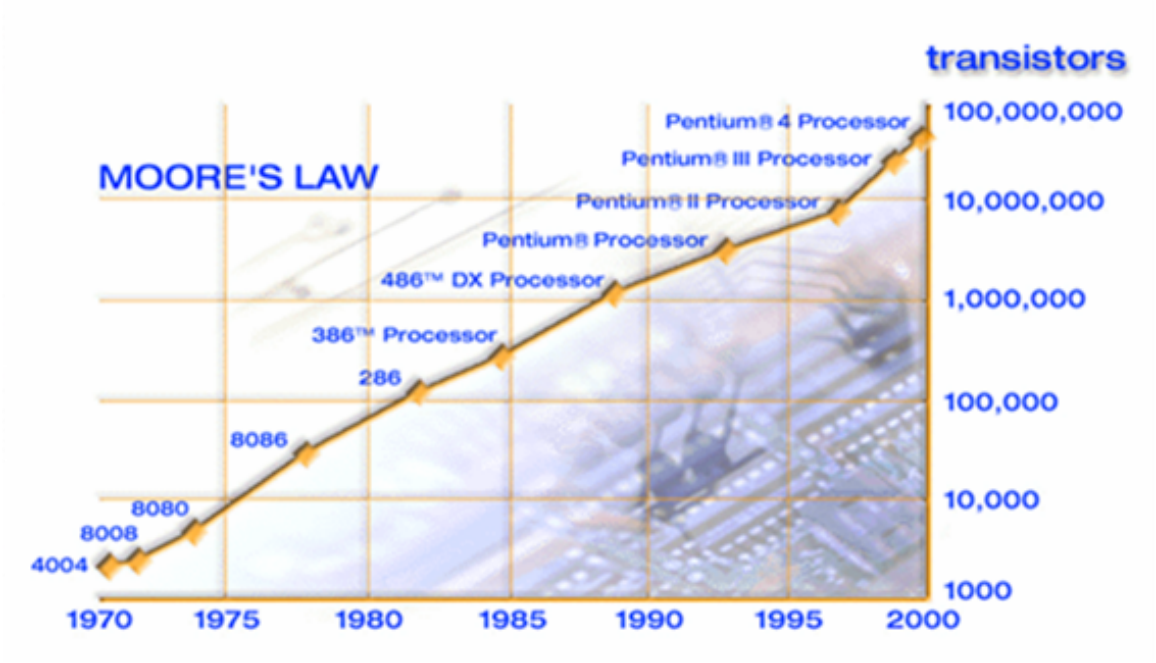

Figure 1.1: Moore's Law says that density of transistors on an integrated circuit increase exponentially over time. This trend has continued for the last 40 years. Image Attribution: [2]

Unfortunately, things can not continue getting smaller forever. While the demise of Moore's law has been prematurely predicted for decades, eventually it will have to end. Faced with this inevitability, the semiconductor industry is in a desperate search for a new type of logic device that will be able to continue a trend that, in addition to all the other aforementioned benefits, has made their shareholders very happy.

1.2 Magnetism at the Nanoscale

The seemingly magical powers of magnetic materials has made them ubiquitous in industry for decades. Here I briefly discuss the origins of magnetism with special emphasis on how magnetic properties manifest themselves at the micro and nanoscales.

1.2.1 Origin of Magnetism

Magnetic fields are caused by the movement of charges [3], [4]. When an electric current flows through a wire, a magnetic field is generated around it.

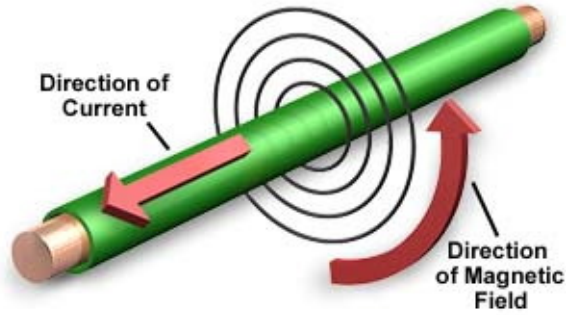

Figure 1.2: When current flows through a wire there is a resulting magnetic field that is generated around it. Image attribution: [5]

However, some materials possess magnetic properties even in the absence of any current flowing through them. While you might not be able to measure any current going through a ferromagnet such as Iron, Nickel, or Cobalt; these materials do have many electrons in them (all materials do), and the properties of these electrons are of fundamental importance for determining a material's electrical and magnetic properties.

Electrons possess intrinsic angular momentum called Spin as well orbital angular momentum as a result of their motion with respect to the nucleus of their atom. These two quantities sum to a quantity J, the total total angular momentum that results in a magnetic moment:

$$m_{atom} = g_J \mu_B \sqrt{J(J+1)} \tag{1.1}$$

μ_B is the Bohr Magneton. g_J is the Landé g factor.

Each of these magnetic moments create their own magnetic field that, not coincidentally, looks very similar to the field that would be created if they instead were a tiny wire loop with current running through it. The field is described by the following equation and can be visualized in Figure 1.3:

$$H_{dipole} = \frac{\mu_0}{4\pi}\left(\frac{3r(m \cdot r)}{r^5} - \frac{m}{r^3}\right) \tag{1.2}$$

1.2.2 Domains and Magnetostatics

In non-ferromagnets, the electronic structure of the atoms that make up the material results in there being 0 net angular momentum. In other cases, there is a nonzero net angular momentum (resulting in a magnetic moment), but the neighboring magnetic moments have no interaction with one another and orient themselves randomly. However, in ferromagnets, neighboring moments exhibit a strong interaction called the exchange interaction which is a force that causes neighboring moments to align themselves. Due to this exchange interaction, large regions of ferromagnetic material with mutually aligned moments add up and create regions of magnetized material.

The exchange interaction is governed by the following equation:

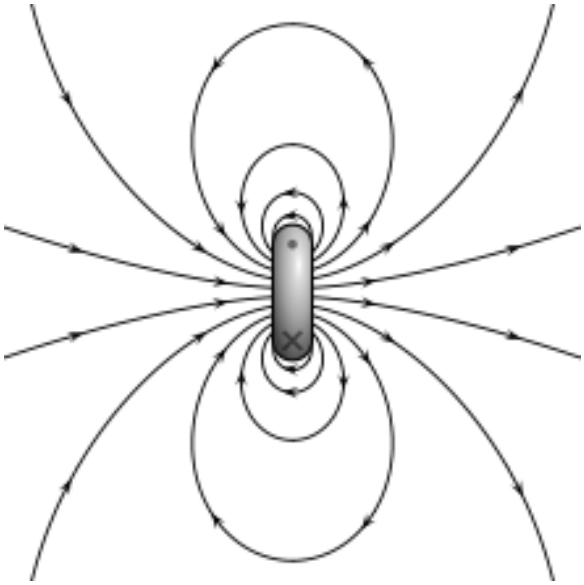

Figure 1.3: The field of a magnetic moment looks like the field of a small current loop. It is known as a dipole field. Image attribution: [6]

$$E_{ex} = -J_{ex} m_1 \cdot m_2 \tag{1.3}$$

In cases where the exchange constant J_{ex} is positive, the exchange energy between two moments is minimized when they point in the same direction.

In addition to the exchange force, moments also are affected by magnetic fields. Specifically the energy of a moment is minimized when it points in the same direction as the magnetic field. This interaction is governed by the following equation and is called the Zeeman energy after the Dutch Physicist most associated with it:

$$E_{Zeeman} = -m \cdot B_{ext} \tag{1.4}$$

As described in Equation (1.2), Each magnetic moment creates its own magnetic field. This magnetic field is felt by all the other magnetic moments in the material as if it were an external field. Thus every magnetic moment in a ferromagnetic feels the force of every other magnetic moment in the material. This is called the magnetostatic energy and can be calculated by integrating over the dipole fields resulting from the other moments in the material:

$$E_{ms} = -\frac{1}{2} \int_V m \cdot B_{ms} \, dV \tag{1.5}$$

By summing up these energy terms one can obtain an expression for the free energy of these moments as a function of the direction that it points. The moment will tend to point along the direction in which the total energy is minimized.

$$E_{tot} = E_{ex} + E_{Zeeman} + E_{ms} \tag{1.6}$$

The exchange term is very strong at short distances (nanometer scale), but weakens quickly and is less dominant then the magnetostatic interaction at the micron scales. The magnetostatic energy on the other hand, tends to favor spins that are oppositely aligned. As a result of these two forces, localized regions of magnetic material, dominated by the exchange force, will tend to align themselves into "domains" of uniformly magnetized areas.

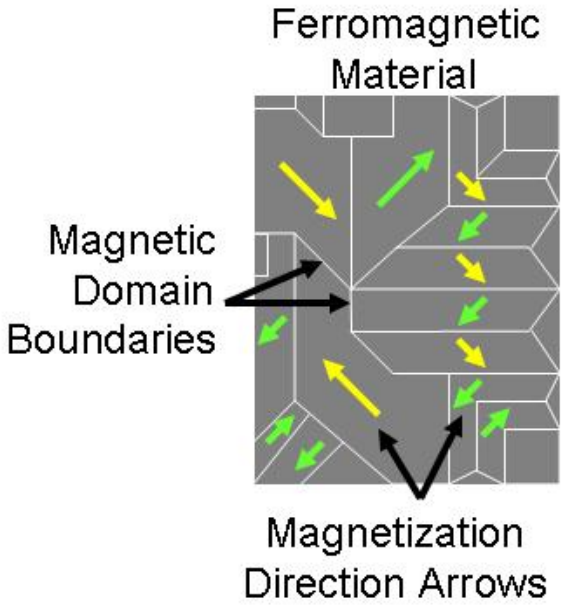

Figure 1.4: In ferromagnets, nearest neighbor spins align themselves in parallel with one another and form regions called domains. [7]

1.2.3 Dynamics and the Landau-Lifshitz-Gilbert Equation

The energies above determine the direction in which a moment will point in a static sense, but they say nothing regarding how the moment will reach this position. The dynamics are described by a differential equation known as the Landau-Lifshitz-Gilbert equation. It says the following:

$$\frac{dm}{dt} = -\frac{\gamma}{1+\alpha^2} M \times H_{eff} - \alpha \frac{\gamma}{(1+\alpha^2)M_s} M \times (M \times H_{eff}) \tag{1.7}$$

The equation describes how the moment will respond when in the presence of an effective field H_{eff} which is derived from the energy E_{tot} in Equation (1.6).

$$H_{eff} = -\frac{1}{\mu_0} \frac{\delta E_{tot}}{\delta M} \tag{1.8}$$

The M $\times H_{eff}$ term in Equation (1.7) causes the moment to rotate or *precess* around the effective field. This precession would occur forever were it not for the $M \times (M \times H)$ term which causes the moment to slowly tilt or *damp* inwards toward the effective field vector. The dynamics of this process as governed by Equation (1.7) can be visualized in Figure 1.5.

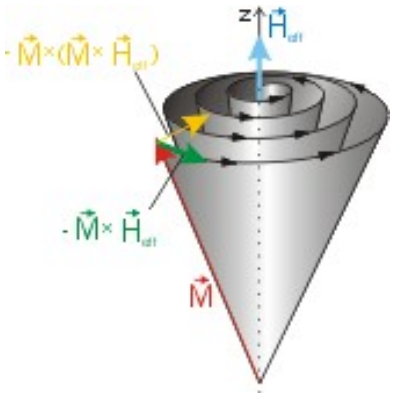

Figure 1.5: This shows how a magnetization vector in the presence of an effective field H_{eff} will behave. It is a visual representation of the Landau-Lifshitz-Gilbert differential equation (1.7). Image attribution: [8]

1.2.4 Nanomagnetism

The formation of magnetic domains as depicted in Figure 1.4 is a result of the competing interaction between the different forces/energies described above. These domains are present in all macroscopic ferromagnetic materials. However, as these ferromagnetic materials are scaled down to smaller sizes, these domains undergo interesting changes. The magnetostatic, or self-energy, described in Equation (1.5) makes it unfavorable for neighboring moments to align themselves parallel to one another. This competes with the exchange energy described in Equation (1.3) which tends to align neighboring moments in the same direction. When the magnetic material is on the order of a few microns the surfaces of the magnetic material become important. At these size scales, the magnetic domains often are able to minimize their energy by forming patterns that are striking in their symmetry and mathematical beauty. An example magnetic structure exhibiting these types of confined domains is shown in Figure 1.6.

At even smaller size scales, it ceases to be energetically favorable to form a domain at all. The exchange interaction (which is very strong but works on very short length scales) wins out and every moment points in the same direction.

This occurs when the dimensions of a magnet are on the order of a few hundred nanometers or below. These so-called single domain nanomagnets are characterized as having a single well-defined magnetization vector with a magnitude equal to the saturation magnetization of the material. In many respects they can be thought of as a single magnetic moment described in Figure 1.3, only much stronger. A single domain nanomagnet gives off a dipole

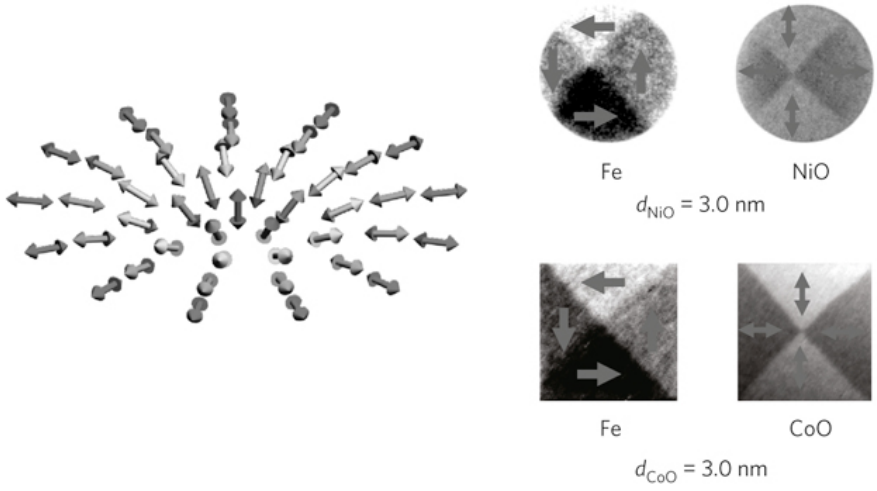

Figure 1.6: These Fe and NiO multilayer structures exhibit curling and vortex structures in this work by Wu, Carlton, et al [9]. The diameter of the discs and length of the squares is 2 um. The thickness is 3.0 nm.

magnetic field described exactly as in Equation (1.2). A schematic of a single domain nanomagnet with its accompanying dipole field is shown in Figure 1.7.

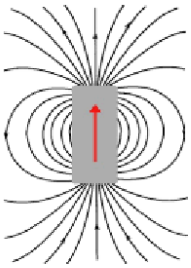

Figure 1.7: A single domain nanomagnet has a well-defined magnetization vector given by the red arrow. The resulting magnetization takes the form of a magnetic dipole, the mathematics of which were already described in Equation (1.2).

Shape Anisotropy

As with confined micron-scale magnets, the shape of a single domain nanomagnet imparts important properties on the way its magnetization vector will behave in the presence of applied fields and other external phenomena. When a single domain nanomagnet has the shape of a circle, its magnetization vector is free to point in any direction. However, this is not the case for non-symmetric elongated structures such as the ellipse. Elliptically shaped nanomagnets prefer to have their magnetization vector pointing along the long direction of the elipse. In Figure 1.7, this equivalent to the magnetization vector preferring to point up/down but not to the left or right. This effect is known as shape anisotropy.

Explaining Shape Anisotropy

Shape anisotropy is extremely important for understanding the concepts in this dissertation, so I will go to some length to explain it in this subsection. First, the following is a quick review of the difference between H and B, the two quantities associated with the magnetic field.

One of Maxwell's fundamental equations of electrodynamics states the following:

$$\nabla \times B = \mu_0 J \tag{1.9}$$

In other words, electric currents (J), are the fundamental cause of magnetic fields. This is the mathematical explanation behind Figure 1.2. However, when dealing with magnetic materials, it is convenient to divide up the currents between currents flowing in wires ("free" current), and those flowing around atoms in materials causing ferromagnets to emit a magnetic field ("bound" current). In this case, Maxwell's equation is modified in the following way:

$$\nabla \times B = \mu_0 (J_{bound} + J_{free}) \tag{1.10}$$

We call the field created by the free current H. M, the magnetization vector, is likewise a result of the bound current. Substituting:

$$\nabla \times M = J_{bound} \tag{1.11}$$

And:

$$\nabla \times H = J_{free} \tag{1.12}$$

We get:

$$B = \mu_0 (M + H) \tag{1.13}$$

In magnetized materials, H points in the opposite direction to M and its magnitude depends on the shape of the magnet and the direction of magnetization. Shape anisotropy is often explained as a being caused by this *demagnetizing* field. When the calculations are carried out, H_D is larger when an elliptically shaped nanomagnet is magnetized along the short axis and smaller when the same nanomagnet is magnetized along the long axis. The larger H_D, the less stable the magnet is in this orientation.

There are several disadvantages to using this approach to understand shape anisotropy, however. One important issue is the relative importance that scientists give to the two fields, H and B. Most physicists understand B as the fundamental quantity. Richard Feynman said, "People tended to think that H was the magnetic field. But, as we have seen, B [... is ...] the physically fundamental field, and H is a derived idea" [10]. B produces the Lorentz force and creates torques on moving charges in magnetic moments and wires, not H.

Material scientists and Electrical Engineers often think of H as the more fundamental field. Part of this has to do with the fact that, to experimentalists, H corresponds most with

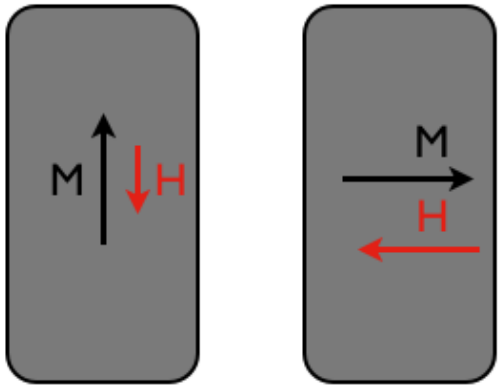

Figure 1.8: A single domain nanomagnet is magnetized along its short and long axes. The relative magnitude of the demagnetizing field, H_D is shown in red. H_D is larger when the nanomagnet is magnetized along the short axis. The relative magnitude of this field is used to explain the preferred magnetization axis in nanomagnets with shape anisotropy.

the types of fields they control. In particular, when fields are generated by current carrying solenoids, J_{bound} = 0 and B and H are related by a simple multiplicative constant, μ_0:

$$B = \mu_0 H \tag{1.14}$$

However, H is at its most "derived" and nonphysical (see Feynman quote above) *inside* a magnetic material. In this case, J_{free} = 0. This lack of free current means (by Equation (1.12)) that:

$$\nabla \times H = 0 \tag{1.15}$$

This doesn't, however, mean that H itself is 0. This says only that H has no curl, but it is this nonzero H, that is often used to "explain" shape anisotropy. This is despite the fact that H was defined as produced by "free" currents that do not exist inside a ferromagnet (Equation (1.12). [i]

While this is the conventional way shape anisotropy is explained in undergraduate courses on magnetism, it is confusing, and based on a field object that Feynman himself called a nonphysical mathematical construct. It turns out that shape anisotropy can also be explained more intuitively as a result of the magnetic moments in the ferromagnet attempting to orient themselves so as to reduce the energy due to their self B (not H) fields. This is, of course, mathematically equivalent to using the demagnetizing H field.

[i] It's worth noting that H *can* be made more fundamental when magnetism is modeled as originating from magnetic charges. This model has the advantage of having no moving parts in the rest frame of the material, but (barring the discovery of magnetic monopoles) is not very physical. For a detailed treatment of the pedagogical arguments for and against B and H, see Reference [11].

Consider an elongated nanomagnet so small that it consists of only 2 moments above and below one another as in Figure 1.9. To minimize their magnetostatic energy (due to their self fields), The two moments will tend to align themselves so their mutual dipole shaped B fields will not exert a torque on one another. There are only a few ways that these moments can align themselves to minimize their energy and bring this torque down to 0. They can align themselves by both pointing up (or down) as in Figure 1.9 a). Or they can align themselves in opposite directions pointing left and right as in Figure 1.9 b). In a larger magnet, b) is a perfectly acceptable way to reduce their magnetostatic energy - this is what a magnetic domain is. However, single domain nanomagnets are by definition small enough that they are dominated by the exchange force and operate under the constraint that both magnetic moments must point in the same direction.

If the moments were to align themselves to the right (or left) as in c) the mutual dipole fields would exert a torques on each other, and the energy would not be minimized. The torque that the moments feel would tend to cause them to point along one of their preferred directions[ii]. The magnet would thus prefer to be uniformly magnetized up or down but not left or right. This can be easily generalized to larger nanomagnets consisting of many moments.

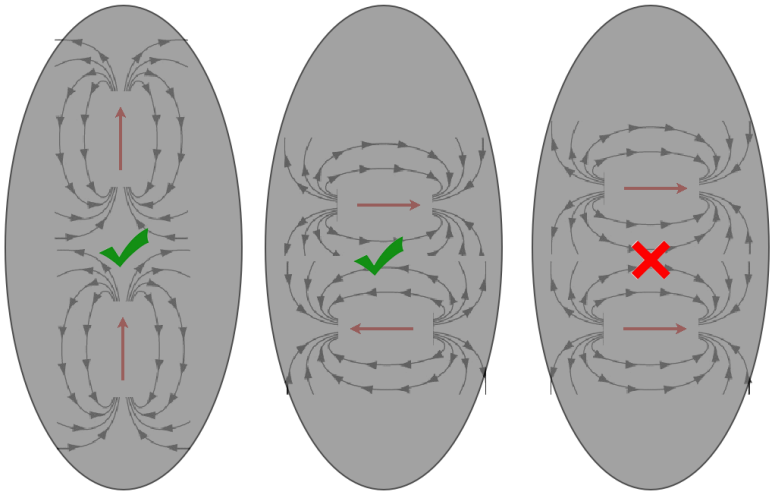

Figure 1.9: A single domain nanomagnet consisting of two interacting moments. To minimize the interaction energy, both moments prefer to align themselves in the same direction, either up or down as in a) or in opposite directions left and right as in b). At this small size scale, the exchange force dominates and the moments are constrained to point in the same direction. in c) the moments are both aligned to the right but in an orientation that does not minimize their energy. This is the origin of shape anisotropy.

Because the magnet has a single axis along which its magnetization vector prefers to point, this type of anisotropy is known as uniaxial anisotropy. The preferred axis (up/down)

[ii] In this simple and highly symmetric model the dipole fields would be pointing exactly opposite to the moments and no torque would be felt due to the cross product going to 0. However this is an unstable equilibrium, and thermal fluctuations would cause the moments to tip out of this unstable point. In a more complicated structure, asymmetries would result in curling of the moments near the edges of the nanomagnet that would also cause torques on the spins.

is known as the “easy” axis. The axis along which the magnetic moment does not prefer to point (left/right)is known as the “hard” axis.

1.3 Introduction to Nanomagnetic Logic

Nanomagnetic logic encodes binary information into the magnetization direction of single domain nanomagnets and transmits and manipulates this information through nearest-neighbor dipole field coupling between neighboring nanomagnets. The seminal experimental work was done at the University of Notre Dame [12]. The nanomagnets are elliptically patterned to give them uniaxial shape anisotropy. They are thus bistable and prefer to be magnetized up or down. This bistability allows the encoding of a bit of information in a nanomagnet based on whether it is magnetized up (‘1’) or down (‘0’) as in Figure 1.10.

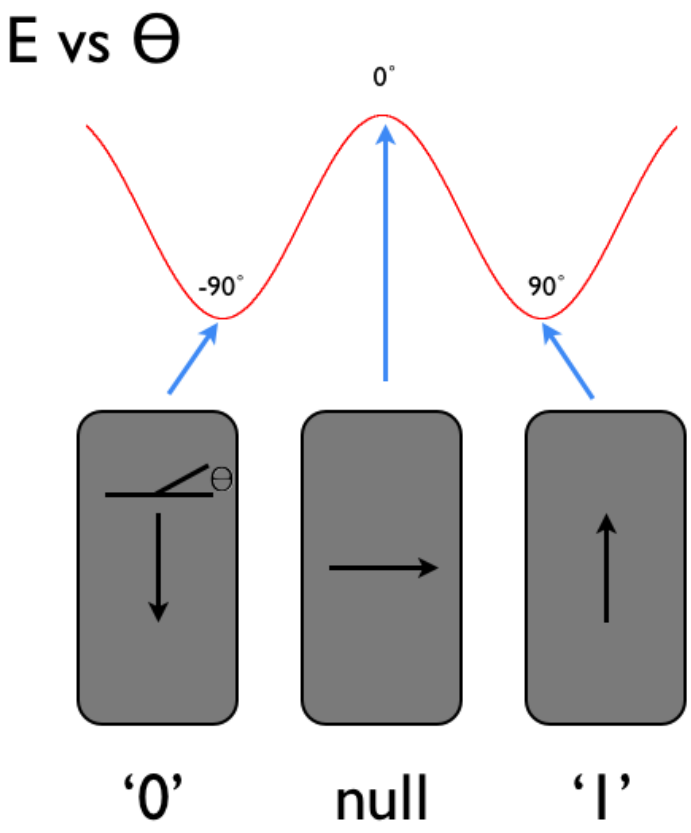

Figure 1.10: The energy landscape due to the shape anisotropy of an elliptically shaped nanomagnet. Binary information is encoded in the direction that a magnet is magnetized along its preferred axis.

1.3.1 Magnetic "Wires"

To carry a bit of information from one area of the circuit to another, magnetic "wires" are needed. These are accomplished by placing a line of identical single domain nanomagnets next to a fixed input bit and forcing them to have their magnetizations point along their unstable "hard" axis as in Figure 1.11 a). In experiments this is done with an external magnetic field for convenience, but an ultra-low power CPU might rely on magnetoelectric clocking to switch the nanomagnets. As this "clocking" field is removed, the magnets must choose a direction to fall into along their preferred axis. This decision is influenced by the dipole coupling of the nearest neighbors which will tend to align themselves antiferromagnetically with one another (alternating directions up, down, up, down). After the field has been removed, the magnetization state of the nanomagnet on the beginning of the chain will be transferred onto the the magnetization state of the nanomagnet on the end of the chain as shown in Figure 1.11 c).

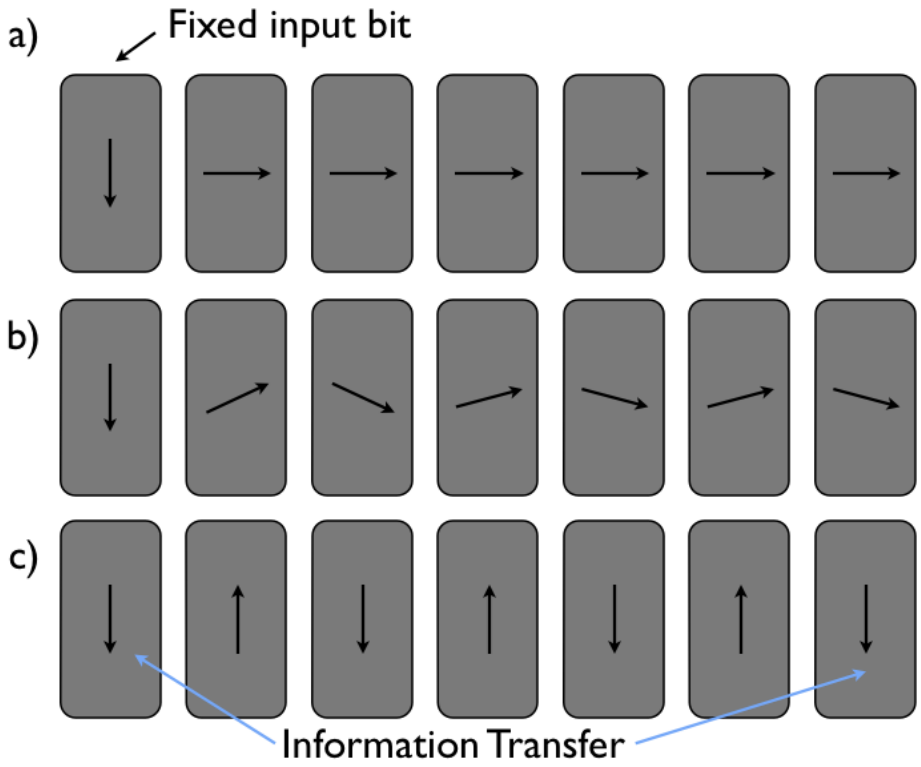

Figure 1.11: A diagram showing how a magnetic "wire" can be used to transfer information from one point in a circuit to another. in a), a single input nanomagnet has been held fixed and the other nanomagnets in the chain have been nulled along their "hard" axis with an external magnetic field. As the field is removed in b), the magnets begin to fall back to their preferred magnetization axis. The direction they fall is mediated by the dipole coupling between nearest neighbors. The chain will tend to align itself antiferromagnetically, and the output magnetization will thus be a function of the input nanomagnet after the field has been completely removed (c).

Wires must be able to transfer information in any direction. The dipole coupling between nearest neighbors in vertical wires results in ferromagnetic coupling, but otherwise the

operation is the same.

1.3.2 The Majority Logic Gate

The magnetic wires above move a signal from point A to point B, but the purpose of these wires is ultimately to shuttle signals to and from magnetic elements capable of performing a logical computation as in Figure 1.12.

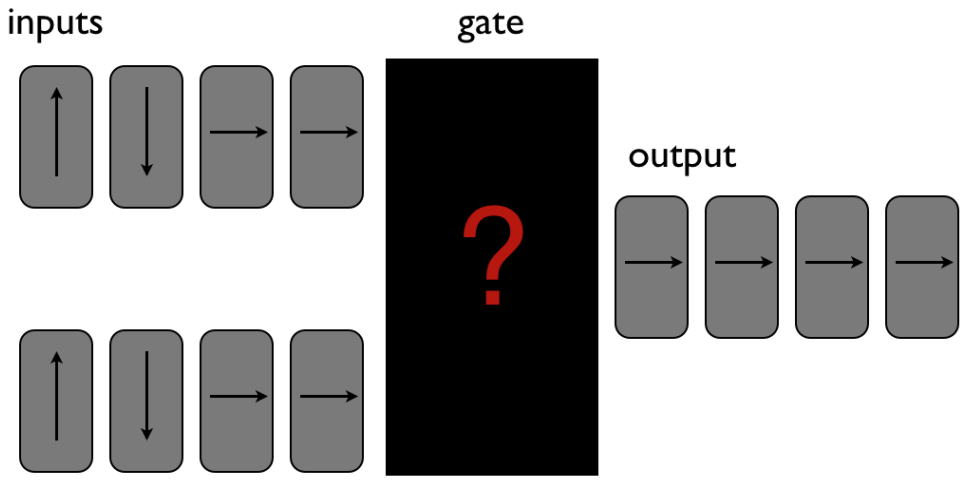

Figure 1.12: In this schematic, the magnetic wires discussed in the previous section are shown carrying and input and output signals to a gate still to be identified.

In prior work, magnetic logic computations have been performed using Majority Logic [12], [13], [14], [15]. As with the more familiar NAND gate, Majority logic gates are functionally complete and can be used to create arbitrarily complex combinatorial logic circuits. The Majority logic gate is a 3 input gate that outputs the majority vote of the inputs. The truth table is shown in Figure 1.13 a).

To perform logic, 3 input nanomagnets surround a central output nanomagnet. During the removal of the aforementioned magnetic "clocking" field, each of the input nanomagnets couple with the output nanomagnet with their dipole fields and vote on a direction for the output bit to fall into as shown in Figure 1.13 b).

By connecting the inputs and outputs of multiple majority logic gates together with the magnetic wires discussed in the previous section, complex combinatorial logic can be performed every time the magnetic "clocking" field is applied

1.3.3 Imaging Techniques

There are many ways that one can characterize the performance and reliability of real nanomagnetic logic circuits. One very common technique is to take a magnetic contrast image

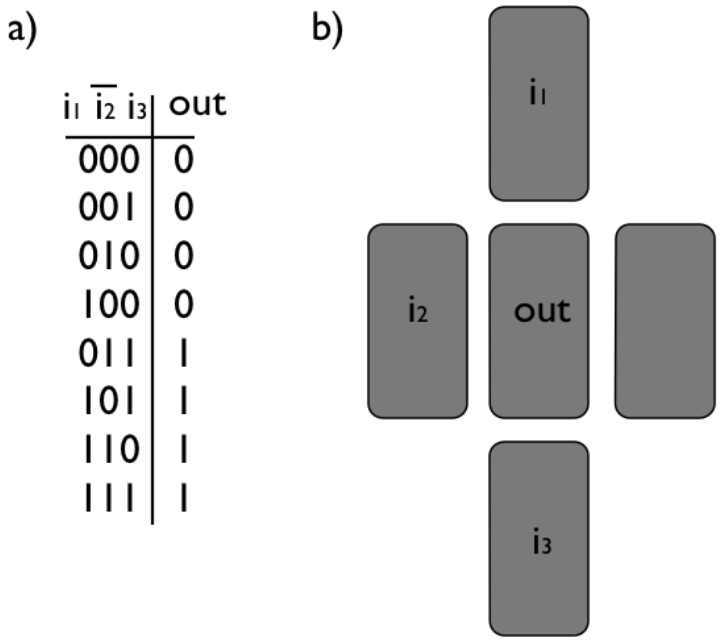

Figure 1.13: a) The truth table for the Majority logic gate. Majority logic gates are functionally complete and can be used to create arbitrarily complex combinatorial logic circuits. b) 3 input bits surround a central output bit. Each of their dipole fields couple with this central bit and vote on the direction the output nanomagnet will fall into.

of a circuit after a computation has taken place and read out the magnetization state of each nanomagnet in the circuit to ascertain whether it functioned as expected. In this work, two imaging techniques were used; MFM, and PEEM.

Magnetic Force Microsopy

Magnetic Force Microscopy (MFM), is a scanning probe technique for detecting magnetic fields near the surface of magnetized material. After obtaining a mapping of the field strength in an area, it is possible to infer what the magnetization state of the material is. A very simplified discussion of MFM follows. A more detailed review of MFM is available at the following reference [16].

In conventional Atomic Force Microscopy (AFM), a cantilever with a sharp tip attached at the end is scanned over a sample. By measuring the interactions that the tip has with the surface and using a feedback loop to keep the tip at a constant distance, a topographic image can be obtained. In MFM, a topographic map is first obtained and then the tip is rescanned over the surface at a constant distance using the previously obtained topographic image as a guide. In MFM, the tip is coated with a magnetic material, and during this second scan the tip sense forces coming from the longer range but weaker magnetic fields. The tip is sensitive to fields that are out-of-plane. The dipole fields of a single domain nanomagnet are shown

in Figure 1.14. There are strong out-of-plane components on either end of the nanomagnet (points p1, and p2). These areas will show up as bright and dark spots on the MFM image. A single domain magnet will always consist of these two spots making it easy to infer which direction the nanomagnet is magnetized.

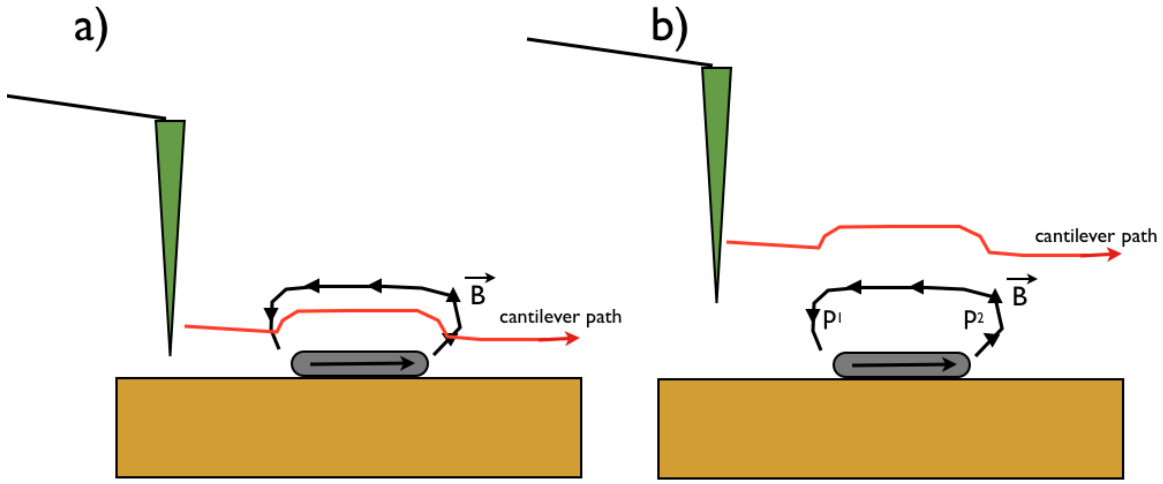

Figure 1.14: a) In AFM, a cantilever is scanned over the surface to obtain a topographic image. b) in MFM a second pass is done further away where surface interactions are minimized and the dominant force on the tip are the weaker but longer ranged magnetic forces. MFM is sensitive to out-of-plane magnetic fields. The dipole field of the nanomagnet in the figure has a large out-of-plane field coming in and out of it at either end (points p1 and p2). In a MFM image these areas will show up as bright and dark spots respectively.

An MFM image showing a chain of nanomagnets that are antiferromagnetically coupled is shown in Figure 1.15 b). A corresponding Scanning Electron Micrograph (SEM) is show in Figure 1.15 a).

Photoemission Electron Microscopy

While MFM measures the magnetization of a material indirectly by imaging stray dipole fields, Photoemission Electron Microscopy (PEEM) is a technique that can directly image the magnetization direction. A brief discussion of PEEM follows. A more detailed treatment is available here [17].

When X-rays hit solid surfaces, photoelectrons are emitted from the material. The properties of these emitted electrons can be used to learn about the sample under irradiation. Magnetic imaging with PEEM relies on an effect called X-ray Magnetic Circular Dichroism (XMCD). If the X-ray beam is circularly polarized, the number of electrons emitted from a magnetized sample will depend on the direction of magnetization and polarization (left or right) of the beam. By irradiating a sample with coherent circularly polarized x-rays and collecting the electrons, an image can be constructed showing the magnetization state of different areas of the sample.

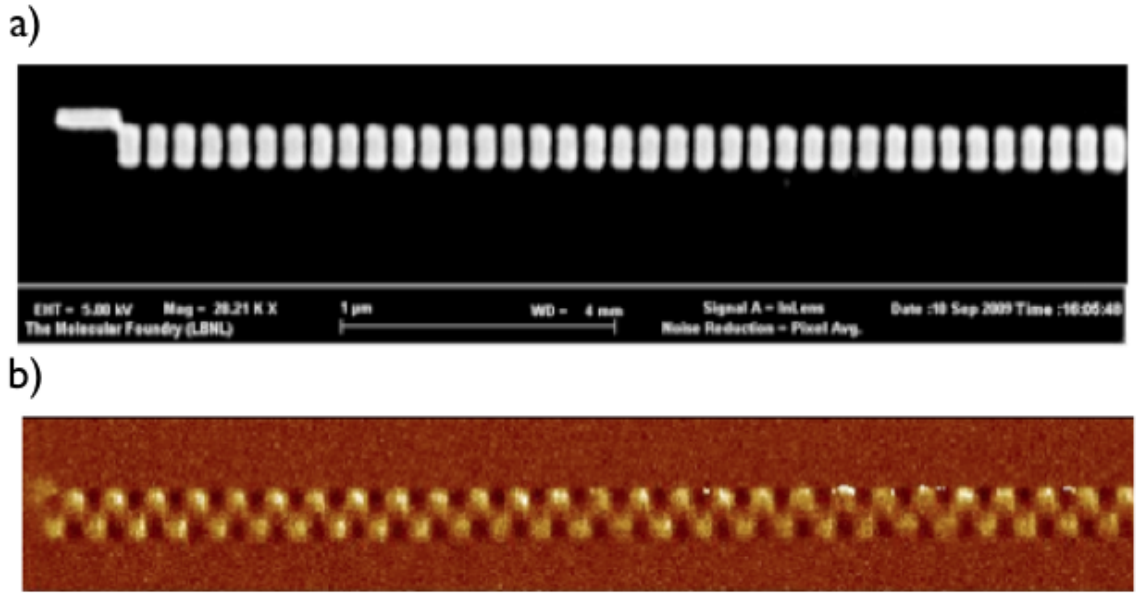

Figure 1.15: a) an SEM micrograph showing a chain of nanomagnet. b) An MFM image showing the magnetic state of a chain of nanomagnets. Each nanomagnet consists of a pair of bright and dark spots corresponding to the out-of-plane stray fields consistent with a dipole field resulting from a single domain nanomagnet.

In Figure 1.17, a PEEM image showing a chain of antiferromagnetically coupled nanomagnets is shown. Because the PEEM directly images magnetization, each magnet is seen as a single color (black, or white), depending on its magnetization state.

1.3.4 Micromagnetic Simulations

Micromagnetic simulations use Finite Element Analysis (FEA) to solve the LLG equation (1.7) to calculate how the magnetic state of a system will evolve in time. Magnetic material is divided into nanometer scale spins and made to interact with the energy terms discussed in Section 1.2.2. After the calculating the total energy of each spin due to these forces, the spins are made to evolve according to equation (1.7) to calculate the new position of the spins at the next time step.

Until recently micromagnetics problems were considered too computationally expensive to be solved with a desktop PC, however this has changed in the last decade. The Object Oriented Micromagnetic Framework (OOMMF) [19] is an open source project at the National Institute of Standards and Technology (NIST) for solving problems in micromagnetics.

The LLG equation in (1.7) does not take temperature into account, but for nanoscale magnets the effect of temperature is particularly important. In these systems, temperature can be modeled as a random fluctuating field with energy proportional to $k_B T$. With this change, the LLG equation becomes:

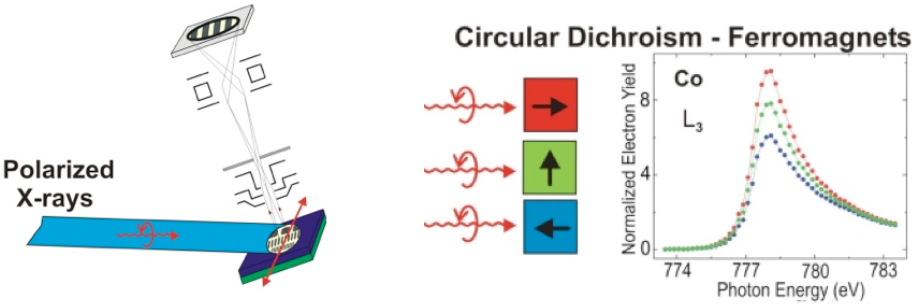

Figure 1.16: a) A schematic showing the experimental setup for a PEEM experiment. Circularly Polarized X-rays irradiate a sample. Photo-emitted electrons are collected with electron optics and used to create a magnetic contrast image. b) A plot showing the normalized electron yield as a function of X-ray energy. The yield changes based on the magnetization direction of the material. Image attribution: [18]

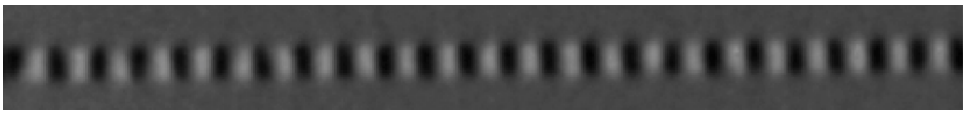

Figure 1.17: a) A PEEM image showing the magnetization state of a chain of nanomagnets. Each nanomagnet consists of a single black or white spot measuring whether the nanomagnet is magnetized up or down.

$$\frac{dm}{dt} = -\frac{\gamma}{1+\alpha^2} M \times (H_{eff} + h_{fluct}) - \alpha \frac{\gamma}{(1+\alpha^2)M_s} M \times (M \times (H_{eff} + h_{fluct})) \quad (1.16)$$

The fluctuating field, h_{fluct}, follows a Gaussian distribution and the angular direction is randomly oriented. Furthermore this field should have 0 mean because temperature variations should not drive the system in any particular direction. The Gaussian distribution is assumed as a consequence of the central limit theorem and the number and independence of the fluctuations. The variance, σ^2, of h_{fluct} is given by the following equation (a more detailed discussion and calculation of the variance can be found in [21]:

$$\sigma^2 = \frac{\alpha}{1+\alpha^2} \frac{2k_B T}{\gamma \mu_0 M_s V} \quad (1.17)$$

Because h_{fluct} has 0 mean, this completely determines its distribution function f(x):

$$f(x) = \frac{1}{\sqrt{2\pi\sigma^2}} e^{-\frac{x^2}{2\sigma^2}} \quad (1.18)$$

This is treated in more detail in Section 8.2 of [22]. OOMMF does not by default support the inclusion of these temperature fluctuations. However, the theoretical framework was implemented in OOMMF as an extension by SPM-Group at the Institute of Applied Physics in Hamburg. It can be obtained at the following reference [23]. OOMMF is often distributed as a precompiled binary. In order to use this extension it is necessary to obtain the raw OOMMF

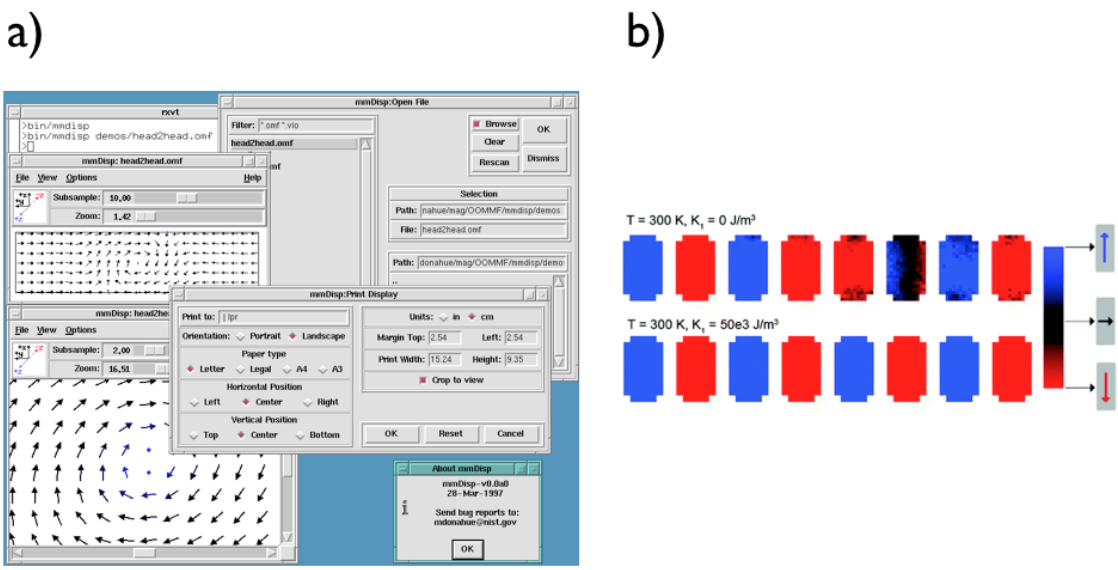

Figure 1.18: a) A screenshot from the OOMMF micromagnetic simulator showing the formation of a vortex state in a micron-scale magnet. Image attribution: [20] b) The results of a micromagnetic simulation showing the final magnetic state in a chain of nanomagnets.

source code and compile it with the extension source files by following the directions in [19] and at [23].

1.4 Dissertation Overview

Creating a device that hopes to compete with conventional CMOS is not easy, but nanomagnetic logic is one of only a few approaches that have shown promise towards achieving this goal. While nanomagnetic logic is never likely to outperform CMOS in terms of speed of operation, there is plenty of room to compete in the realm of power efficiency. There also still remains a great deal of investigation needed to overcome hurdles and achieve the full potential of this device. This dissertation will explore the current state-of-the-art and suggest future research goals directed at solving these remaining challenges. First, the dynamics of nanomagnetic logic will be explored in detail. A model for signal propagation will be developed taking into account the role thermal effects play in the relaxation of the magnets to their low energy state. This model will be demonstrated theoretically with micromagnetic simulations and then experimentally with time-lapse PEEM imagery. The reliability and robustness of nanomagnetic circuits will be analyzed in the context of this new model. Next, biaxial anisotropy will be investigated as a method for increasing speed and reliability in nanomagnetic logic circuits by altering nanomagnet dynamics to occur as a cascade. The biaxial mode will be studied theoretically and demonstrated experimentally. Reliability and speed in this mode will also be investigated. Lastly, the consequences of operating nanomagnetic logic circuits in the biaxial mode will be considered. Challenges associated with race conditions and the majority logic gate will be discussed along with a proposed logic structure to solve this problem. The biaxial mode will also be investigated as part of a Register Transfer Logic (RTL) compatible computing architecture. As part of this discussion, a nanomagnetic memory register element will be developed to allow the creation of long pipeline stages and finite-state machines

Chapter 2

Adiabatic Clocking

Contents

The properties of the magnetic clocking field used to reset the nanomagnets between computations is a very important factor in determining the operating characteristics of nanomagnetic logic systems [24]. One of the most important parameters is the rate at which the magnetic clocking field is removed. This chapter will focus on the operation of nanomagnetic logic circuits in which the clocking field is removed slowly relative to the time it takes for the nanomagnets to reach a new equilibrium position after a change in the external field. These "adiabatic" changes allow the magnetic system to remain near thermal equilibrium throughout operation and will be defined in this dissertation as a clock removal time that is longer than several nanoseconds. This mode is important because the majority of experimental work to-date has been done in this mode [12], [14], [25].

I will first discuss experiments and theory exploring the dynamics of nanomagnet chains in this mode. Then I will show experimental and simulation work on robustness and error rates for circuits operating adiabatically.

2.1 Adiabatic Dynamics

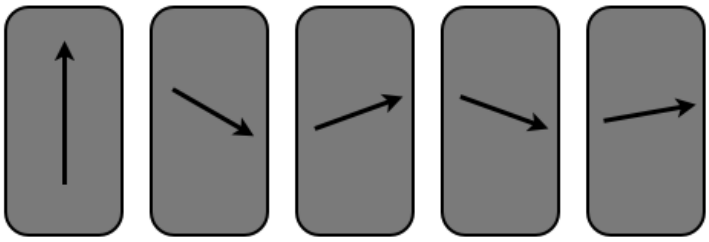

Figure 2.1: When the nanomagnets are clocked adiabatically, the system has time to reach a new equilibrium and every nanomagnet rotates continuously and simultaneously into their ground state.

When the magnetic clocking field is removed adiabatically, every nanomagnet in the chain ideally rotates simultaneously and continuously into the final antiferromagnetic ground state as shown in Figure 2.1. However, when operated at room temperature, the dynamics by which the nanomagnets fall into their ground state during the adiabatic removal of the clocking field is greatly influenced by thermal fluctuations. In previous work, Cowburn studied the effect of thermal fluctuations in the relaxation of ferromagnetically coupled magnetic islands in rotating fields [26]. We suggest a closely related model to describe the dynamics of signal propagation for the present system, and we verify it with micromagnetic simulations and experiment. In this model, as the magnetic field is lowered, thermal fluctuations inevitably introduce ferromagnetically aligned defect pairs. Defects can also be induced by stray magnetic fields or lithographic irregularities. However, these defects obtain enough thermal energy to diffuse along a nanomagnet chain until a lower energy, error-free state is reached. Defects are able to diffuse rapidly because they are not as thermally stable as nanomagnets in the antiferromagnetically aligned ground state.

2.1.1 Defect Random Walk

Each nanomagnet in the chain is affected by its nearest neighbors, however, it is useful to first consider the magnetization energy of an *isolated* nanomagnet (this simplified "isolated" nanomagnet model will be expanded to take into account the nanomagnet's neighbors shortly):

$$U(q) = K_u cos^2(\theta) - H_{hard} M_s cos(\theta) \tag{2.1}$$

where K_u is the uniaxial shape anisotropy energy constant, H_{hard} is the magnitude of the clocking field, Ms is the saturation magnetization, and θ is the magnetization angle with respect to the hard axis. When H reaches a critical value, H_{crit}, the energy barrier between the up and down states is less than the thermal energy, $k_B T$, as illustrated in Figure 2.2 a). Consequently, the isolated nanomagnet undergoes spontaneous transitions between its two low-energy states at an appreciable rate [27].

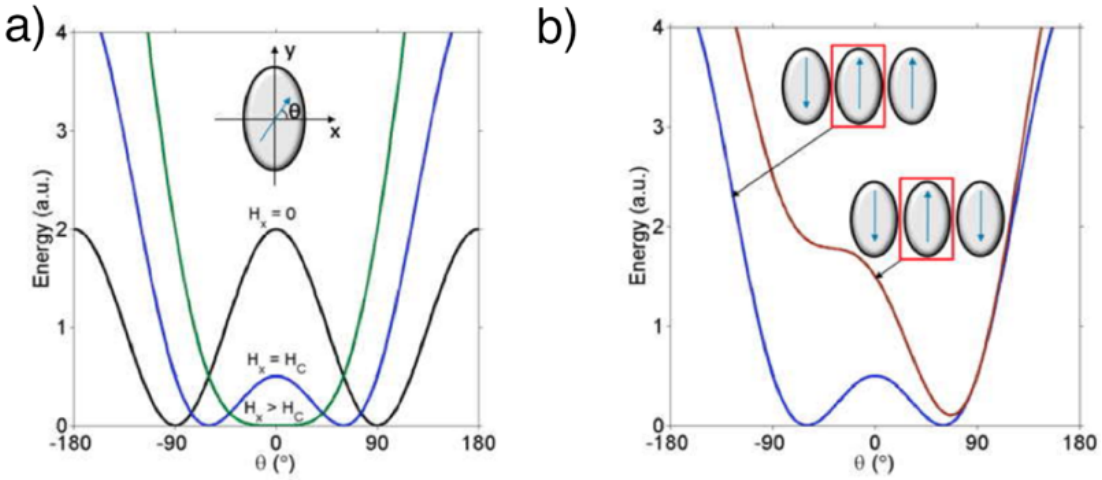

Figure 2.2: Magnetization energy at the critical field. a) Magnetization energy as a function of angle for an isolated single domain elliptically shaped nanomagnet. A magnetic field applied parallel to the hard axis modulates the energy barrier between the two stable magnetic states. For applied field values greater than H_{crit} the barrier between the 'up' and 'down' states is less than k_BT. b) Magnetization energy as a function of angle for a nanomagnet at the critical field in the presence of two nearby neighbors. A nanomagnet that is part of a defect pair has the same energy profile as an isolated nanomagnet because the dipole fields of its nearest neighbors cancel out. The energy barrier for an antiferromagnetically aligned nanomagnet is increased by the nearest-neighbor interactions.

The transition rate of a nanomagnet in a closely spaced array (no longer isolated) is modified by the dipole fields from its neighboring nanomagnets. In the case of an antiferromagnetically aligned chain, the nearest neighbors to the left and right of a given nanomagnet are oriented in the same direction, so their dipole fields add constructively. This field decreases the probability that the central nanomagnet will transition out of its current magnetization direction. This is in contrast to nanomagnets that are part of a defect pair. The nearest neighbors of these nanomagnets are of opposite polarity. In this case, the neighboring dipole fields cancel each other out, allowing either of the nanomagnets that make up the defect-pair to undergo spontaneous transitions when $H_{hard} >= H_{crit}$. We compare the energy profiles of nanomagnets in either antiferromagnetic or ferromagnetic configurations in Figure 2.2 b).

When a transition occurs in a nanomagnet that is part of a defect pair, the defect shifts by one position to the right or left. The direction that the defect moves depends on which nanomagnet within the defect pair undergoes a random switching event, as illustrated in Figure 2.3. Due to symmetry, the defect moves one way or the other with equal probability, causing it to undergo a random walk. Eventually the defect reaches a terminal nanomagnet, at which point it ceases to exist. Alternatively, two defects can combine with one another, which results in their annihilation. Every time a defect is removed from the circuit, the collective energy of the system decreases, making it energetically unfavorable for defects to be reintroduced.

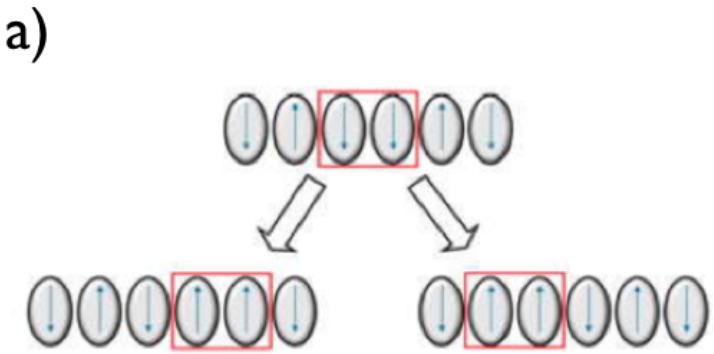

Figure 2.3: At the critical field, nanomagnets that are part of a defect pair transition states at an appreciable rate, resulting in a random walk of the defect.

2.1.2 Micromagnetic Simulation of Random Walk

We ran micromagnetic simulations using the publicly available OOMMF simulator [19], [28], [22], [29] that included the effects of thermal fluctuations as discussed in Chapter 1 to investigate the accuracy of this model. In our simulations, a linear chain of 15 nanomagnets was modeled using the material parameters of permalloy with dimensions 60 nm x 120 nm x 5 nm and nearest neighbor separations of 20 nm. A magnetic field along the x-axis was held fixed at the critical field (37 mT) for the duration of the simulation. The magnetization of all 15 nanomagnets was initialized along their hard axes. Once the simulation began, the nanomagnets quickly ($<$ 1 ns) fell into a state in which only a few defects remained. The remaining defects then began to undergo a random walk as predicted by our model. The results of a micromagnetic simulation at several points in time showing a random walk and subsequent annihilation of a single defect are presented in Figure 2.4 a)-e). The total duration of the simulation was 6 ns.

2.1.3 Experiment

PEEM Fabrication Considerations

To demonstrate the behavior predicted by our model experimentally, magnetic contrast images of the nanomagnet chains were taken using PEEM [17]. There are several important considerations that must be kept in mind to obtain good PEEM data. I will briefly discuss them here. PEEM is a very surface sensitive measurement. The majority of electrons that are excited with enough energy to escape the surface when the x-rays illuminate the substrate are within several nm of the surface. This affects the fabrication procedure in 2 important ways. First, because the magnetization signal is coming from the surface of the nanomagnet, it is important that top layer of the magnetic material be undamaged. Oxidization is a common problem with ferromagnetic material and is it even more so here. While a few nanometers

Figure 2.4: Defect diffusion in nanomagnet chains. a)-e), Micromagnetic simulation of the magnetization of a line of nanomagnets with a defect pair highlighted in the first 4 frames. A hard axis field is held at a fixed value of 37 mT. The magnetization of the first nanomagnet on the left is held fixed as an input to set the antiferromagnetic ordering of the chain. A defect that has formed in the wire moves in a random walk until exiting the chain to the right in e).

of oxidation may not be enough to effect the functionality of the nanomagnet chain, it can destroy the ability to obtain a good PEEM image because the oxidized magnet will be the only material visible to the PEEM.

It is therefore very important to control oxidation by having a capping layer. This capping layer creates its own set of challenges however. Very thin capping layers are required because of the PEEM's surface sensitivity, however thin capping layers are not always able to adequately protect against oxidation. When choosing capping layer thickness there is a thus a tradeoff between adequate oxidation protection and PEEM signal reduction. The best capping layer for these experiments was found to be 1.5-2 nm of Aluminum. Al oxidation in ambient conditions is self limiting to $\sim$1nm so very thin capping layers can be used that still protect the underlying magnetic material from oxidation.

Another fabrication consideration that was necessary to keep in mind with PEEM is the need for a conducting substrate. PEEM is similar to conventional electron microscopes in that charge buildup can occur if the substrate being imaged is insulating. P-type silicon substrates were found to have enough conductivity so to not hamper imaging. However, in the next chapter I will discuss the use of epitaxially grown nanomagnets in PEEM experiments. Here, the substrate cannot be chosen arbitrarily as the substrate is used as a template for growing the single crystalline nanomagnets on top. For example, single crystal Fe can be grown epitaxially on MgO substrates. MgO is an insulator, however, and cannot be imaged in the PEEM without causing arcing of the beam and damaging the sample. When an insulating substrate is required for epitaxial growth, a conducting underlayer with a lattice parameter that is compatible with epitaxial growth of the ferromagnetic material can be used. For ex-

ample, in the MgO/Fe system, Vanadium is an underlayer that can be used. The thickness of this underlayer needs to be thick enough to allow for overetching the ferromagnetic slightly.

Chain Random Walk

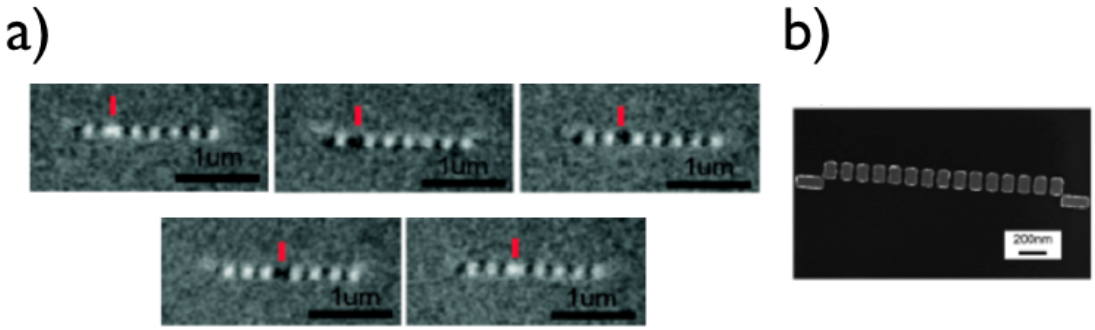

Figure 2.5: a) Time-lapse PEEM images showing a defect pair diffusing through a nanomagnet chain. The defect pair is highlighted with a red marker. b) an SEM micrograph shows a nanomagnet chain with logically opposite input nanomagnets on each end.

We fabricated an array of permalloy chains with varying nanomagnet aspect ratios in order to find an aspect ratio at which the random walk occurs at a measurable rate, i.e., neither too fast nor too slow for individual defect shifts to be captured by PEEM. The defect diffusion rate, which is governed by Arrhenius statistics, is an exponential function of nanomagnet aspect ratio and temperature. We varied these parameters to achieve a defect hopping time on the order of minutes. The nanomagnets in the array were patterned with standard electron beam lithography, electron beam evaporation and liftoff of permalloy. The nanomagnets in the array of chains were fabricated to be 80nm wide, 6nm thick, and with aspect ratios ranging from 1:1 to 2:1 stepped by 2nm. Each aspect ratio had a slightly different anisotropy energy, which in turn causes slightly different defect diffusion rates. The nanomagnet chains had two inputs, one at either end, set to oppose one another so that every chain contained at least one defect. This frustration between neighboring nanomagnets is similar to past work on artificial spin ice [30]. An SEM image of our test pattern is shown in Figure 2.5 b). We took magnetic contrast images of the sample in PEEM without applying a magnetic clocking field. To obtain time-lapse images, we first scanned the sample to find an aspect ratio at which we could observe defect diffusion and adjusted the substrate temperature to control the diffusion rate. Then, we took a time lapse series of 600 images at intervals of 25 seconds. In Figure 2.5 a), a subset of these images show the magnetization state of a nanomagnet chain in which a defect undergoes a random walk. Similar images taken of different nanomagnet aspect ratios indicate that the defect diffusion rate is strongly dependent on nanomagnet aspect ratio, as our model predicts.

Logic Gates

Using a similar approach, we demonstrate thermally driven combinatorial logic in a three-input nanomagnet majority logic gate [12]. In our experiment, three elongated nanomagnets serve as thermally stable inputs for the majority gate, while the remaining nanomagnets are sized to achieve defect diffusion. To show that the gate is able to compute the answer to different sets of inputs, we randomize the input bits by heating the system over its Curie point. We then reduce the system temperature back to the critical temperature at which the nanomagnets can perform random walks to find their ground state energy configuration. Note that this heating cycle is used only as an experimental technique to randomize the inputs. A real computing architecture would use some other means such as magnetic tunnel junctions, for example, to set the inputs for a new computation. The total energy dissipated to perform a computation would be the energy to set the magnetization state of these input nanomagnets. We use PEEM imaging to observe the final magnetization state of the gate and test for correct output behavior. This process is repeated so that many different input configurations can be applied to a single gate. In Figure 2.6 a)-c), we show PEEM images of the magnetization state of a majority logic gate before and after thermal cycling, all of which have computed the correct output for their random inputs.

2.1.4 Computing in Thermal Equilibrium

Unlike previous work demonstrating functional nanomagnet chains and majority logic gates, no magnetic clocking field was used in these experiments. This is a consequence of the fact that control of nanomagnet aspect ratio and temperature allows the critical field, Hc, to be tuned to any value, including Hc = 0. While this was done for experimental reasons, it implies that by designing the nanomagnets to have the proper energy barriers, nanomagnetic logic circuits can operate using only the ambient thermal energy with no clocking field necessary. This observation could help to overcome one of the key roadblocks to using nanomagnetic logic circuits in low-power applications: the energy required to generate the external magnetic clocking field.

This thermally-driven nanomagnetic logic scheme is closely related to the thermally activated computer, first proposed by Bennett as a path to performing computations near the fundamental limits of energy dissipation [31], [32], [33]. Bennett suggested several close analogs to thermally activated computation in nature, but to our knowledge no system capable of general-purpose logic with these properties has been demonstrated before.

One challenge facing logic architectures that rely on thermal energy alone is their slow speed of operation. Random walk travel times increase as the square of the number of nanomagnets in the chain, so long pipeline stages are not practical. This limitation can be partially addressed by using nanomagnetic logic devices in massively pipelined, segmented clocking architectures in which only a few nanomagnets are clocked at a time to increase throughput. Nanomagnets have been investigated for use in these architectures [34]. In the manner discussed by Bennett [32], [33], these segmented pipeline stages can be thought of as feeding energy into the system to impart a positive drift velocity to the otherwise random rate

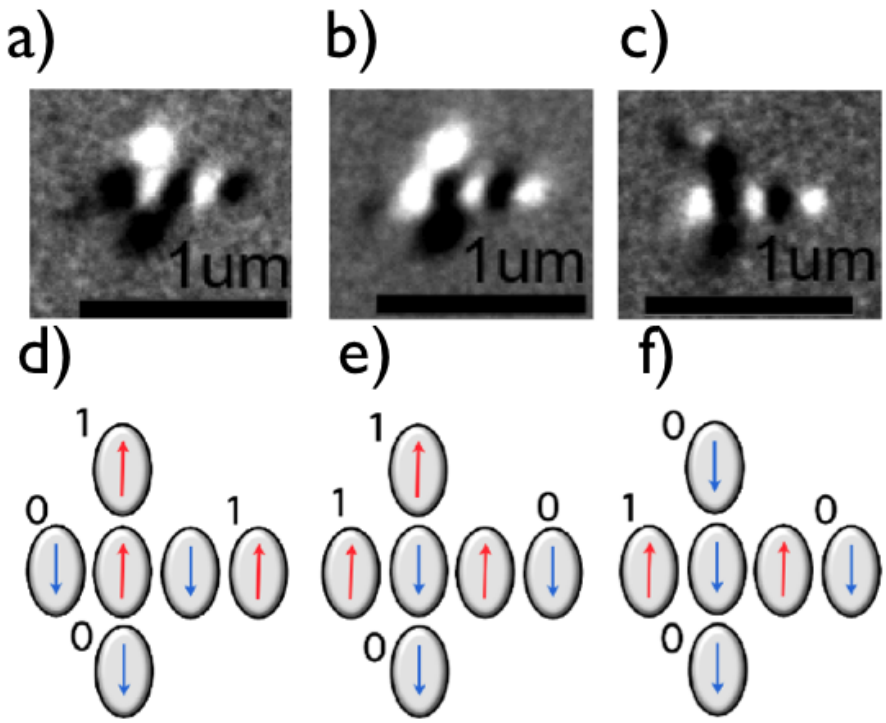

Figure 2.6: Thermal switching of a majority logic gate. a)-c), PEEM images show the final magnetization state of a single majority logic gate structure performing computations for several input combinations using only thermal energy. d)-f), Schematics show the direction each nanomagnet in the gate is magnetized. The nanomagnets were randomized by raising the temperature over the Curie point. As the gate is cooled through the critical point, random fluctuations allow the nanomagnets to find their correct ground state orientation containing the answer to the computation.

of progress. As discussed earlier, in the limit of long pipeline stages, nanomagnetic logic circuits relying on an adiabatically removed clocking field operate very similarly to circuits operating in thermal equilibrium with no external clock.

2.2 Errors and Reliabilty

In adiabatically clocked circuits (or circuits designed to operate in thermal equilibrium), the chains of nanomagnets do not always consistently align themselves in the ideal antiferromagnetic arrangement [12]. When two neighboring nanomagnets align themselves ferromagnetically instead of antiferromagnetically, they form a defect pair. These imperfections represent a corruption of the data transfer along the magnetic wire. An example of a nanomagnet chain containing ferromagnetically aligned defect pairs is shown in Figure 2.7. In this section, I will analyze defect rates and discuss a model that helps predict how errors form and in what numbers.

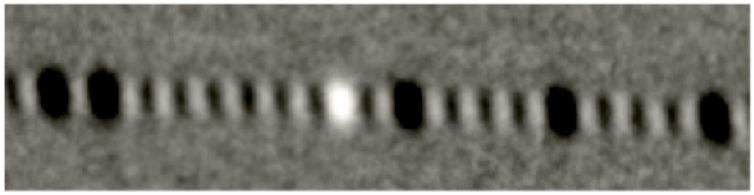

Figure 2.7: A PEEM contrast image showing a chain with ferromagnetically aligned defects in it.

2.2.1 Modeling Defect Rates

There are many potential sources of fabrication variation as well as thermal fluctuations that could lead to imperfections and corrupted signal transfer. However, it is desirable to have a simulation model that is as simple as possible yet can predict how errors form and in what numbers. Here we show that modeling the nanomagnets as single spins with an easy axis that deviates from the vertical axis by a Gaussian angular distribution gives good quantitative agreement with experiment and allows predictions to be made about how to improve circuit reliability.

The nanomagnets are modeled as single spins obeying the stochastic Landau-Lifshitz-Gilbert (LLG) equation [29] using the finite difference midpoint technique. Thermal fluctuations are included using a random field fluctuation model as discussed in Chapter 1. The magnets were given dimensions 120nmx80nmx10nm, an intra-island spacing of 30nm, and a saturation magnetization, Ms, of 800 kA/m. Imperfections were simulated by introducing a different random small angular deviation to each of the magnets′ easy axis alignment in the chain. Each nanomagnet in the chain received a different small angle rotation calculated using a Gaussian distribution with a standard deviation of 1-3 degrees. The temperature parameter was set to 300 K, and the hard axis clock field was applied and removed over the course of 10 ns. To study error rates, we look at how error rates change as the nanomagnet chains get longer. For each chain length, 100 simulations were done and the number of errors present were divided by the number of magnets in the chain to obtain a normalized per island error rate for each chain length. The results of the simulation are plotted in Figure 2.8 a). The results indicate that short chains of 1-2 nanomagnets can be quite reliable even with the angular rotations, however longer chains have an error rate of 7-8% per island.

2.2.2 Experimental Comparisons Supporting the Single Spin Model

To see how well this model agrees with experiment, arrays of permalloy nanomagnets with the same dimensions as simulated were fabricated using electron beam lithography, electron beam evaporation, and liftoff processing. The magnets were magnetized along their hard axes with an external magnetic field with magnitude 2000 Oe and then allowed to relax. We then counted the defects in the chains by imaging the magnetization state using PEEM. The arrays of chains that were fabricated had variable lengths just as in the simulations, and each chain length was repeated several hundred times for the purpose of gathering statistics on variation.

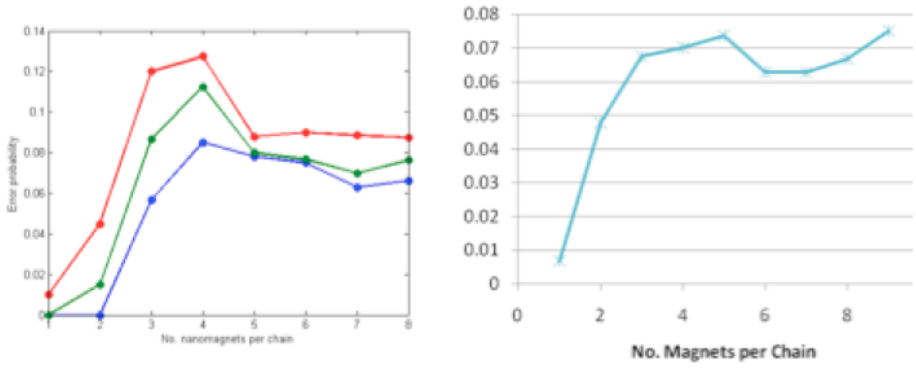

Figure 2.8: a) Per island error rate vs. nanomagnet chain length as predicted by stochastic LLG model with Gaussian angular deviation. b) Experimentally determined error rate as measured in PEEM for chains of permalloy nanomagnets.

The results are shown in Figure 2.8 b) and show very good agreement with the simple angular deviation model described above.

The model was also used to make predictions about the repeatability of errors in nanomagnet chains. The simulations predict that errors in nanomagnet chains are randomly distributed but repeatable. Resetting a single chain multiple times results in defect sites that are correlated from one cycle to the next. The areas along the chain that are error free after one reset are likely to be error free over and over again. Figure 2.9 a) shows a histogram of error frequency binned by location along a chain of nanomagnets with random angular rotation over the course of 100 clock/reset cycles.

To verify validity of the model‘s predictions we performed experiments with chains of permalloy nanomagnets fabricated in the same manner as discussed above. The chains were clocked multiple times with a magnetic field and the errors and their locations were tabulated. In Figure 2.9 b) we show the error frequency vs. location histogram for a chain that was clocked a total of 20 times. The sign of the magnetic field vector sets the direction of rotated nanomagnet on the far side of the chain and can be used to change the polarity of the antiferromagnetic alignment. The chain was clocked 10 times in the positive direction and 10 times in the negative direction. The results show the same correlated defect positioning predicted by the LLG simulations above.

2.2.3 Magnetic Force Microscopy Measurements

This study on error distribution during multiple clock cycles in nanomagnet chains was conducted with Magnetic Force Microscopy instead of PEEM because of the ability to easily reapply the external clocking field. While the basics of MFM were already discussed in the introductory chapter of this dissertation, there are several details specifically relevant to nanomagnetic logic circuits that I will now consider.

First, the amplitude that the cantilever is tuned to is an important parameter in MFM.

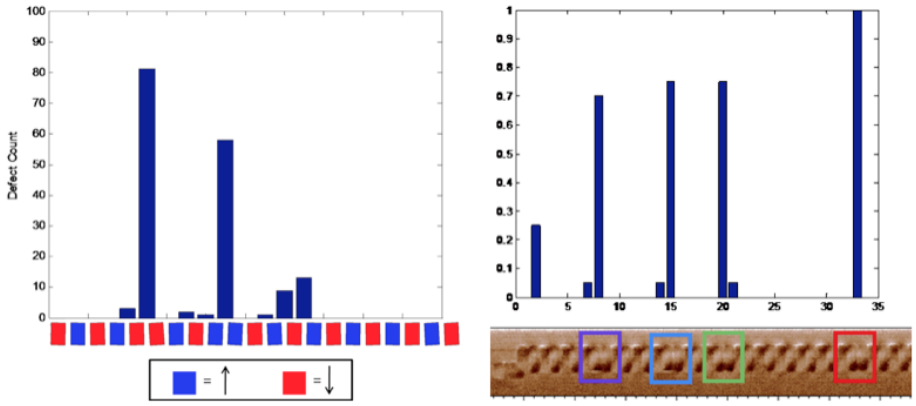

Figure 2.9: a) Histogram showing defect locations in a single chain clocked many times simulated with Gaussian angular deviation in each nanomagnet. b) Histogram of defects locations in a permalloy nanomagnet chain clocked many times and measured with Magnetic Force Microscopy.

Signal-to-noise goes up with increasing amplitude, but sensitivity can be degraded when sensing the shorter range magnetic forces of interest in MFM. For large amplitudes, the cantilever spends a greater portion of its time far away from the surface (during the backswing) where there are no magnetic fields present. This is schematically shown in Figure 2.10. For MFM measurements, this tradeoff favors smaller cantilever amplitudes than would be used for conventional AFM. The default amplitude on the Asylum Atomic Force Microscope uses a cantilever amplitude of 2 V. However, for MFM mode, 200 mV was found to give the increased sensitivity needed to detect the relatively weak signal. At 200 mV the amplitude in nm of the cantilever was measured to be approximately 50 nm. This is only an estimate as the cantilever amplitude voltage to nm ratio can vary based on the condition of the tip and laser alignment.

The sensitivity of any MFM measurement is proportional to the field strengths leaving the magnetic material under measurement. As the nanomagnets are scaled and become thinner, this field strength will gradually be reduced making it more difficult to obtain magnetic contrast. One option for increasing sensitivity that was explored for this project and that may become necessary in the future is doing the measurements in a low pressure environment. At $10^{-}2$ Torr, signal-to-noise ratio is known to be more than 10 times better. Vacuum systems are readily commercially available and should considered if the need for higher sensitivity MFM arises.

Another important MFM technique is the compensation of Electrostatic forces. In any MFM measurement, the cantilever is affected by both magnetic as well as electric forces. Minimizing these electric forces is critical for obtaining a reliable image. One way that electrical forces cause problems and can even come to dominate the signal is if there is a surface potential on the substrate. A potential difference between the grounded cantilever and the surface of less than 1 Volt is enough to drown out the weak magnetic forces. To avoid these forces, it is desirable to perform a standard measurement of the surface potential using force

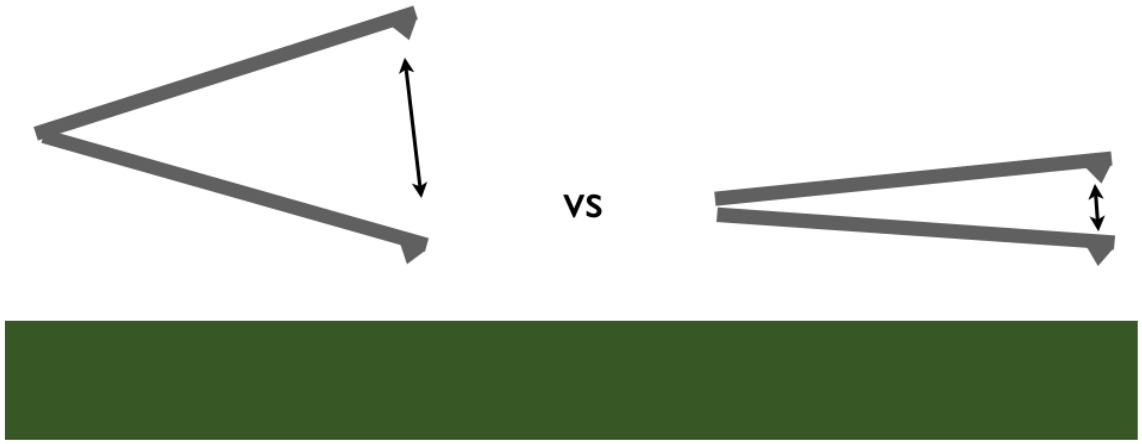

Figure 2.10: A schematic comparing the distance a cantilever is from the surface being measured for different amplitudes. For larger amplitudes, the cantilever is far away from the surface during the backswing and will not sense the short range magnetic fields during this period.

measurements and electric tuning in AFM mode. Once done, a compensating Voltage can be applied to the cantilever during measurement to mitigate these electric forces. A schematic showing the cantilever's interaction with the surface in the presence of an uncompensated surface potential is shown in Figure 2.11

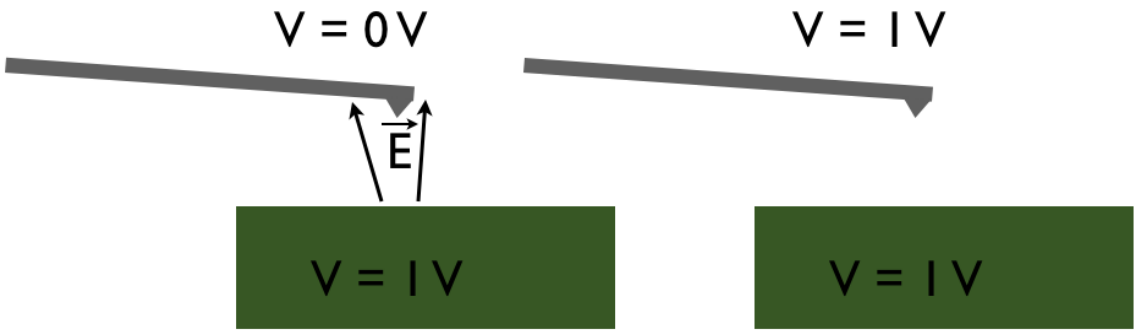

Figure 2.11: A schematic comparing the interaction the cantilever has with the surface when it is uncompensated/compensated for the surface potential.

The choice of the magnetic tip, a highly application specific variable, can also be important for getting good magnetic contrast. MFM tips are characterized by the radius of the tip as well as the type of magnetic material that it is coated with. As with most engineering decisions, tradeoffs are involved. A smaller radius tip has the ability to give higher resolution images because it senses magnetic forces in a smaller area. However, it is often less sensitive because to obtain the smallest tip radii, the magnetic coatings often have to be made very

thin. When troubleshooting a weak or absent signal in samples that have high frequency oscillating patterns such as the ones in nanomagnet chains (very quick changes between dark and light), it is not always clear whether the problem is a lack of resolution or sensitivity. For this reason it's important to explore many tips. The type of magnetic material can also be important. One can purchase commercially tips that are coated with magnetic material that is high moment or low moment, high coercivity or low coercivity, etc. The effectiveness of these coatings will depend on the material being imaged. A tip with a higher moment may have higher sensitivity, but it has the potential to interact with the magnetic material under inspection. Choosing the correct tip is a trial-and-error process and is not an exact science. Many commercial tip vendors sell small "variety packs" of magnetic tips to allow for more economical experimentation. The tips used in these experiments that were found to have the best contrast were "High Coercivity" made by Asylum Research, Inc.

Lastly, measuring the defect rates in the nanomagnet chains over the course of many magnetic "clock" cycles, requires the ability to perform MFM measurements of the same area after many applications of an external field. To perform this experiment, we used a specialized magnetic stage manufactured by Asylum. This "Variable Field Module", allowed us to apply in-plane magnetic fields with an amplitude of up to +-2500 Oe with a resolution of +-1 Oe. The magnetic field is controlled by aligning a motorized magnet with a soft Fe yoke. Figure 2.12 shows the Variable Field Module along with schematics of the magnet in its high and low field configurations.

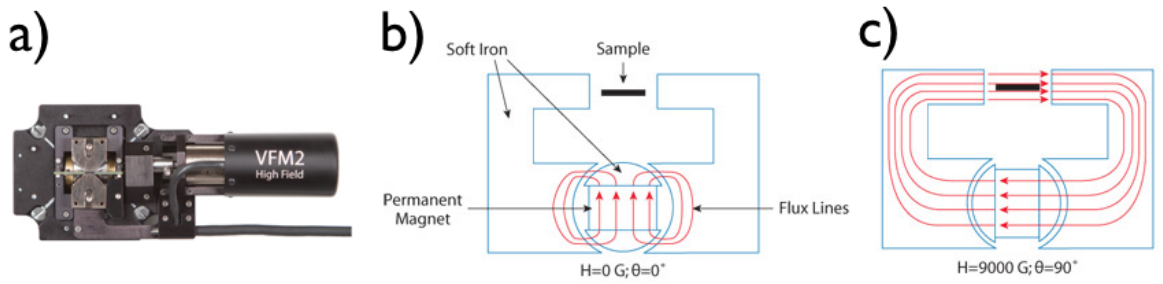

Figure 2.12: a) A photo of the Asylum, Inc. Variable Field Module. The magnetic field is controlled by aligning a motorized magnet with a soft Fe yoke. b) A schematic showing the field module in its low field configuration. c) A schematic showing the field module in its high field configuration. Image attribution: [35]

2.2.4 Single Spin Model Predictions and Experiment

As was discussed earlier, the dynamics by which these nanomagnet chains reach their ground state is a complicated stochastic process governed by random walks. However, the simple "angular rotation" model that we have developed can inform the degree of process control required to achieve reliable operation. To determine sensitivity to angular misalignment we simulated a chain of nanomagnets with perfect alignment with the exception of a single nanomagnet in the middle whose angular misalignment was swept as a parameter. For each angle, 100 simulations were run with the temperature parameter at 300K. The plot in Figure 2.13

shows the error rates for nanomagnets with an Ms of 800 kA/m, 1200 kA/m, and 1600 kA/m. The figure shows that nanomagnet chains in their current form are very sensitive to angular misalignment of the easy axis of even 1 degree.

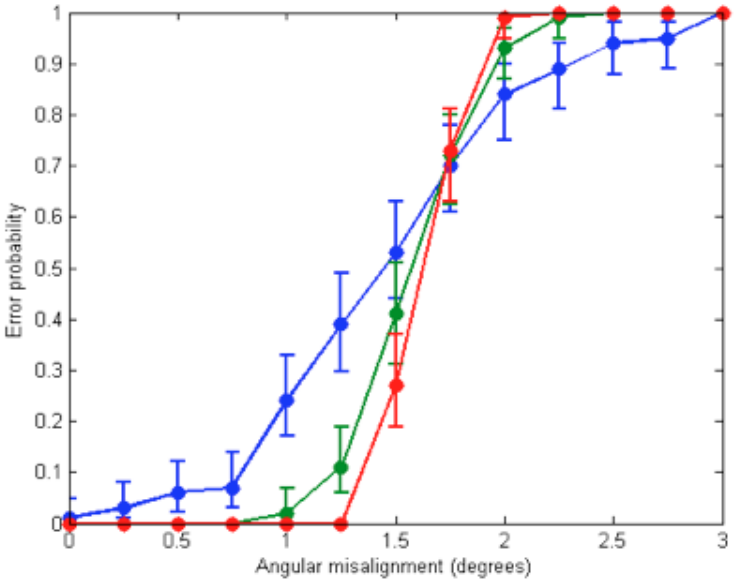

Figure 2.13: A plot measuring the error probability in an otherwise ideal chain of 7 nanomagnets with a single nanomagnet in the middle whose magnetic easy axis is treated as a variable.

Process variation can lead to numerous types of irregularities and nonuniformities in nanomagnet chains, but this model's agreement with experiment suggests that nanomagnet easy axis alignment may be a fundamental cause of errors in nanomagnet chains. In particular, lithographic variation can result in nonuniformities in the shape of a patterned nanomagnet that can result in a deviation of the desired easy axis direction. Factors other than edge roughness can contribute to variations in the direction of a nanomagnets easy axis, however, permalloy's lack of other anisotropies make measuring the contribution of this factor an important part of characterizing this non-ideality. To quantify the effect of nanomagnet edge roughness on easy axis angle deviation, we imaged a large number of permalloy nanomagnets with high resolution scanning electron microscopy (SEM) and used edge detection software to extract the as-patterned nanomagnet profile. We then used these shapes as the input to a micromagnetic simulation and extracted the total magnetostatic energy as a function of magnetization angle as in [36]. We repeated this process for many nanomagnets and plotted the easy axis deviations as a histogram shown in Figure 2.14 the histogram shows the patterned nanomagnets in this study have easy axis rotations with a standard deviation of 3.75 degrees.

The results in Figure 2.13 indicate that nanomagnet chains fabricated with current fabrication techniques are sensitive to even 1 degree of easy axis misalignment. On the other hand, the results, particularly those in Figure 2.9 showing the repeatability of errors, support the hypothesis that errors are process related and not fundamental to the reset process. However,

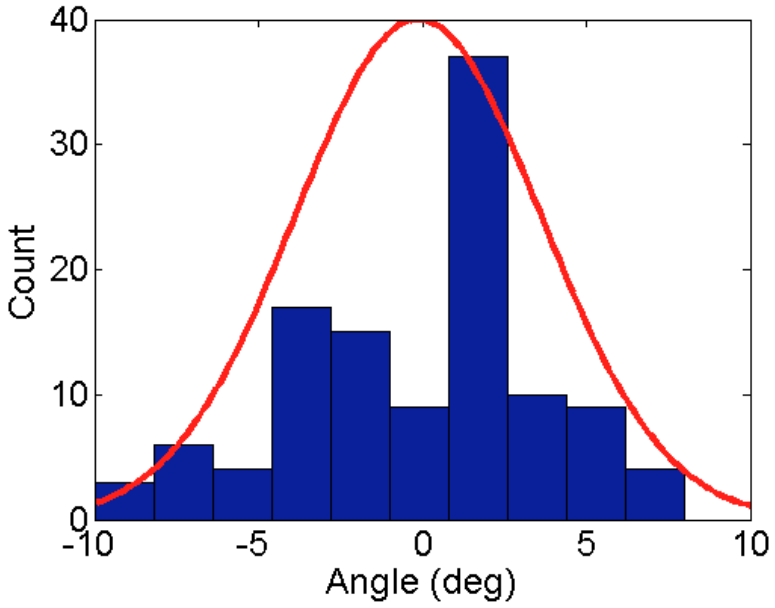

Figure 2.14: A histogram of easy axis angular deviation in nanomagnets with edge noise extracted from fabricated nanomagnets and calculated with micromagnetic simulations.

increasing this error threshold will be critical to making this technology viable.

The error probability vs. angular deviation curves for different magnetic moments in Figure 2.13 show the importance of increasing the coupling between neighboring nanomagnets. When the nanomagnets have a larger magnetic moment, they are able to tolerate greater angular deviations of their easy axis. Decreasing nanomagnet separation distance and increasing nanomagnet thickness (volume) are all ways of raising the intra-island coupling.

The histogram showing angular deviation resulting from edge noise in Figure 2.14 suggests another possible path to improving nanomagnet error robustness. The shapes of the nanomagnets in this study were uniform rectangles, but this is not a necessary condition for the signal propagation to occur. Future work is needed to determine whether it is possible to engineer a shape that is more robust to shifts in easy axis misalignment in the presence of edge noise.

Lastly, nanomagnet architectures have been proposed that use biaxial anisotropy to stabilize the magnetization of the nanomagnets along their hard axes in the presence of thermal noise. This results in fundamentally different signal propagation dynamics. Because the propagation dynamics are so different, the robustness results of this study are not applicable to architectures using this type of anisotropy engineering, and future work targeting this architecture is necessary to determine its sensitivity to lithographic noise [37].

2.3 Summary

In this chapter, I closely analyzed the operating characteristics, function, and reliability of a nanomagnetic logic system in the adiabatic or "slow clocked" mode. The dynamics in this mode were demonstrated theoretically and then experimentally to occur via a random walk. A reliability study was carried out to investigate the cause and frequency of errors that corrupt the signal propagation. A model was developed that showed strong evidence for the theory that a dominant cause of errors is a small effective rotation of the easy axis of the nanomagnets along the chain. The addition of nanomagnet rotation to simulation model's of signal propagation in chains introduces errors that correlate very strongly in both number and distribution found experimentally.

Chapter 3

The Biaxial Mode

Contents

The reliability, error rates, and speed of adiabatically clocked nanomagnet chains discussed in the previous chapter show that there remain many challenges to making a practical computing device based on nanomagnets. In the adiabatic mode discussed in the previous chapter, the circuit is performing computations through annealing with random walks – a mechanism that is unlikely to be of practical use in the near future. In this chapter, I investigate ways of altering the signal propagation mechanism in nanomagnet chains so that the dynamics occur in a non-stochastic, well-defined fashion.

In adiabatic architectures, a slow removal of the clock is required to allow the nanomagnet chain to "find" its ground state energy via a thermally induced random walk process. One very different signal propagation mechanism that has been envisioned is one in which the clock is instead removed quickly, and the information contained in the input nanomagnet propagates from nearest neighbor to nearest neighbor one nanomagnet at a time as a cascade. A schematic showing the difference between these two propagation mechanisms is shown in Figure 3.1.

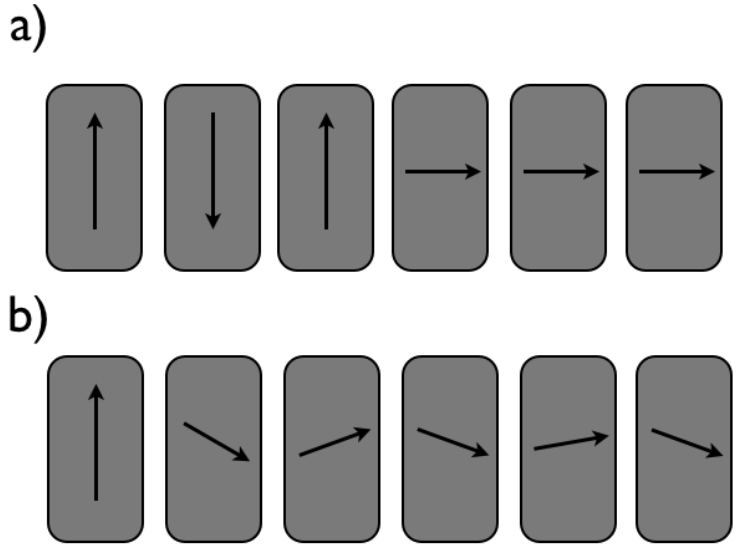

Figure 3.1: a) A schematic of a nanomagnet chain in which the signal is propagating one nanomagnet at a time as a cascade. The nanomagnets further down the chain remain magnetized along their hard axes until the signal has reached them. b) A schematic of a nanomagnet chain in which the signal is propagating in the adiabatic mode. Every nanomagnet in the chain is rotating simultaneously into the ground state. Defects present (not shown), would be annealed out of the chain as a random walk.

3.1 Magnetic Energy Landscape Engineering

In order for the signal to propagate as a cascade, the nanomagnets further down the chain must remain magnetized along their hard axes until the signal can reach it. However, the energy landscape of a nanomagnet with only uniaxial shape anisotropy make this unlikely to occur. The hard axis of a nanomagnet with uniaxial anisotropy, in addition to being an energy maxima, is an unstable equilibrium. Any stray field or thermal fluctuation can cause a nanomagnet with only uniaxial anisotorpy to quickly choose an easy axis direction to fall into well before the signal has reached it. A mechanism to achieve some hard axis stability is needed to keep the nanomagnets aligned along their hard axes during signal propagation.

Here I introduce the concept of enhancing hard axis stability by adding a biaxial anisotropy term to the net magnetization energy of each nanomagnet. Experimentally, biaxial anisotropy can be added to each nanomagnet by patterning them from an epitaxial film known to exhibit cubic anisotropy (e.g., fcc Co epitaxially grown on single crystal Cu(100) substrates) [38], or through other means such as shape, or strain [39]. With the introduction of the biaxial anisotropy, the magnetostatic energy landscape becomes:

$$U(\theta) = K_u cos^2(\theta) + \frac{K_1}{4} sin^2(2\theta) \tag{3.1}$$

where K_1 is the biaxial anisotropy constant and the biaxial and uniaxial anisotropy axes are coincident. In this single domain picture, the biaxial term reduces or even inverts the

curvature of U(θ) at θ = 0°, thereby enhancing hard axis stability. For our simulations we use OOMMF and use a cell size of 5 nm^3, saturation magnetization (for Co) Ms = 106 A/m, and exchange stiffness A = $1.3 \times 10^{-}11$ J/m. U(θ) plots are generated for a 100 nm x 50 nm rectangle (with 10 nm x 10 nm squares removed from each corner) by first saturating the magnetization at an angle θ, then removing the saturation field, and returning the total energy 0.1 ps later. For all nanomagnet dimensions studied in this work, reversal is observed to be domain wall-dominated, likely due to the highly nonuniform dipole fields that drive the signal propagation, but the U(θ) plots for nanomagnets coerced to be single domain illustrate the stabilizing effect of the biaxial anisotropy. We plot U(θ) for K_1 = 0, 30, and 60 kJ/m^3 in Figure 3.2. Fitting Equation (3.1) to each curve reliably yields K_u = 34 kJ/m^3.

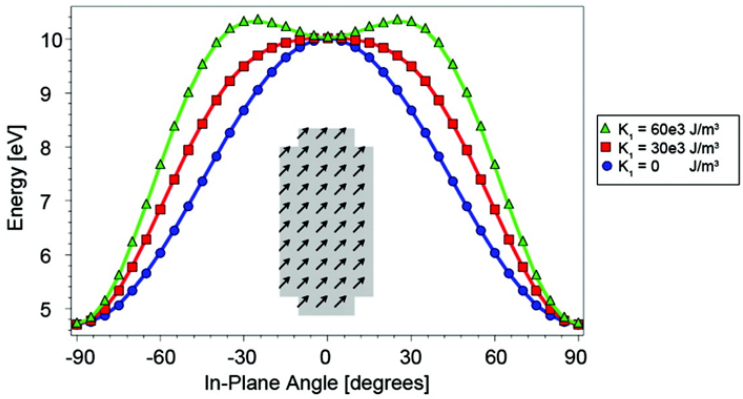

Figure 3.2: Magnetic energy U(θ), from OOMMF simulations of the nanomagnet shown in the inset (at θ = 45°), for K1 = 0, 30, and 60 kJ/m^3. The biaxial anisotropy term alters the curvature of the U(θ) plot near θ = 0°, making that point (hard axis) more stable.

Because the nanomagnets in the chain have a metastable point along their hard axis, they no longer all fall uniformly into their ground state as the clock is removed. Instead the dynamics are characterized by a cascade in which one nanomagnet falls over at a time. As each nanomagnet falls over from its metastable hard axis to easy axis, its dipole field rotates to tip the next nanomagnet in the chain. Micromagnetic simulations were carried out at T = 300 K to compare the dynamics of chains with and without biaxial anisotropy. Temperature dependence in the micromagnetic simulations is implemented in the manner discussed in Chapter 1.

For comparison, the dynamics of a chain of uniaxial only nanomagnets are shown in Figure 3.4. Nanomagnets with only uniaxial anisotropy all fall into place simultaneously after the clock has been removed, and the result is many errors. The clock is removed instantly in both these simulations. If the clock had been removed adiabatically over the course of several nanoseconds, the random walk dynamics discussed in the previous chapter would have been observed.

To quantitatively explore the impact of K_1, we simulate a horizontal wire of 15 rectangular Co nanomagnets and visualize the success of the cascade propagation as a function

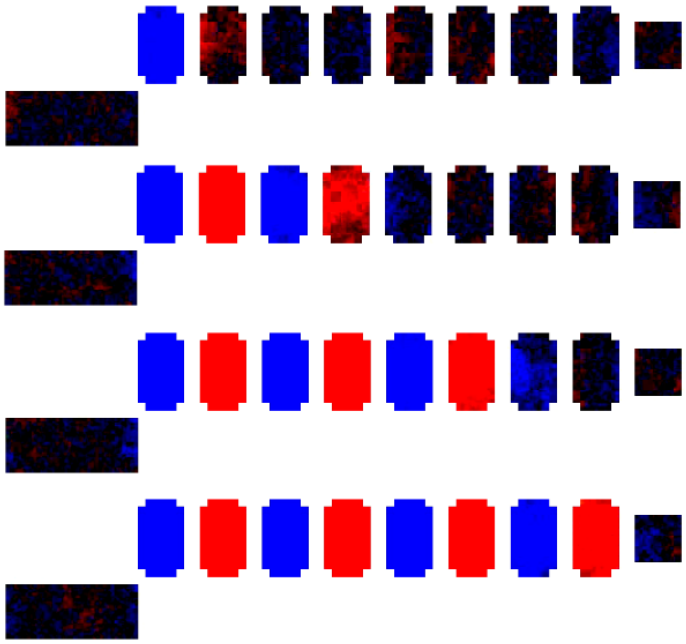

Figure 3.3: Simulated wires of eight nanomagnets at T = 300 K with a biaxial anisotropy term K_1 = 50 kJ/m^3. The dynamics show a cascade along the chain with one nanomagnet flipping after the other. The nanomagnets further down the chain remain magnetized along their metastable hard axes until the cascade reaches them.

of nanomagnet length, width. Nanomagnet thickness and separation were held constant at 5nm and 20nm respectively. The results of the parameter space study are shown in a Shmoo parameter space plot [40]. Total length of the simulations was 3 ns. Shown in Figure 3.5, the Shmoo plot consists of three distinct regions, identified by their x-y plane coloring: light gray, where logic propagation fails due to incorrect switching of nanomagnets whose aspect ratios (length:width) are too large, rendering them unstable; dark gray, where logic does not propagate within the 3 ns simulation time because the nanomagnets are too stable (aspect ratios are too small); and white, where logic propagation is successful within 3 ns. The wedge of parameter space with successful logic propagation (white region) demonstrates a working range of nanomagnet aspect ratios and shows that scaling nanomagnet dimensions into the sub-50 nm dimension regime is possible.

Signal fanout and arbitrary routing of the logic is also necessary, which requires junctions of vertical and horizontal wires where the logic signal must branch out and form copies of itself. Vertical wires, where the nanomagnets are stacked with their short axes abutting one another, in addition to horizontal wires are necessary for realizing a general nanomagnetic interconnect scheme. Logic propagation along a vertical wire is also initiated by aligning all the moments along their hard axes, where they must remain until the logic cascade arrives and reorients them to all align parallel, up or down. Unlike horizontal wires, nearest neighbor dipole fields in vertical wires oppose the magnetization direction and thereby hinder hard axis stability. For values of K_1 that stabilize horizontal wires, the added biaxial anisotropy is

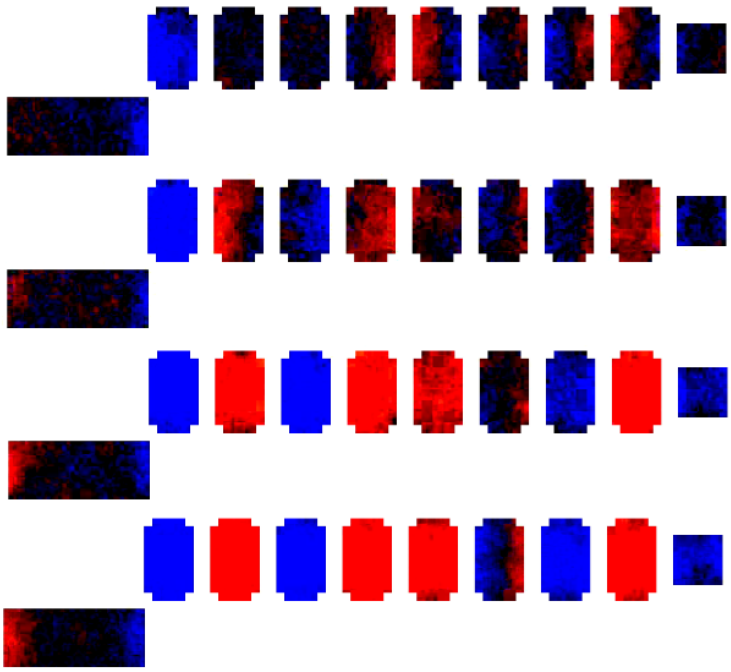

Figure 3.4: Simulated wires of eight nanomagnets at T = 300 K with no biaxial anisotropy. The dynamics show that without the hard axis stability provided by the biaxial anisotropy all the nanomagnets fall at once.

insufficient to ensure successful logic propagation in vertical wires. A solution to this nearest-neighbor-induced instability is to place square stabilizer nanomagnets to the left and right of each nanomagnet in the vertical wire. The external field of these stabilizing nanomagnets provides an additional Zeeman energy term to the nanomagnet that they surround that acts to keep this central nanomagnet magnetized along its hard axis until the signal reaches it. With their magnetization directions set by H_{ext}, dipole fields from the stabilizers compensate for those from the nearest neighbors, and because of their shape, shape-induced anisotropy is minimal. The biaxial anisotropy, in conjunction with their large moment, makes them relatively impervious to stray dipole fields from the nanomagnetic wires. A time series of key frames in a micromagnetic simulation showing signal propagation in a corner junction is shown in Figure 3.6.

These vertical wires can be generalized to demonstrate fanout. Figure 3.7 has the results of a micromagnetic simulation showing how the addition of biaxial anisotropy in conjunction with the stabilizer nanomagnets makes it possible to send a signal over long distances and create copies of itself.

Dynamics of the cascade are controlled by the hard-to-easy axis relaxation rate of individual nanomagnets and the strength of the dipolar coupling between them. Because of this, logic propagation times will be considerably longer than electrical signals in conventional electronic interconnects. Propagation times from the simulations shown in Figure 3.5 are

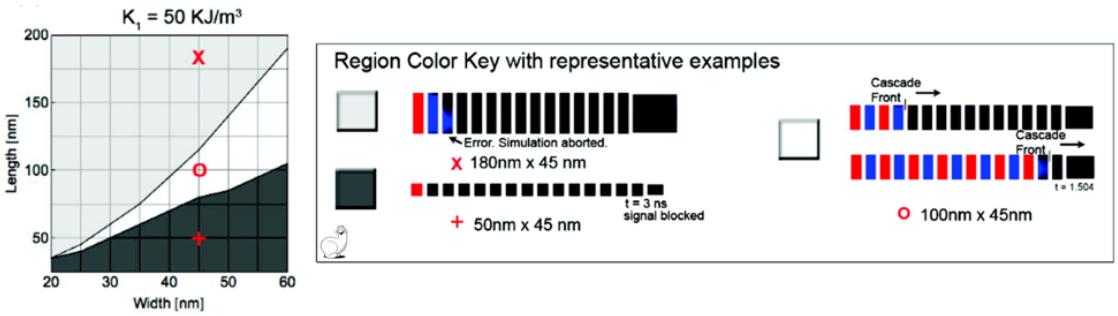

Figure 3.5: A Shmoo plot showing whether the signal propagates successfully as a function of nanomagnet length and width. The nanomagnets have a biaxial anisotropy constant K_1 = 50 kJ/m^3. White wedge-shaped area indicates regions of parameter space for which the signal propagates correctly with all nanomagnets flipping in the correct order within the 3 ns simulation time. Grey areas are where signal propagation was unsuccessful. Failure mechanisms are explained in the main text. False positives, where an instability along the wire led fortuitously to proper alignment of the magnetizations, are accounted for in the analysis.

1-2 ns for 15 nanomagnets, or 100 ps per nanomagnet. Energy dissipation, which comes from viscous damping forces during magnetization reversal, is estimated in our simulations for nanomagnets of several different sizes. Our choice of initial conditions, where all nanomagnets begin uniformly magnetized to the right, is equivalent to H_{ext} being instantaneously removed at time = 0. This means that an upper bound for the energy dissipation for our simulations can be approximated by the single domain nanomagnet energy barrier arising from the uniaxial shape anisotropy term of its energy landscape. Because this estimation uses the entire energy barrier, it should be considered a worst-case value for the dissipation. If the nanomagnets were instead engineered to relax adiabatically at a time scale much larger than the magnetization relaxation time, energy dissipation can be reduced significantly [14]. For a nanomagnet of dimensions 100 nm x 50 nm x 5 nm, a barrier of 5.3 eV is found directly from Figure 3.2 and scales with both the volume as well as aspect ratio of the nanomagnets.

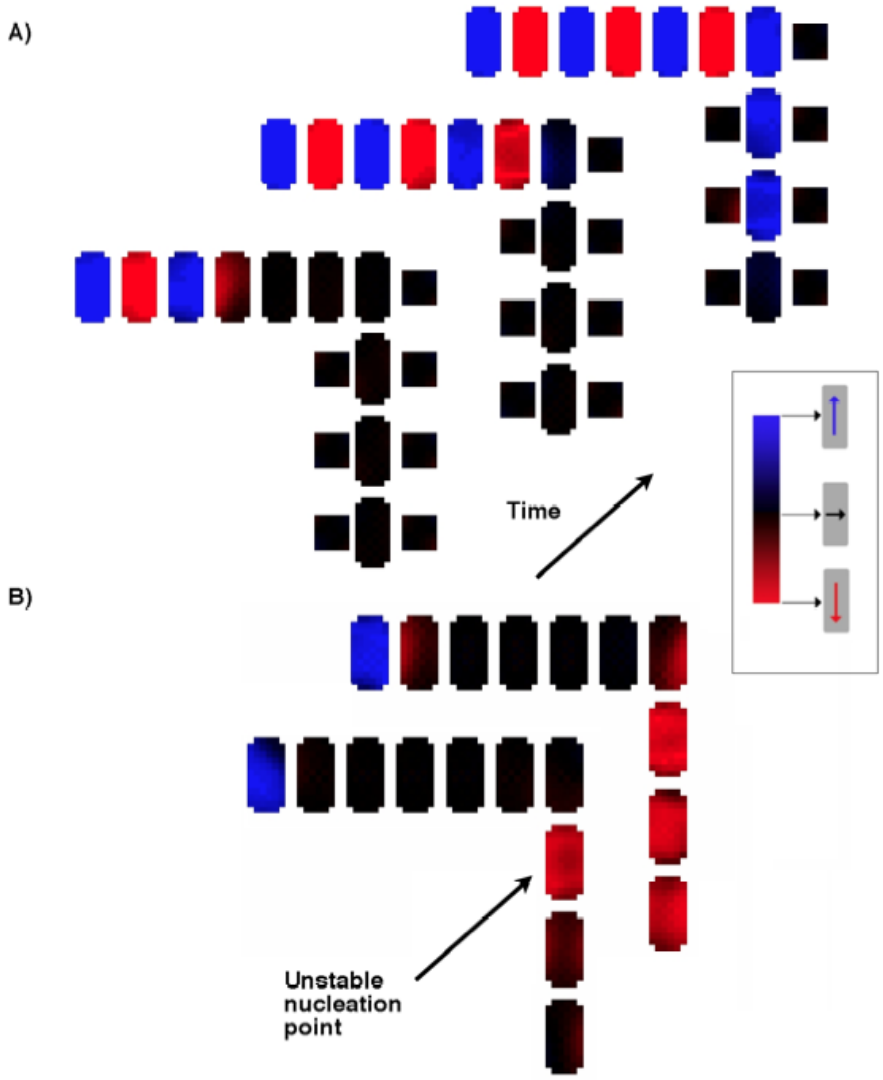

Figure 3.6: A right angle junction between the incoming signal (horizontal) and outgoing (vertical) wire, where the latter is simulated both with a) and without b) square stabilizers. Without stabilizing elements surrounding the nanomagnets in the vertical segments of the wires, the moments do not remain metastable long enough for the signal to reach them.

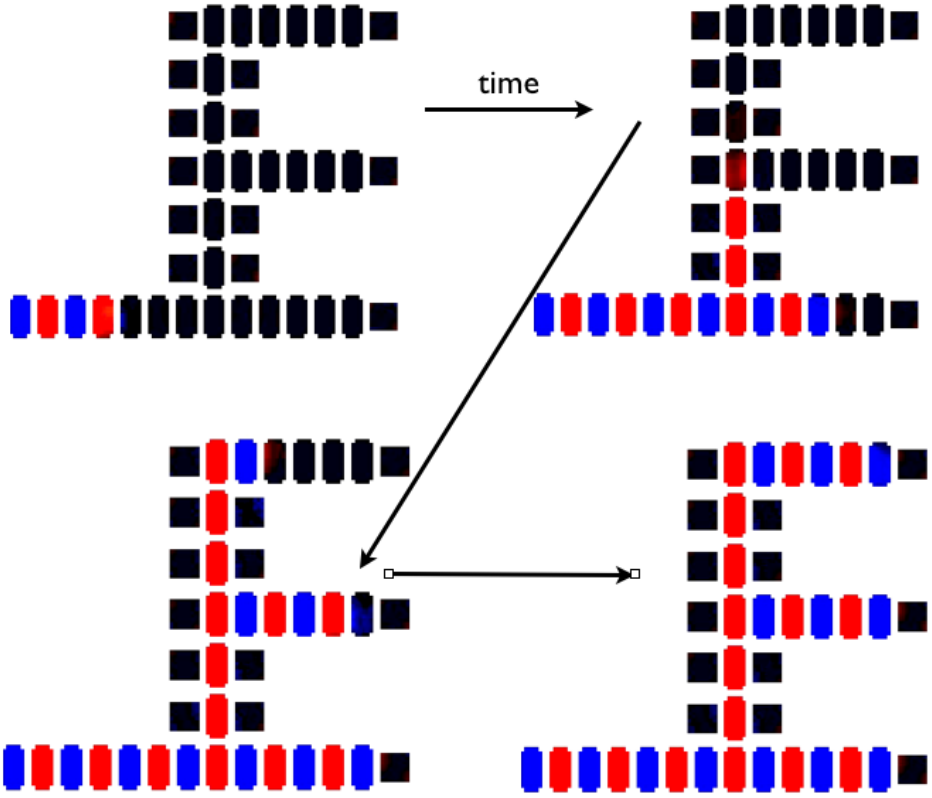

Figure 3.7: The results of a micromagnetic simulation showing how the addition of biaxial anisotropy in conjunction with the stabilizer nanomagnets makes it possible to send a signal over long distances and create copies of itself.

3.2 Grid Sizing Considerations for Micromagnetic Modeling

In Finite Element Modeling (FEM), the size of the grid is an important parameter to consider when attempting to model a physical system [41]. The more grid points that are used in the simulation, the more accurate, but the longer it will take. To understand quantitatively the tradeoff between simulation time and accuracy, we study how the measured rate of signal propagation in a coupled chain of nanomagnets is affected by grid size. If the cell size is not chosen to be dense enough, then the propagation time, t_{prop}, will be a function of the cell size. This is undesirable because it means the same physical system is giving a result that is dependent on a nonphysical simulation parameter. The optimal choice of the grid element length, L_g, should be chosen such that the derivative of $\frac{dt_{prop}}{dL_g}$ is approximately 0. The proper cell size choice is also expected to be a function of the dimensions of the nanomagnets that are being modeled.

Micromagnetic simulations of the propagation in a chain of nanomagnets were carried out with grid sizes ranging from 1nm to 10nm. The chains were 15 nanomagnets in length, and the time for the cascade to reach the end of the chain was recorded for each simulation. To test for size affects, chains with nanomagnets with dimensions 30 nm x 60 nm and 50nm x 100 nm were chosen. The results of the simulations are plotted in Figure 3.8.

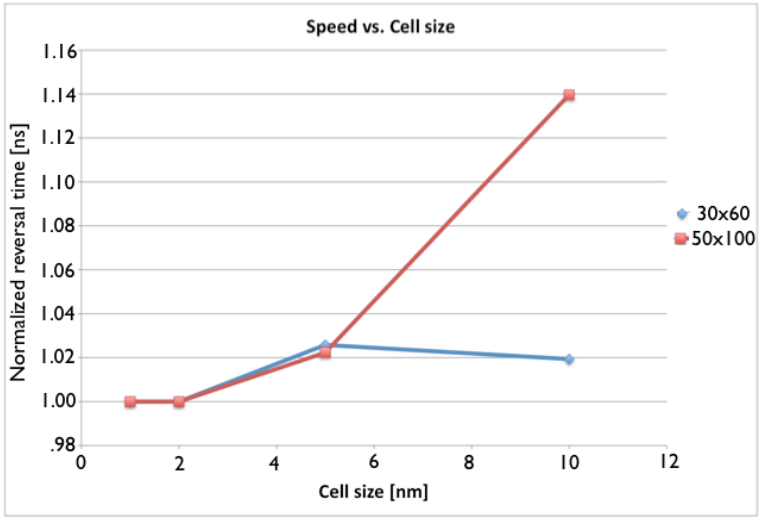

Figure 3.8: A plot showing the normalized propagation times in 2 chains of 15 nanomagnets as a function of grid size. As the grid size is shrunk, the propagation times converge. The grid size should be chosen to be the largest value that still gives good convergence to this quantity. For the majority of the simulations in this dissertation, a grid size of 5 nm was chosen as it gives the best tradeoff between speed and accuracy.

Intuitively one might suppose that the smaller the nanomagnets being simulated, the smaller the grid size would be required to obtain convergent simulation results. This turns out to be wrong. The likely reason is that the smaller the nanomagnets, the more close they are

to being truly single domains. A true single domain nanomagnet can be modeled as a single spin which is equivalent to 1 grid point. The larger 50 nm x 100 nm actually end up requiring smaller grid sizes to obtain good results. Their larger size means that the exchange force is not completely dominant and more information is needed to accurately model nonuniformities of spins near the edges of the structures. When a grid size of 5 nm is chosen for these larger nanomagnets, the simulation is within 2% of the nominally correct value (which is taken to be the propagation time at the smallest grid point simulated after convergence to this value has occurred).

The difference in simulation times when a smaller grid size is chosen can be dramatic. The number of calculations per time step goes as the square of the grid so a 10nm grid size is expected to be approximately 100 times faster per time step than a comparable simulation using a 1nm grid spacing. However, the effect is actually much larger than this in practice. OOMMF solves the LLG equation through an iterative method that uses a variable time step chosen to minimize simulation error. For larger grid sizes of 10nm, the time step chosen by the solver can be 100's of times larger than when a grid size of 1nm is chosen. These combined effects can thus change the simulation time by 4 orders of magnitude or more making even small scale calculations impractical. Taking these factors into account, a grid size of 5nm has been chosen for the majority of the simulations in this dissertation unless otherwise stated.

3.3 Biaxial Anisotropy Experiments

In the previous section, I showed that engineering biaxial anisotropy into a nanomagnet's energy landscape is important for achieving reliable circuit operation when the clocking field is removed rapidly. Biaxial anisotropy can potentially be integrated into the energy landscape of nanomagnets in various ways: shape, strain, etc. However, this dissertation will focus on the use of magnetocrystalline anisotropy with single crystal epitaxially grown thin films.

3.3.1 Fabrication of Single Crystal Nanomagets with Magnetocrystalline Biaxial Anisotropy

Magnetocrystalline anisotropy is the result of spin-orbit interactions. In single crystals these spin-orbit interactions result in preferred magnetization axes along specific crystallographic symmetries. Cubic crystals have a cubic symmetry resulting in 3 easy axes (two in-plane, one out-of-plane). In a thin film, the shape anisotropy resulting from the thickness of the film forces the magnetization vector in-plane removing the out-of-plane easy axis. This results in 2 preferred magnetization axes, and this "bi"-axial anisotropy is precisely the anisotropy needed to stabilize the hard axis of a nanomagnet with uniaxial shape anisotropy.

Magnetocrystalline anisotropy can also result in uniaxial anisotropy. A common misconception is that a properly tuned uniaxial anisotropy along the shape induced hard axis of a nanomagnet could also be used for stabilization purposes. This is not the case, however. The energy landscape of biaxial + uniaxial anisotropies shown in Equation (3.1) results in a

metastable region along the hard axis shown in Figure 3.2. Adding two perpendicular uniaxial contributions together, however, gives Equation (3.2). Simple trigonometric manipulation of the two uniaxial terms results in uniaxial anisotropy with a shift in the easy axis and cannot be used to induce biaxial behavior.

$$U(\theta) = K_{u(shape)}cos^2(\theta) + \frac{K_{u(crystalline)}}{4}cos^2(\theta - 90) = K_{u(effective)}cos^2(\theta - \delta) \quad (3.2)$$

3.3.2 Fabrication Techniques

Fabrication of single crystal nanomagnets is nontrivial. In this section, I will discuss the methods and techniques by which the nanomagnets were fabricated.

Molecular Beam Epitaxy

Single crystal magnetic films were grown with Molecular Beam Epitaxy (MBE) [42]. In MBE, the desired material is heated until it evaporates and condenses onto the substrate upon which it is being deposited. It is in many ways similar to conventional evaporation deposition techniques, but with some very important differences. First, in order for a single crystal film of the deposited material to form, the substrate on which it is being deposited must be chosen very carefully. The substrate must form a template or seed for the crystal to grow from so it must have a similar lattice constant a_0. Cleanliness is also very important, so the deposition must be done at very high vacuum and the surface of the substrate must be very clean and polished to be nearly atomically flat. The rate of deposition must also be very slow to allow for the deposited atoms to diffuse into the favored crystallographic locations. The substrate is often heated to facilitate this diffusion. If any of these parameters are not met, the deposited material will be polycrystalline, and the desired magnetic properties will be lost. A schematic for an MBE chamber is shown in Figure 3.9.

Patterning

Once the film has been deposited, it is necessary to pattern it into the desired nanomagnet shape. This is achieved by etching away the magnetic material using ion milling. Ion milling etches material by accelerating charged Argon ions through an electric field against the surface that is being etched. The high energy Ar ions physically sputter atoms away causing the material to be etched. Because the process is physical, it works on all materials and is ideal for patterning hard to etch metals that do not have reliable chemical or reactive ion etching techniques [44]. A schematic showing the inside of an ion mill chamber is shown in Figure 3.10.

The sputtering relies on being able to transfer the energy from the incident ions to atoms on the surface to be etched. To first order, the efficiency of the energy transfer is related to the mass of the etching ion species (M_1) and the mass of the atoms being etched (M_2) [44]:

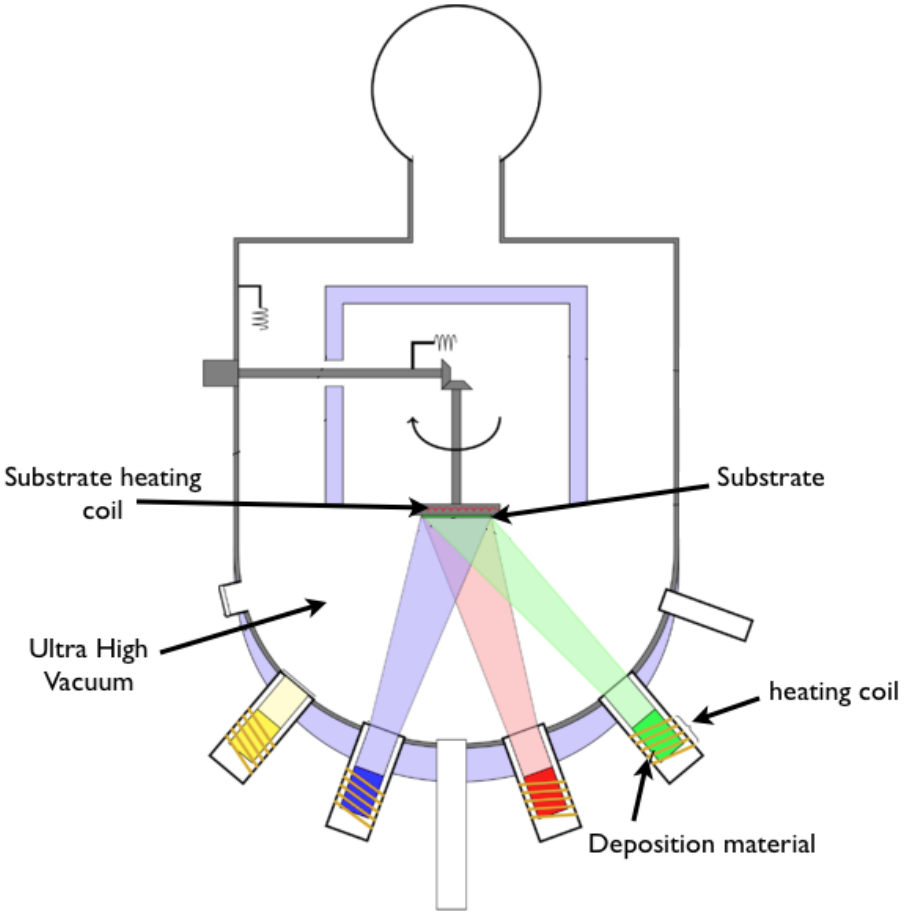

Figure 3.9: A schematic for the inside of an MBE chamber. A single crystal substrate is heated in ultra high vacuum, and a compatible material is slowly evaporated onto the surface using the substrate as a seed from which to grow. Image attribution: [43]

$$\gamma = \frac{4M_1M_2}{(M_1 + M_2)^2} \tag{3.3}$$

The etching efficiency is maximized when $M_1 = M_2$. This means that different materials will be etched with different rates based on their molecular weights. One challenge associated with ion milling magnetic materials is that they are often etched slowly compared with the polymer based ebeam resists used to lithographically create the ion mill mask. If the mask is etched away too quickly, it is not possible to etch the magnetic material.

One obvious potential solution is to use a thicker mask, however, this is not ideal for several reasons. First, patterning thicker resists is more difficult, and resolution will go down the thicker the resist height. The close spacing of the nanomagnets requires a very high resolution, and using a thicker resist would make patterning much more difficult. Second, thicker masks do not work well for ion milling. For closely spaced structures, the ejected

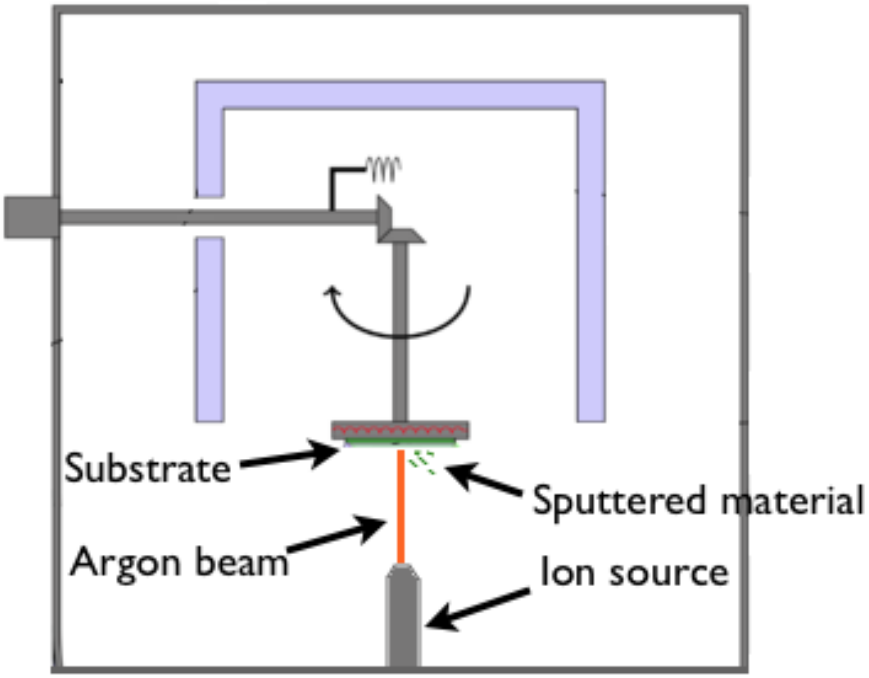

Figure 3.10: A schematic for the inside of an ion mill chamber. A high energy Argon beam physically sputters away material from the substrate to be etched.

material has a more difficult time exiting past taller masks. Taller masks tend to exhibit an effect called "crowning" in which the sputtered material agglomerates on the sidewalls and creates raised areas along the edges that look like a crown. These crowns make subsequent removal of the mask very difficult and are not desirable. A schematic for crowning is shown if Figure 3.12 a). An AFM image showing crowning is shown in Figure 3.12 b).

To solve these issues it is sometimes desirable to pattern a hard mask that is more impervious to ion milling that can be made thinner. There are a variety of options for creating this hard mask with advantages and disadvantages.

One approach to patterning a hard mask is to use diamond-like Carbon (DLC). DLC is extremely hard to Argon-based ion milling and can easily be patterned with an oxygen plasma [45]. The process steps are as follows:

1. Deposit DLC. Spin on sacrifical Durimide layer. Pattern ebeam mask with Hydrogen Silesquioxane (HSQ).

2. Use oxygen plasma to anisotropically pattern the DLC and Durimide using HSQ as the mask. To achieve the anisotropic etch, the O_2 plasma etch should be done at low temperature (-100 °C).

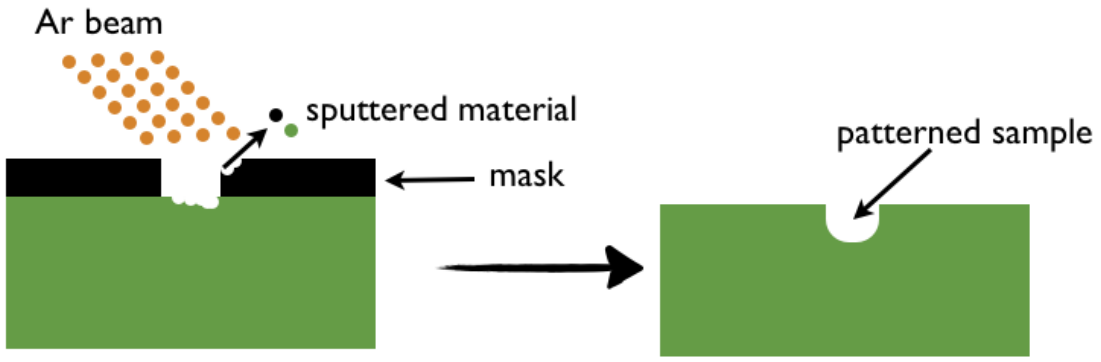

Figure 3.11: A schematic of the etching process during ion milling. Image attribution: [43]

3. Dissolve the sacrifical Durimide layer to remove the HSQ and leave behind the patterned DLC hard mask. Durimide dissolves easily in hot N-Methylpyrrolidone (NMP), a common laboratory solvent.

4. Ion mill using the DLC as a hard mask. If desired the DLC can be removed with an O_2 plasma.

A schematic showing the aforementioned process steps is shown in Figure 3.13. SEM's showing steps 2 and 3 are shown in Figure 3.14.

The DLC hard mask suffers from several disadvantages due to its complexity. DLC exists in 7 different forms of various hardness depending on the amount of sp^3 bonding between the carbon atoms. It is desired to maximize the number of sp^3 bonds which is not trivial. The cryo 0_2 plasma etching complicates matters because overetching can cause oxidation of the metal surface underneath the DLC. During this same etch step, the Durimide is also etched. The purpose of the Durimide layer is to remove the HSQ so that only the DLC is left behind. This results in a thin yet hard etch mask. The DLC etches significantly slower than the Durimide in this step and can make timing the etch difficult. Because PEEM is surface sensitive any oxidation present is very deleterious to the magnetic imaging capabilities, so care must be taken. At the same time, due to the surface sensitivity of the PEEM, the second O_2 plasma step is also very critical because all the DLC must be removed.

We successfully fabricated nanomagnet chains using this process and imaged them using PEEM. However, reliability of the process was an issue which caused our group to investigate the use of other processes. Through extensive discussion and collaboration with IBM Almaden, another hard mask process was developed using a chrome liftoff mask. This technique has the advantage of being simpler in that it requires only one plasma etching step and uses the comparatively simpler process of evaporating and lifting off metal instead of the more complicated DLC process. The composition of the evaporated chrome is significantly easier to control and less prone to variability issues compared with the DLC. The process steps are as follows:

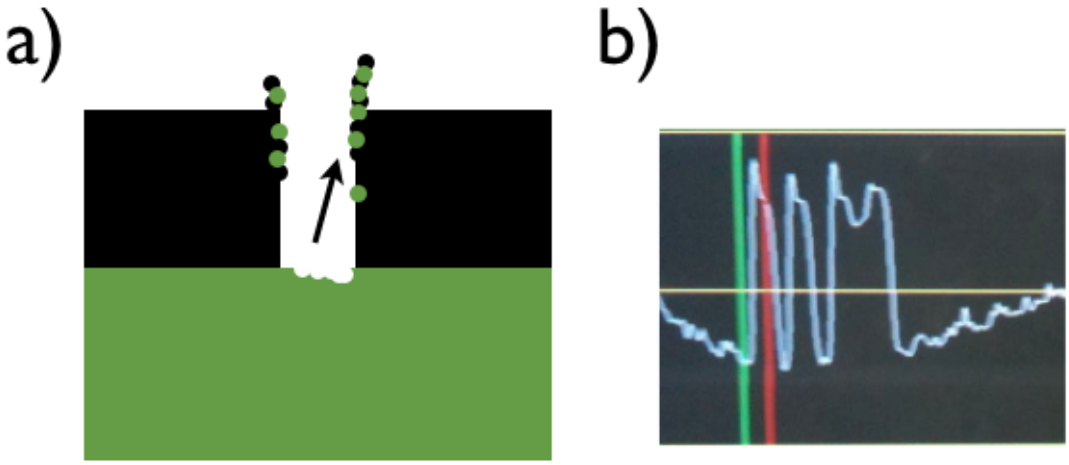

Figure 3.12: a) A schematic showing how crowning can occur in thicker ion mill masks. b) An AFM image showing crowning in an ion milled sample.

1. Spin on sacrifical Durimide layer. Pattern e-beam mask with Poly(methyl methacrylate) (PMMA).
2. Evaporate Chrome film onto mask (20nm).
3. Lift off the Cr by dissolving the PMMA in Acetone. Note that NMP, the preferred solvent for PMMA, cannot be used as the solvent for this purpose because it will also dissolve the Durimide layer underneath. Acetone dissolves PMMA very quickly and results in a poor liftoff unless it is diluted with isopropyl alcohol (IPA). A mixture of 10:1 IPA:Acetone was used successfully for this purpose.
4. Use oxygen plasma to anisotropically pattern Durimide using Cr as the mask. To achieve a more anisotropic etch, the O_2 plasma etch can be done at low temperature (-100 °C). The low temperature step is not strictly necessary and an undercut can be desirable. In the DLC process the anisotropic etch was critical because it was being used to directly pattern the hard mask.
5. Ion mill using the Cr as a hard mask. The Cr can now be removed by dissolving the Durimide layer in hot NMP.

This method is more reproducible and has a quicker turnaround time compared to the DLC method. However, it has a few disadvantages. First, the mask height is taller than the DLC method due to the sarificial durimide layer underneath of 20-30nm. This limits the resolution compared to what is potentially possible with the DLC. This is not as large a problem as it seems, however, as the DLC method uses the negative resist HSQ which is more difficult to control then PMMA making the achievable resolutions for both processes

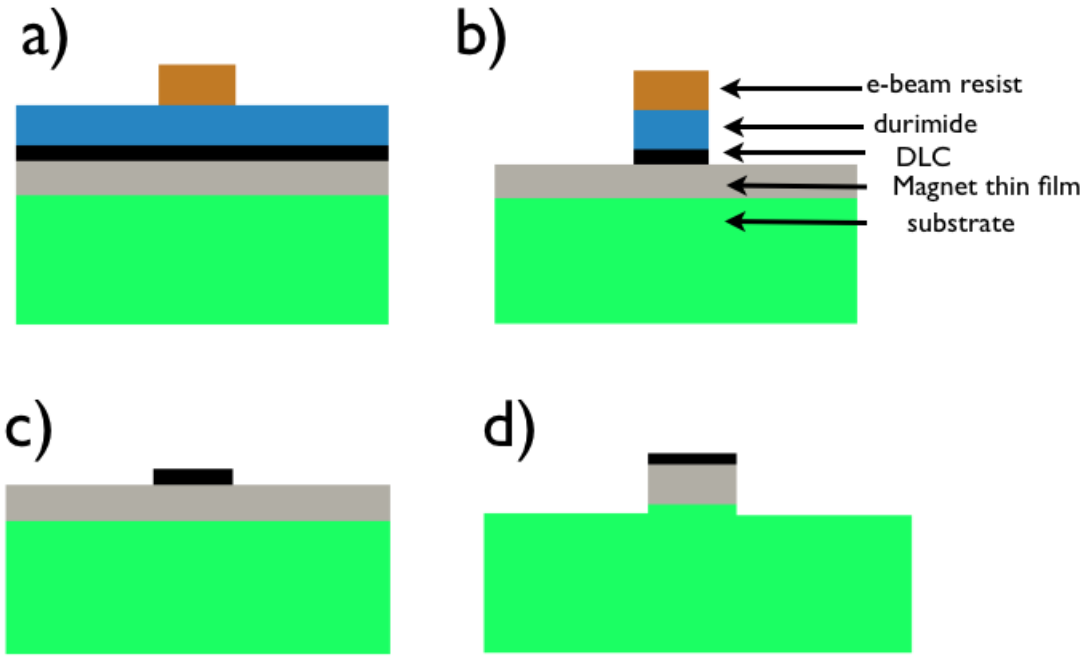

Figure 3.13: a) Patterned HSQ on Durimide, on DLC. b) DLC and Durimide are anisotropically etched in a cryo Oxygen plasma. c) Durimide is dissolved to remove the HSQ leaving behind the DLC hard mask. d) Sample is ion milled using the DLC as a hard mask.

comparable. The other disadvantage of using the thicker Durimide and Cr etch mask is that the removal of this mask is somewhat challenging. During the the etch, redeposition of sputtered material on the sidewall (see Figure 3.12) can completely cover the Durimide making it resistant to removal in the hot NMP. Sonication for long periods of time, alternated with CO_2 snow cleans have been found to help with the removal of the mask. Snow cleaning is discussed in detail in [46]. This remains an ongoing challenge, however.

3.3.3 Experimental Evidence of Hard Axis Stability

Arrays of nanomagnet chains were fabricated with the Cr hard mask method. The nanomagnets were etched from 6nm thick epitaxially grown Fe films on an MgO substrate.[i] The arrays were designed so that the shape of the nanomagnets swept a large parameter space. This allowed us to the study the operation of the chains in various configurations and compare the results directly with the theoretical parameter space studies in Figure 3.5. The simulation work predicted that the nanomagnet chains would behave in different ways based on the relative amount of biaxial and uniaxial anisotropy present. At the low aspect ratios, the biaxial

[i]The author would like to acknowledge the assistance provided by IBM Almaden. Specifically, the help of Brian Hughes, Charlie Retter, Li Gao, and Stuart Parkin was greatly appreciated.

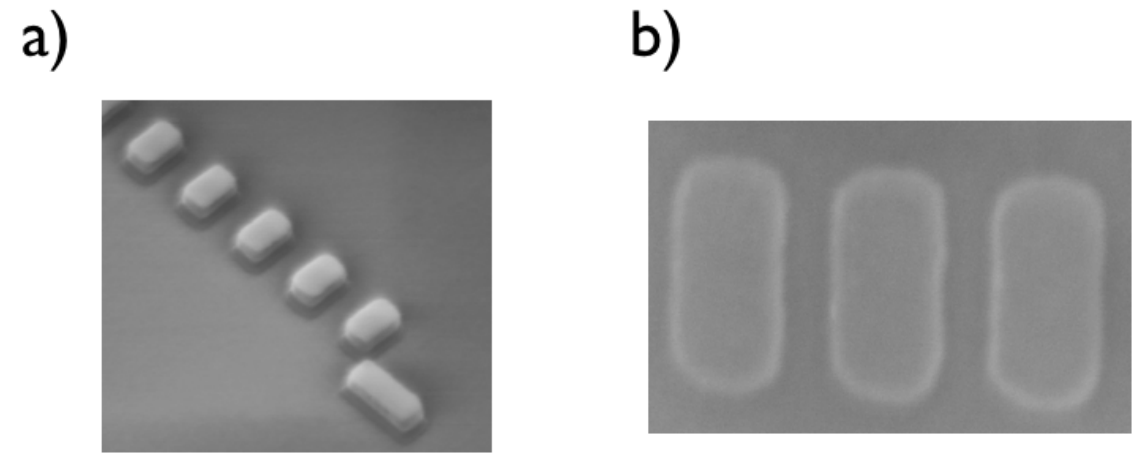

Figure 3.14: a) A SEM showing the patterned DLC, Durimide, and HSQ layers (Figure 3.13 b). b) A SEM showing the patterned DLC hard mask after the Durimide has been dissolved to remove the HSQ.

anisotropy dominates, and the nanomagnets will remain locked along their hard axis and no signal will propagate.

In the experiment we found chains that were partially blocked lying right on the transition between the "unblocked" and "blocked" regions predicted by the simulation. The first few nanomagnets were able to propagate the signal by flipping out of the hard axis alignment, but became blocked further down the line due to an anisotropy in the energy barrier of the metastable nanomagnet hard axis. The signal is frozen mid propagation unable to propagate further. When the temperature of the system is increased to approximately 100 C, the phase boundary shifts and the signal becomes unfrozen. The frozen signal propagates the rest of the way down the chain. This process is shown in Figure 3.17.

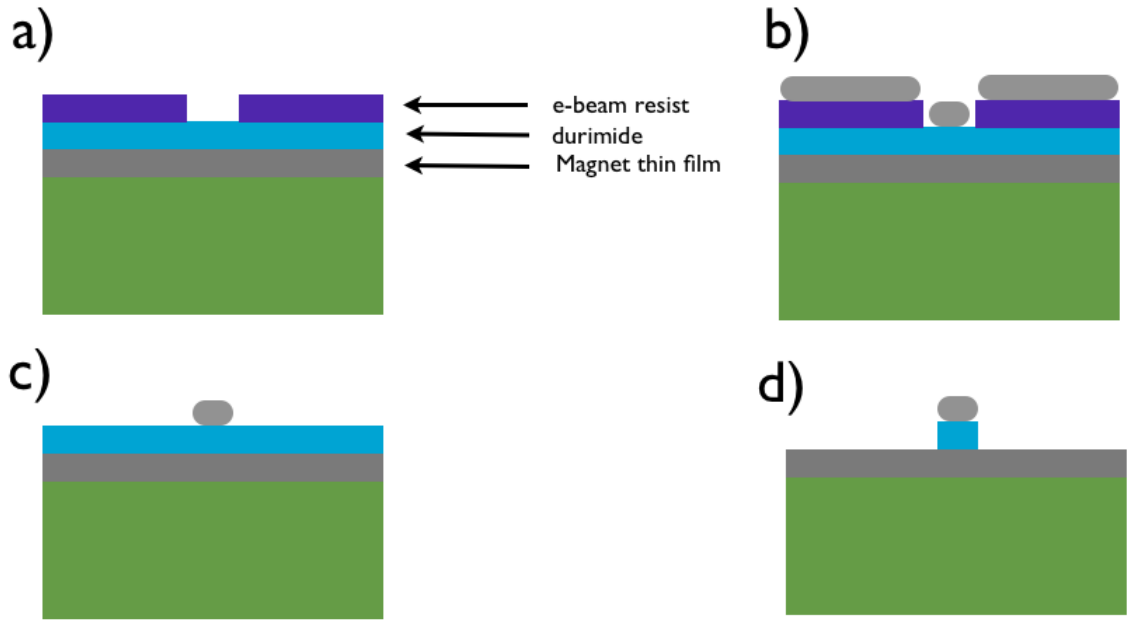

Figure 3.15: a) Patterned PMMA on Durimide. b) Evaporated Cr. c) Cr lifted off. d) Cryo O_2 plasma etch to pattern the Durimide. The ion mill can now be performed using the Cr as a hard mask. The chrome can be removed with hot NMP.

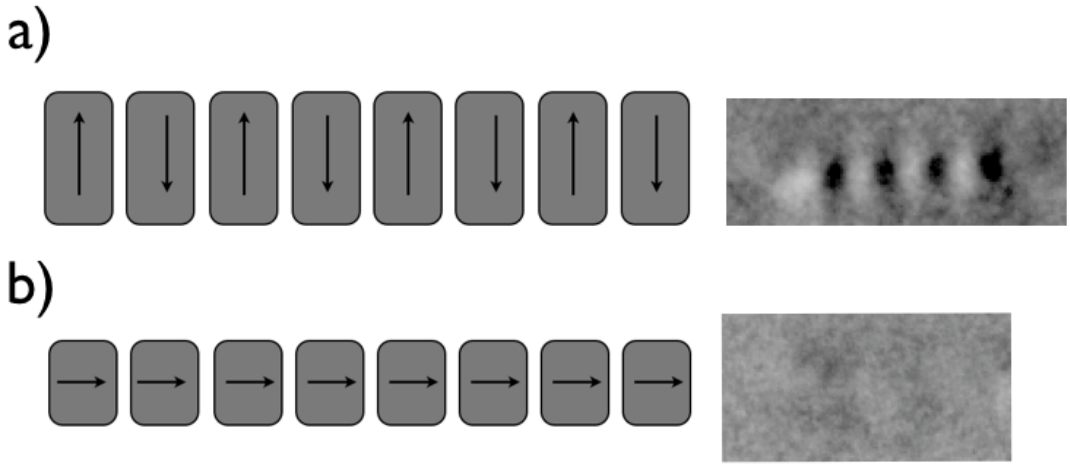

Figure 3.16: a) A PEEM image and schematic showing a nanomagnet chain with an aspect ratio that allowed the signal to propagate correctly along the chain. b) A PEEM image and schematic showing a nanomagnet chain with a smaller aspect ratio that resulted an imbalance in the amount of biaxial and uniaxial anisotropy. The nanomagnets in the chain remained magnetized along the hard axis and no signal propagates. The PEEM image shows no magnetic contrast because it is sensitive to only one axis of magnetization (up/down not left/right).

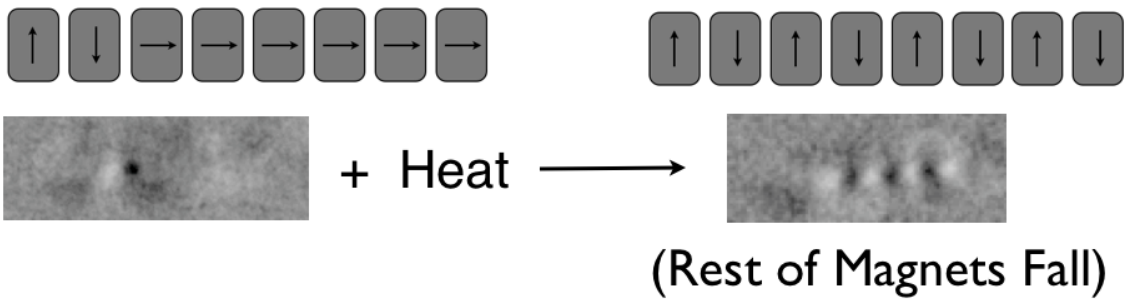

Figure 3.17: A nanomagnet chain in with the signal is frozen mid propagation, unable to propagate further. The uniaxial anisotropy is balanced on the phase boundary between completely blocking the signal and letting it pass. The temperature is increased to approximately 100 C. The phase boundary shifts and the signal becomes unfrozen.

3.4 Summary

In this chapter, I discussed altering the nanomagnets' energy landscapes with a biaxial anisotropy to give them stability along their hard axes. This allows them to remain magnetized along the hard axis after the clocking field has been removed and until the signal cascade can reach them. After discussing the general concept, micromagnetic simulations were shown demonstrating the signal cascade with the biaxial term and comparing it to a chain of nanomagnets without the additional anisotropy. A Shmoo plot showing the operating window of this mode was plotted as a function of island dimensions and further micromagnetic simulations were shown with the cascade operating in vertical wires as well as fan-outs and wire bends. Next, fabrication work was discussed to implement these structures in real materials. The choice was to use magnetocrystalline anisotropy inherent in certain single crystal materials. Finally, PEEM images exhibiting evidence of hard axis stability in nanomagnet chains were shown.

Chapter 4

Architecture Design in the Biaxial Mode

Contents

4.1 Reliability of the Biaxial Mode

In chapter 2, I presented several studies on the reliability of nanomagnet computing architectures in the slow clocked adiabatic mode. The biaxial mode has very different dynamics, and in this chapter I will characterize its robustness and consider new challenges that result from this new operating regime. I will also discuss how energy dissipation and speed are affected by the biaxial anisotropy term.

4.1.1 Parameter Space Studies

In the previous chapter, a parameter space study was carried out on nanomagnet chains with biaxial anisotropy to understand the dynamics and operating envelopes for this mode. The results were graphed as a Shmoo plot [40] which is reproduced here in Figure 4.1. The middle white colored triangular region of the plot in Figure 4.1 represents the nanomagnet dimensions for which the signal propagates as expected. Other parameters that may affect

propagation of the signal, such as the amount of biaxial anisotropy in the nanomagnets and nanomagnet separation, are held fixed. Understanding how these fixed parameters affect the robustness of the nanomagnet signal propagation is also important, and in this section I will discuss the role these parameters play. These parameters cover a large parameter space, and before discussing them I will briefly discuss the distributed computing architecture that was created to make the study possible.

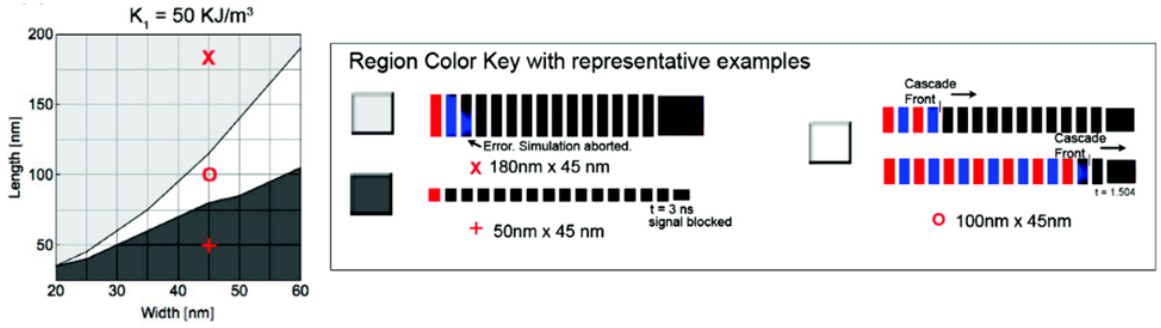

Figure 4.1: A Shmoo plot showing whether the signal propagates successfully as a function of nanomagnet length and width. The nanomagnets have a biaxial anisotropy constant $K_1 = 50$ kJ/m^3. The white wedge-shaped area indicates regions of parameter space for which the signal propagates correctly with all nanomagnets flipping in the correct order within the 3 ns simulation time. Grey areas are where signal propagation was unsuccessful. Failure mechanisms are explained in the main text. False positives, where an instability along the wire led fortuitously to proper alignment of the magnetizations, are accounted for in the analysis.

Xgrid Distributed Computing

To create each parameter space plot (as exemplified in Figure 4.1), several hundred micromagnetic simulations had to be run and the results analyzed. Due to the length of the simulation (3ns), grid size (5nm), and simulation area (severalμm^2), each micromagnetic simulation takes on the order of an hour to run on a 2.6 Ghz CPU. The number of simulations required to explore the desired parameter space is large enough as to be impractical on a single desktop machine. The use of a supercomputer facility was considered but rejected in favor of a local computing grid that made use of spare CPU cycles of desktop machines in the laboratory. The grid made use of Apple Inc.'s free Xgrid distributed computing software [47]. The structure of the Xgrid network is detailed below as well as graphically in Figure 4.2.

1. First, a Python script creates a "Job" of OOMMF simulations to explore the desired parameter space.

2. The "Job" is transferred to the "Controller". The output of the script in step 1 is a text file readable by "GridStuffer", a program developed at Stanford for their own grid simulating protein folding. GridStuffer is a GUI used by the client to manage the transfer of "Jobs" to the "Controller"

3. The "Controller" sends individual OOMMF simulations to "Agents" on the network. The "Controller" is part of the Xgrid framework.

4. Each "Agent" performs the OOMMF simulation. The Agent downloads a fully compiled copy of OOMMF and runs a micromagnetic simulation with the desired parameters. Graphic input files of the magnet dimensions are generated with a Python script that initiates the simulation once OOMMF has downloaded correctly, and the input files have been created. The OOMMF simulation outputs a data file containing the magnetization information every time step. As the simulation progresses, these files are converted to a graphic format. A python script is used to analyze the graphic content to determine the state of the simulation (whether the signal is "blocked" or errors are present). The script also cleans up the files and can terminate the simulation when errors or signal blockage has been detected.

5. Agents return the results. When the simulation is over the Python script creates a movie out of the magnetization data as well as a text file containing the results of the simulation.

6. Results are transferred back to the client. When all the results are in, a final Python script is used to compile data into a single text file for plotting.

The simulations for this project were run on a grid of Macintosh computers in the former Device Group offices of 373 Cory Hall. These computers were desktop machines in use by other members of the laboratory mainly for office work and were not originally meant to be used as part of a cluster. However, the Xgrid agent runs as a low priority user in a sandbox and is only able to use spare CPU cycles not needed by the machine owner. It's operation is thus transparent to the computer owner. At its peak in 2007, the grid had a performance of equivalent to around 100 Ghz and could run approximately 50 OOMMF simulations in parallel.

Biaxial Anisotropy Strength

The strength of the biaxial anisotropy is an important parameter in signal propagation along wires as it directly determines the amount of hard axis stability in the nanomagnets. In Figure 4.1, the biaxial anisotropy coefficient K_1 was fixed at 50 kJ/m^3. This value is approximately the amount of biaxial anisotropy of crystalline Fe, one of the candidate materials for implementing biaxial anisotropy in nanomagnets experimentally that was discussed in the previous chapter. In Figure 4.3, 3 Shmoo plots are shown to visualize how the operating region changes as the amount of biaxial anisotropy constant is varied. As K_1 is increased, the stabilization from the biaxial anisotropy gets stronger, and the operating window grows larger. Note that as more biaxial anisotropy is added, the lower operating envelope shifts upward meaning higher aspect ratios are required before the signal can be passed correctly. For example, in Figure 4.3 a), a chain with 50nm wide by 70nm tall nanomagnets will propagate the signal, but the same aspect ratio is part of the "blocked" region in Figure 4.3 c). The cause of this shift is

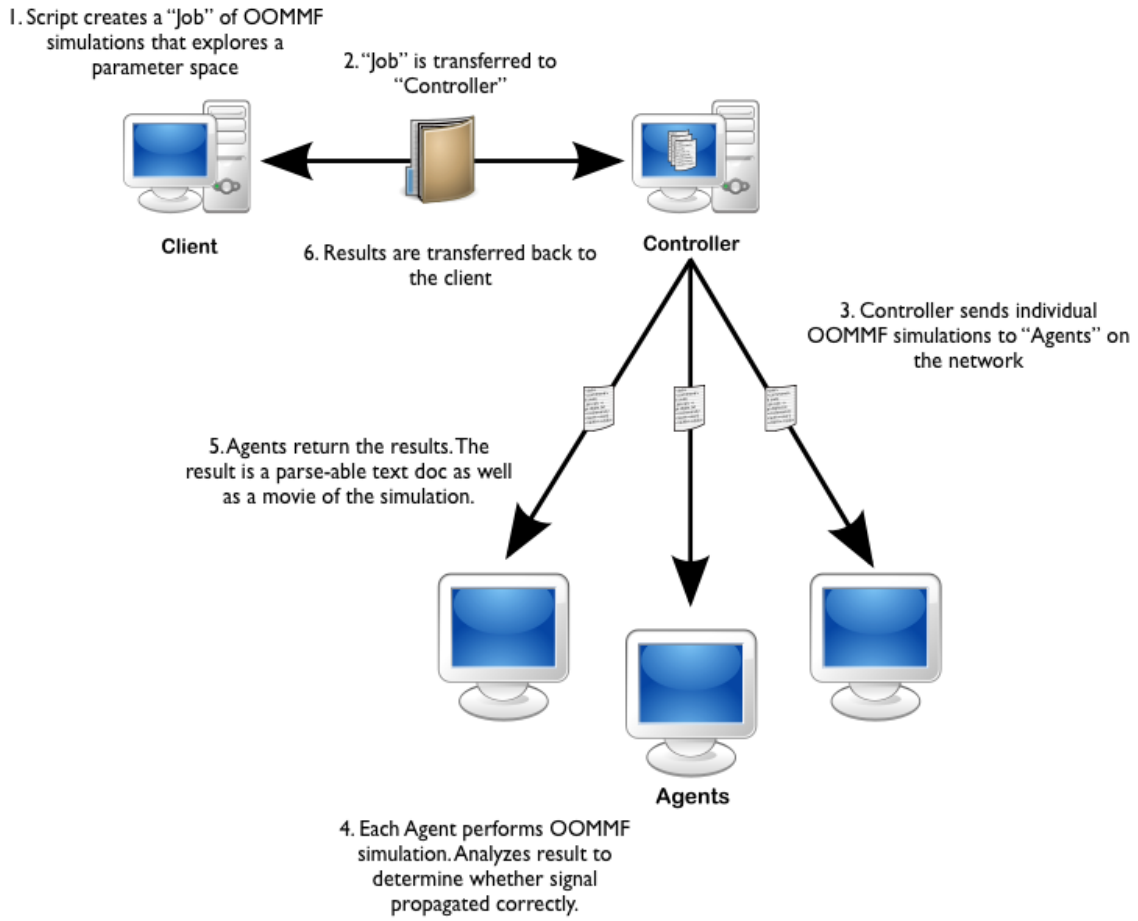

Figure 4.2: A schematic of the Xgrid network for performing the distributed OOMMF calculations. A detailed description of the different steps in the diagram is in the main text. Image attribution: [43]

explained by the added stability provided by the biaxial anisotropy which puts lower aspect ratios into this "over stable" region. This potentially deleterious effect on the lower envelope is more than made up for on the upper envelope, however, resulting in an operating region that is wider overall.

Nanomagnet Separation

The separation of the nanomagnets from their nearest neighbors is an important parameter in signal propagation along wires as it directly determines how strongly the nanomagnets couple to each other. As the nanomagnets get closer to one another, the operating window grows larger. In Figure 4.4, Shmoo plots are shown for nanomagnet separations of 20nm, 15nm, and 10nm in a)-c) respectively. Notice that the increased operating window grows from the top, not the bottom. Nanomagnet chains with higher aspect ratios that did not function correctly before begin to propagate the signal correctly when the nanomagnet spacing is reduced. The

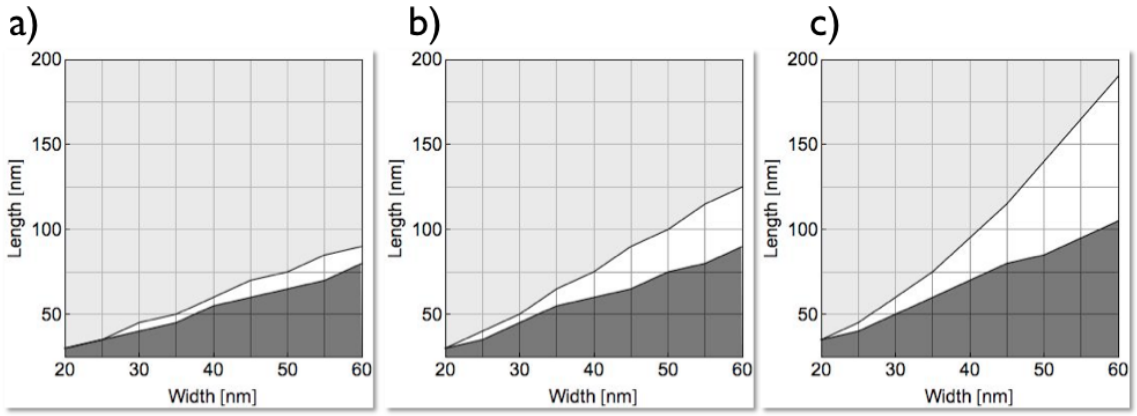

Figure 4.3: Shmoo plots showing how the operating regions change as the amount of biaxial anisotropy constant K_1 changes. a) K_1 = 30 kJ/m^3, b) K_1 = 40 kJ/m^3, a) K_1 = 50 kJ/m^3

reason for this trend is the added stabilization the nanomagnets feel when locked up along their hard axes when placed closer together. This stabilization strengthens the hard axis alignment in the same way that the "helper" nanomagnets in vertical chains discussed in Chapter 2 increase hard axis stability.

One might expect that this increased stability for the upper envelope would be detrimental to the lower operating envelope below which the nanomagnet chains become "over stable". The reason this does not occur (the lower envelope remains mostly unchanged) is that the increased coupling associated with more hard axis stability also increases the ability of a nanomagnet to tip its neighbor and propagate the signal. These two forces offset each other, and the net effect is no change in the lower operating envelope.

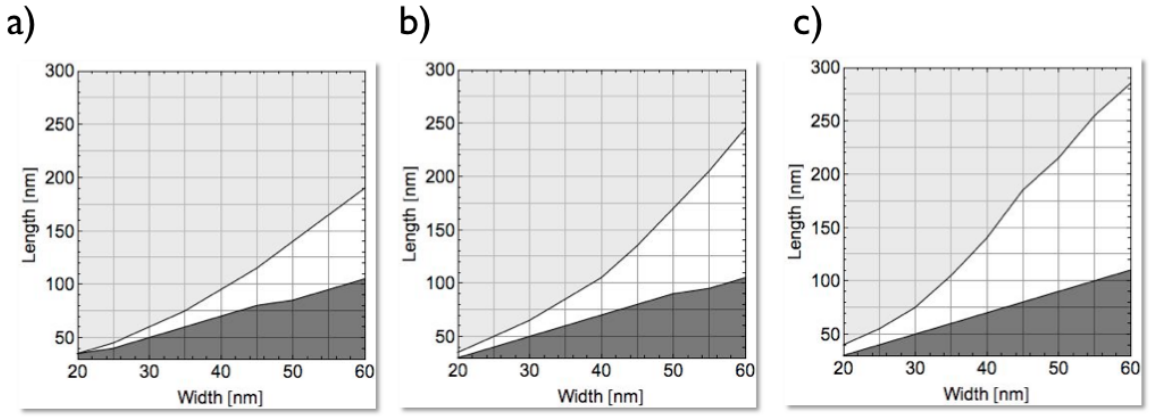

Figure 4.4: Shmoo plots showing how the operating regions change as the nanomagnet separation changes. a) s = 20 nm, b) s = 15 nm, a) s = 10 nm

4.2 Computing in the Biaxial Mode

4.2.1 Race Conditions and the Majority Logic Gate

As mentioned previously, the 3-input majority logic (MLG) gate [12] introduced in Chapter 1 is the current basis for computing with nanomagnet-based logic. Three magnetic wires serve as input to the gate by surrounding and terminating at a central nanomagnet whose magnetization is set along its hard axis. When the logic signals arrive at the central nanomagnet, the combined effects of the dipole fields from the three adjacent nanomagnets determine the final orientation, up or down, along the easy axis of the central nanomagnet. Each of the three inputs thus supplies a vote for the direction of the central nanomagnet, and whichever direction receives the majority of votes wins.

One issue with this approach is that if the inputs do not arrive at precisely the same time the gate cannot be made to behave predictably. Consider the example shown in Figure 4.5. Here the two top/bottom inputs arrive first simultaneously with opposite votes (Figure 4.5 a). Because these inputs cancel themselves out, the central moment is unaffected, and the output must be determined solely by the vote of the third input when it arrives (Figure 4.5 b). *This left input nanomaget must therefore have sufficient coupling strength on its own to affect the output*.

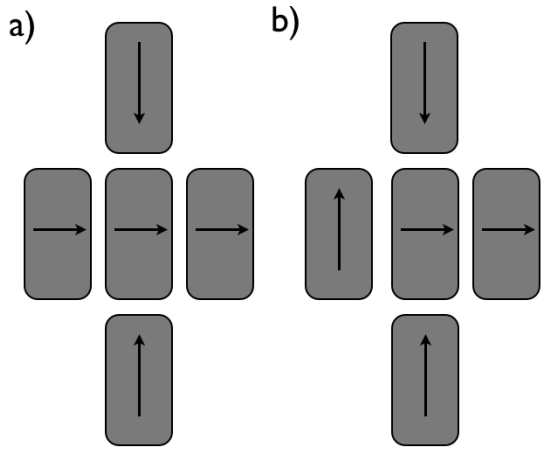

Figure 4.5: a) The top/bottom inputs arrive at the MLG first with opposite votes canceling themselves out. b) When signal from the left input nanomagnet arrives, the strength from this input must be strong enough on its own to affect the output of the gate.

However, in the opposite case *where the left input arrives first, its one vote must not be sufficient to flip the central nanomagnet*. This is shown in Figure 4.6 a). When this happens, there is not enough information to determine what the final output value will be, and the gate should wait for the other two inputs to arrive (Figure 4.6 b) before making a decision. In one case, the left input needs to be strong enough to flip the output on its own (Figure 4.5). In the other situation, the same input needs to not be of sufficient strength (Figure 4.6). Thus,

we have two contradictory scenarios with the distinction between them resting only in the arrival timing of the three inputs. The problem of this so-called race condition would be eliminated from the MLG if all inputs are forced to be synchronous. This condition may be achievable in a cellular automata information processing architecture. However, for complex combinatorial logic circuits with relatively large numbers of nanomagnets in a single clocked pipeline stage, this is very difficult to achieve.

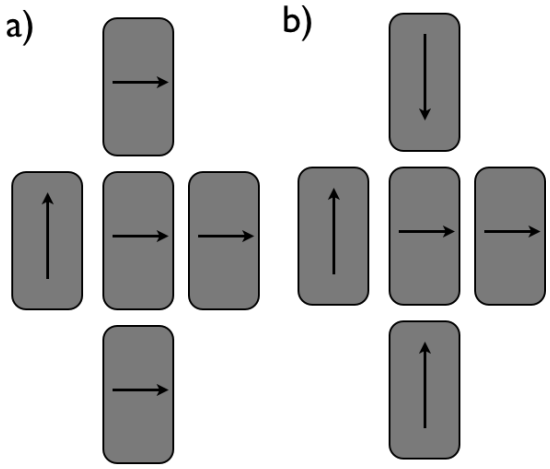

Figure 4.6: a) The signal from the left input nanomagnet arrives first. There is not enough information to determine the output of the gate, so this input nanomagnet should not be strong enough on its own to affect the output of the gate. b) The gate should wait for the other two inputs to arrive. This scenario is not compatible with the scenario in Figure 4.5 so the MLG suffers from race conditions.

4.2.2 The Bgate

Due to the race conditions described above, the design of a different logic gate that does not suffer from this issue is desirable. We introduce a modified, two-input universal logic gate that solves the problem of asynchronous inputs by breaking up the logic operation into two complimentary subgates.

The Dictator Gate

The first subgate is a modified MLG, where the strength of inputs 1 and 3 are designed to have weaker coupling to the central nanomagnet and so can only affect an output when their votes agree. Weaker coupling is achieved by spacing the two inputs slightly further from the central nanomagnet. This removes the need for inputs 1 and 3 to arrive synchronously as the weaker coupling effectively gives each input only half a vote. Input 2 must then be given majority rule through stronger coupling as it alone must cause the central nanomagnet to flip if inputs 1 and 3 disagree. The race conditions for all three inputs could then be removed if input 2 is engineered to supply a potentially deciding vote, if needed, in the case of a tie

between inputs 1 and 3. Due to the asymmetry in voting power of the input islands, we refer to this modified majority logic gate as the 3-input Dictator gate (D-gate) to emphasize the role played by input 2 in determining the output. While the D-gate solves the race condition problem for inputs 1 and 3, it is not a complete logic gate on its own. If input 2 arrives first, the output would immediately be decided. A second structure is necessary to control the flow of input 2, blocking it or sending it through only when necessary. This is accomplished by the second complimentary subgate.

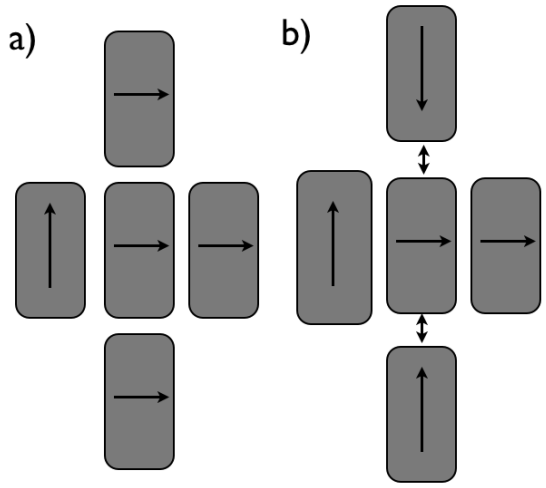

Figure 4.7: a) A schematic showing the layout of a normal MLG. b) A Schematic showing a modified MLG in the Dictator gate configuration. The top/bottom inputs are spaced further away so each has less than 1 vote. One of these inputs is not enough to set the output of the gate. Conversely the left input is engineered to be a "Dictator" input. It can be slightly larger, or spaced slightly closer so that it is strong enough on its own to flip the output bit.

The Lazy AND Gate

The second subgate, which completes our modified two-input universal logic gate, has a truth table as shown in Figure 4.8 b). The gate acts as a logical AND gate with the exception that when it should output a '1', it outputs nothing at all. We refer to it, then, as the Lazy AND gate. As will be shown below, in order for this gate to work it must have the ability to discriminate and block different incoming signals. We achieve this by including nanomagnets that can only switch in one direction: only down in our implementation. Although this unidirectional bias can be achieved using antiferromagnetic pinning layers, doing so would lead to considerable fabrication complexity. In this implementation, the unidirectional anisotropy is engineered by placing stabilizer nanomagnets at opposite corners of those nanomagnets in the incoming signal wire, as shown in Figure 4.8 b). The combined dipole field from these two new stabilizers is preferentially down, does not switch the nanomagnet down, but does prevent the nanomagnet from switching up. We refer to this as a magnetic diode because a

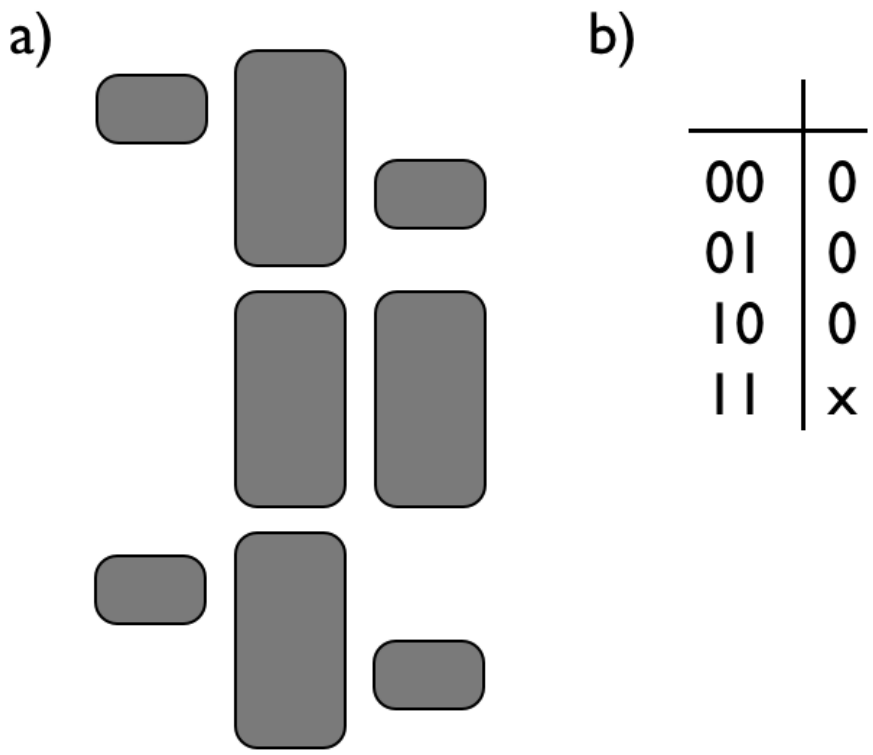

Figure 4.8: a) A schematic showing the layout of a Lazy AND gate. b) A truth table of the Lazy AND Gate.

signal is propagated only if it possesses the correct polarity when it arrives at the unidirectional nanomagnet. The energy landscape of the magnetic diode is shown in Figure 4.9.

The complete Lazy AND gate consists of two of these magnetic diodes that surround and strongly couple to the central nanomagnet so that either vote alone is sufficient to output a result. A schematic of this subgate is shown in Figure 4.8 a). If both inputs to the magnetic diodes are up (logic 1), both are blocked and the central nanomagnet is unaffected. In all other cases one of the signals will be a down (logic 0) and will be passed through, as indicated by the truth table in Figure 4.8 b). The results of a micromagnetic simulation showing how signal blockage and passage occurs in this gate is shown in Figure 4.10.

The Bgate

The complete, two-input universal logic gate is created by connecting the inputs to the Lazy AND gate to inputs 1 and 3 of the Dictator gate and then connecting the output of the Lazy AND to input 2 of the Dictator gate. This arrangement is shown in Figure 4.11. The gate is given the name “Bgate” due to it’s resemblance to the letter ’B’. In each case where the Lazy AND provides an output (01, 10, 00), that signal is passed to the D-gates strongly coupled input (input 2) and the output is immediately determined. Because the other inputs

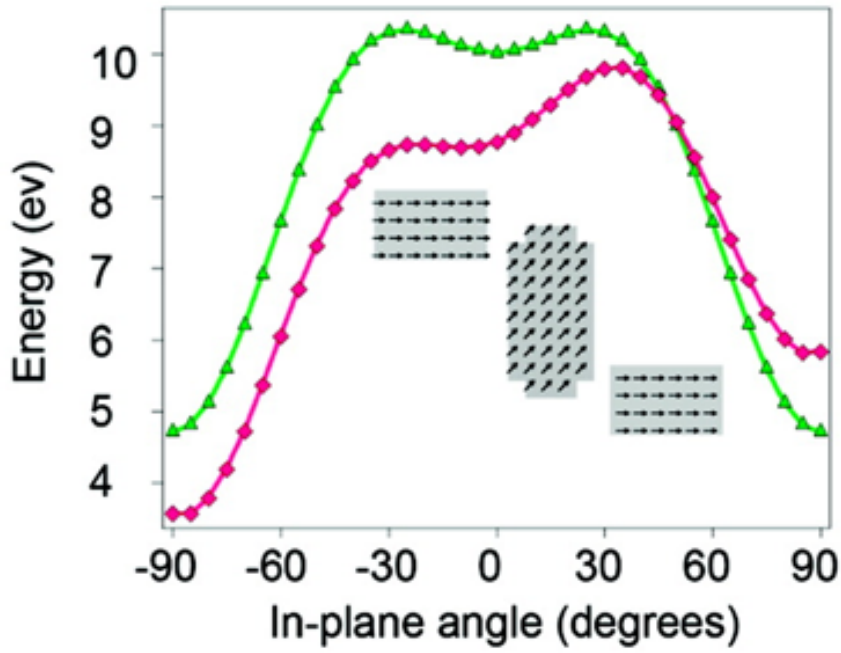

Figure 4.9: The energy vs. magnetization angle plot of an unmodified nanomagnet with uniaxial and biaxial anisotropy and a nanomagnet with offset stabilizers that make up the Lazy AND Gate. The stabilizer islands bias the magnet to switch in one direction without completely removing the energy barrier. This island can flip in one direction but not the other.

to the D-gate will either be canceling (01, 10) or in agreement with input 2 (00) the arrival of the inputs 1 and 3 is not important. In the only case where the Lazy AND gate does not produce an output due to both signals being blocked (11), the output will be determined by inputs 1 and 3 of the D-gate whose two "up" votes are enough to produce the desired output. Micromagnetic simulations for this gate are shown for two different inputs at two times in Figure 4.11.

The truth table of this gate can correspond to that of a standard NAND gate. However, since the NOT operation in this architecture can be implemented by adding/subtracting an extra nanomagnet to/from any input or output signal, this same structure can easily be used with no alteration to create a NOR, AND, or OR gate. The logical operation that this structure performs is thus only dependent upon the number of nanomagnets in the wires connecting it with the next gate.

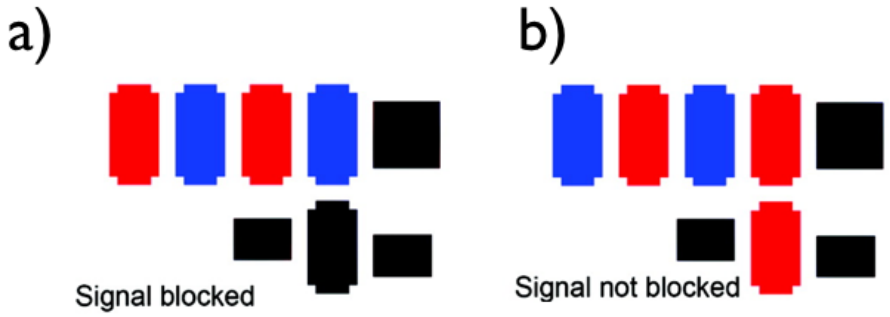

Figure 4.10: a) The signal is blocked by the "magnetic diode" because the bias provided by the stabilizers prevents the nanomagnet from flipping up. b) The signal passes through normally. The bias provided by the stabilizers is in the correct direction to allow the nanomagnet to flip down.

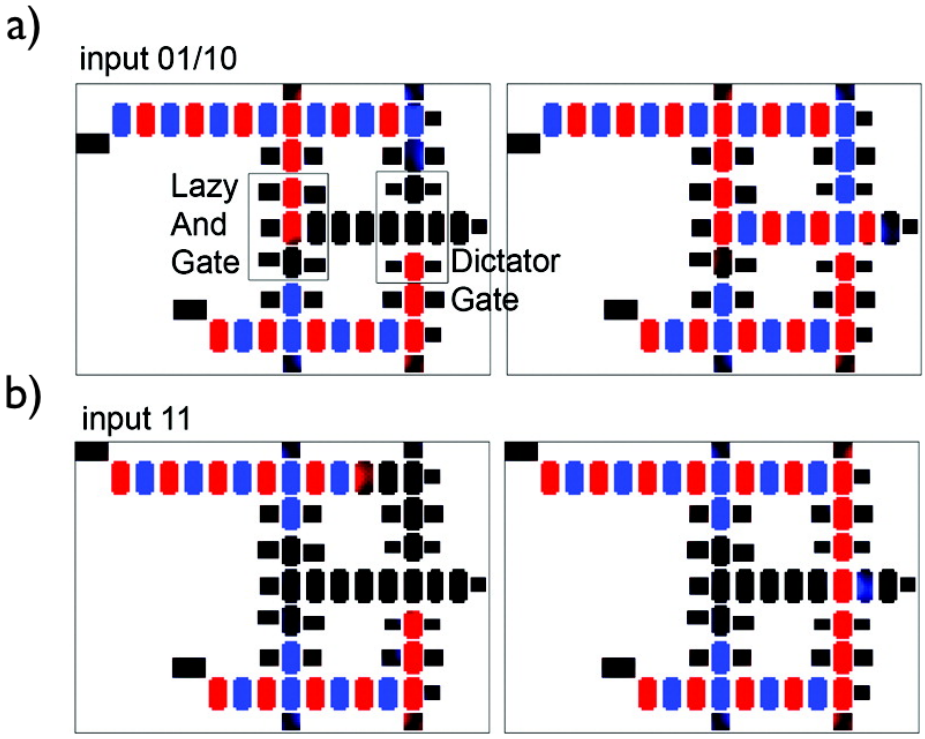

Figure 4.11: a) Bgate gate showing how it is constructed from a Lazy AND and a Dictator gate. Operation of the Bgate gate at two different times with input 01, 10. The first input is blocked, but the second input passes through the Lazy AND and determines the output. Input 00 (not shown) operates in a similar manner with both inputs being passed through by the Lazy AND. b) Operation of the NAND gate at two different times with input 11. Both inputs are blocked by the Lazy AND. The output is determined the by two inputs going into the D-gate.

4.3 Clocking Architectures

The choice of a clocking architecture has very important effects on reliability, speed, and energy dissipation in nanomagnet circuits. I will briefly return to the adiabatic mode of operation discussed in Chapter 2 and discuss the types of exotic architectures that are most appropriate for it given its stochastic nature. Then I will contrast those requirements with the challenges and opportunities raised by going to the biaxial mode.

4.3.1 Systolic Architectures and the Adiabatic Mode

In the adiabatic mode, the slow removal of the clock and the stochastic nature of nanomagnet signal propagation discussed in Chapter 2 mean that long pipeline stages are not practical. As was mentioned in Chapter 2, this limitation can be partially addressed by using nanomagnetic logic devices in massively pipelined "systolic" architectures to increase throughput [34]. However, these types of architectures have not seen much commercial adoption.

In that same vein, the adiabatic mode could also lend itself to even more exotic computing architectures completely removed from their use as elements of a conventional von Neumann computer architecture with wires and Boolean logic gates. For example, a homogenous array of nanomagnets interacting with nearest neighbors implements a cellular automaton. Cellular automata are of interest in the field of complexity theory and computer science because the patterns they generate have been shown to be capable of computation [48]. When the nanomagnets are near thermal equilibrium, the random thermal switching events stochastically advance the state of the cellular automaton to create subsequent generations. This probabilistic cellular automaton rule is known to be P-Complete in 3 dimensions and implies that an array of nanomagnets interacting in this manner is able to simulate any other cellular automata rule no matter how complex [49]. In particular, this cellular automaton would be able to simulate a universal Turing machine capable of universal computation. New generations of this cellular automaton are computed without external input from the environment and would operate near the thermodynamic limits of computation.

However, while these exotic computing architectures appropriate for the adiabatic mode show a great deal of promise and show potential for computing near the thermodynamic limits, they represent a radical departure from the way computing is done today. This represents a significant barrier to the adoption of nanomagnetic logic in commercial systems.

4.3.2 Fine State Machines and the Biaxial Mode

One of the near term advantages of the biaxial mode is that, unlike the adiabatic mode, it could potentially be used in a more conventional "long pipeline", von Neumann computer architecture implementing Register Transfer Logic (RTL).

In conventional computer architectures, memory elements called registers are read from and written to at the beginning and end of every clock cycle, and for the biaxial mode to be useful it must also be able to do this. In systolic architecures, this capability is built-in because the register can be built into one of the small pipeline stages. However, for larger

"globally" clocked structures that reset every nanomagnet in the circuit, a memory element is needed that can store information from one clock cycle to another without being erased by the external field.

One could imagine a completely different memory element that the nanomagnets interface with between computations. However, using an unaltered nanomagnet is desirable for a number of reasons. Nanomagnets are intrinsically nonvolatile and make natural memory elements. If the data can remain in its magnetic form encoded in the magnetization direction of the island, there would be no need for potentially energetically costly conversions between storage types. The challenge, however, is that the external field that is used to align the rest of the magnets along their hard-axes to ready them for performing calculations will also destroy the data in the register bit.

One approach to solve this issue is the use of an out-of-plane, fin-like structure for the register bit. In this approach, the register bit is a nanomagnet that has been turned on its side 90 degrees. As discussed in Chapter 1, in patterned nanomagnets, shape anisotropy creates preferred magnetization directions. For thin film magnets, the magnetostatic energy is minimum when the magnetization points along the long or "easy" axis and is larger when it points along the short or "hard" axis. It is even more difficult to magnetize the magnet out of the plane so we refer to this axis as the "super-hard" axis (Figure 4.12). A fin-like nanomagnet has a similar set of axes, but with the orientation of its "super-hard" and "hard" axes reversed relative to the axes of the normal in-plane nanomagnets.

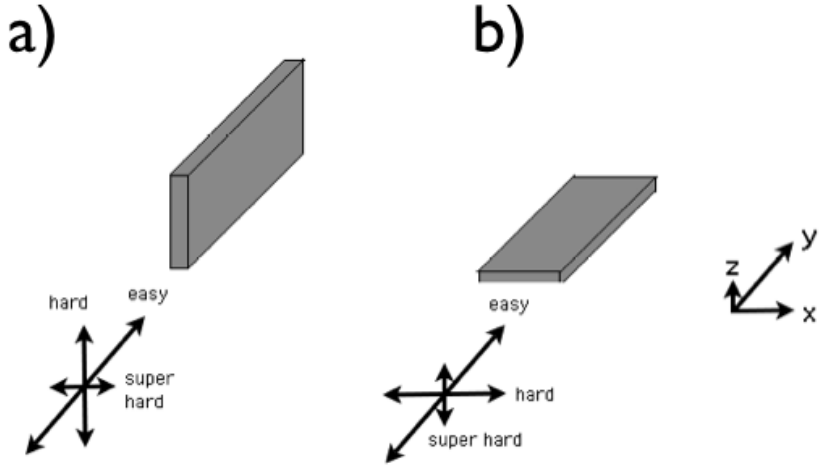

Figure 4.12: The easy and hard axis orientations for a nanomagnet patterned from a thin film with shape anisotropy as well as a nanomagnet with a fin-like structure.

The result is that an external magnetic field applied to the right sufficient in magnitude to coerce the flat nanomagnets along their "hard" axes will be insufficient to magnetize the fin-like register bit. Once the field is removed, the dipole fringe field of the register bit will act in the same manner as the rest of the islands and cant the magnetization of its neighbor

up or down. In this matter it can serve as the input bit to the cascade. Another way to do this would be to use a material with perpendicular magnetic anisotropy. This requires using a different material, but the fin requires a different thickness, so both require an extra mask.

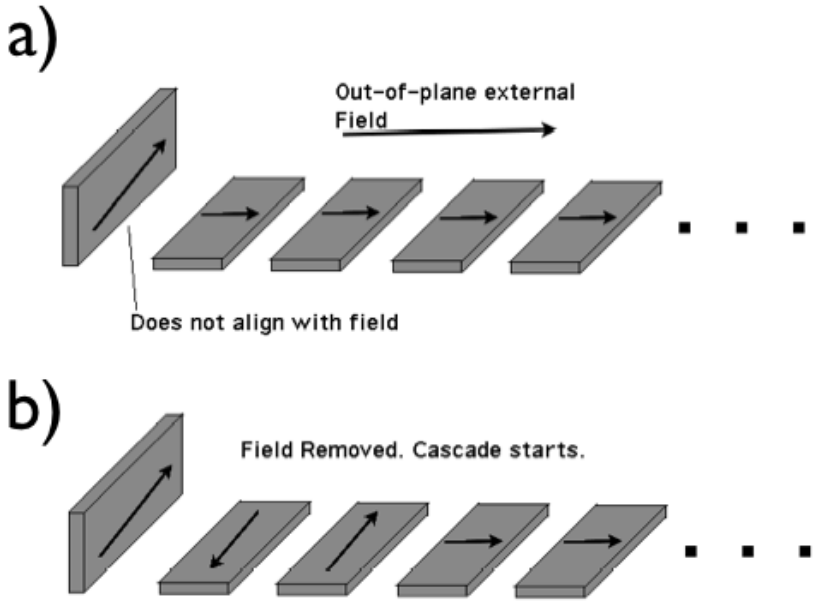

Figure 4.13: a) The external field aligns all the nanomagnets for computation along their "hard" axes except for the register bit whose magnetization remains pointing along its "easy" axis. b) The dipole fringe fields of this register can now act as the input to start the magnetic cascade once the external clocking force is removed.

In conventional computer architectures, once a computation has been carried out given an input from a register, a new value must be written to the register. In Figure 4.14, a register with the value of "up" (+y) has successfully started the propagation of a signal to the right. After some computation, a signal with a new result for the register is arriving from the left. Once the signal arrives, it is observed that the new desired value for the register is a "down" (-y) value.

In order for this new value to be written the register must be biased along its metastable "hard axis". In Figure 4.15, it is observed that through the application of an external out-of-plane field only the register bit is affected. This out-of-plane plane field is in the direction of the other magnets super-hard axes so no magnetization change will be observed in them. With the register bit magnetized along its "hard axis" it can now be affected by the magnet immediately to its left, and a new value will be written. Further application of the clocking field can now be repeated in the same manner described above to perform computations with the new input value. This system is equivalent to a finite-state machine. The states are stored in the register bits, and each application of the clocking fields give rise to logic that puts the system in a new state.

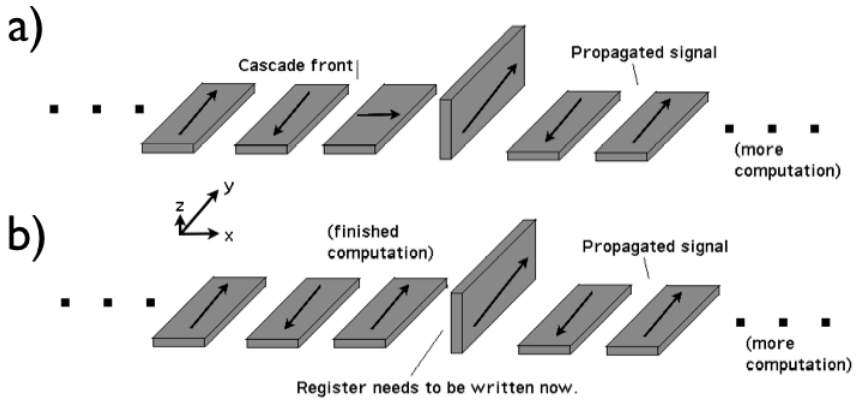

Figure 4.14: a) The register has value of "up". This input caused a signal to propagate to the right. Computations are performed (not shown) and now a signal containing the result is nearing the register bit from the left. b) The signal has arrived at the register bit and a new value of "down" should be written in this case.

The size and stability of the islands immediately to the left and right of the register bit are important considerations when designing a working register. These islands will be referred to as the input register contact (IRC) and output register contact (ORC), respectively. The ORC must be more easily written to then the IRC. If the two contacts were symmetric, the fringe fields from the register would cause both contacts to flip and there would be both a forward and backward propagating signal. The signal must only propagate in the forward direction, so the dipole fringe fields from the register must only be large enough to flip the ORC. Similarly when the register bit is being written to, the IRC must be a more powerful force than the ORC. As can be seen in the situation in Figure 4.15, both the register contacts will have dipole fringe fields that will push the register in different directions. For the register to move in the correct direction (down in this case), the field from the IRC must overpower the field from the ORC. The IRC should therefore be both more stable and have a larger fringing dipole field. One approach to creating this situation is to enlarge/shrink the two respective contacts. In addition, because the ORC is the first island in the cascade chain, the biaxial anisotropy can be omitted from this island. These choices have been illustrated in Figure 4.16.

This register architecture has been discussed in a horizontal configuration with the IRC and ORC to the left and right of the register bit. The register is not limited to this configuration, however, and it can be advantageous to have a register architecture in a vertical configuration as shown in Figure 4.17. The vertical configuration has the advantage that large stabilizer islands can be added for further stabilization of the IRC.

The increased size and potential addition of large stabilizer islands that are designed to make the IRC impervious to back-propagation from the register can also make it difficult to flip by the conventional islands in the cascade from which it receives the value that will be written. This potential issue can be solved through the use of a structure we call the magnetic

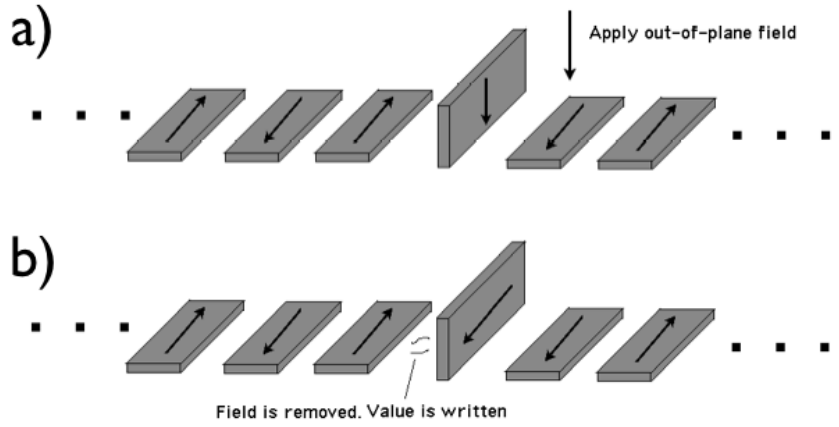

Figure 4.15: a) An in-plane magnetic force is applied to bias the register bit along its hard-axis. This in-plane field is in the direction of the other islands super-hard axes so they are not affected. In b), the field is removed and the register is pushed to the down position due to the force from its neighbor to the left.

amplifier (MA). By creating a chain of islands of increasing size, the flipping force of a signal can be increased while still propagating the signal correctly. With the MA, the signal arriving at the IRC can be made powerful enough that the overly stabilized IRC can still be flipped.

Once a global clock compatible register element has been implemented, it can be combined with complex combinatorial logic circuits already enabled by the biaxial mode to create finite state machines. Finite state machines are the building blocks of digital logic and are at the foundation of the modern CPU. In Figure 4.19, two nanomagnet-based registers are combined with several Bgates to form a globally clocked finite state machine that computes the 2-bit counter function.

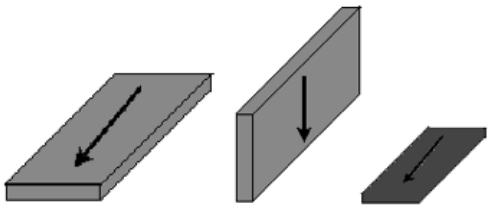

Figure 4.16: The IRC is enlarged giving it greater power to flip the register bit than the ORC. The ORC is smaller and lacks biaxial anisotropy (shown in a different color to represent a different material). This makes it easier to flip then the ORC then the IRC, which is desirable to avoid back-propagation of the signal.

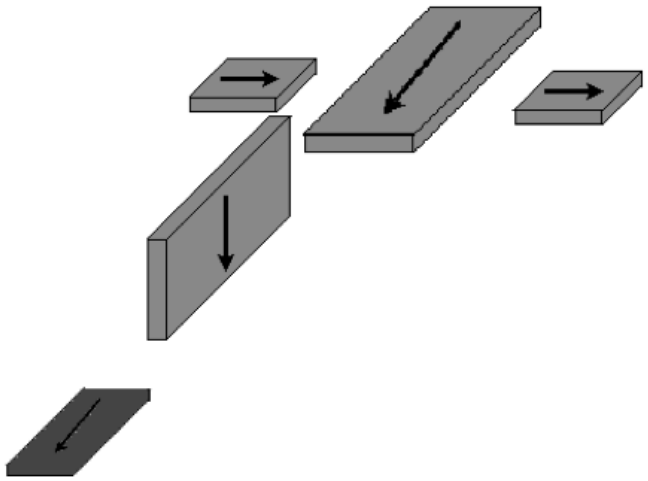

Figure 4.17: The register is shown in a vertical configuration with respect to its contacts. Additional stabilizer islands have been added to the IRC to increase resistance to flipping by the register bit.

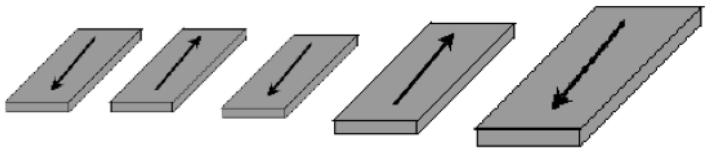

Figure 4.18: The magnetic amplifier structure is shown in a horizontal configuration (vertical configurations are also possible). A gradual enlargement of islands in the wire can create a signal with significantly more flipping power or dipole fringe fields. This increased flipping power is necessary to flip the IRC, which is more resistant to flipping to avoid back-propagation of the signal.

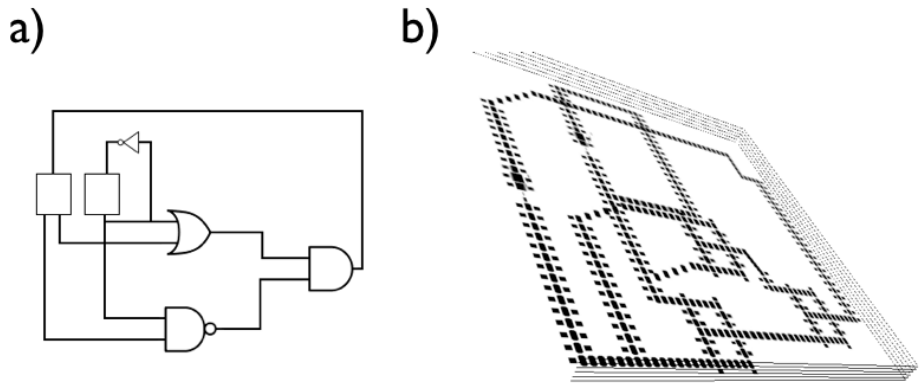

Figure 4.19: a) A circuit diagram for a 2-bit counter finite state machine. b) A nanomagnetic logic circuit combining register elements, wires, and Bgates to implement to two-bit counter function.

4.4 Summary

In this chapter, I discussed some architectural considerations of using the biaxial mode in a nanomagnetic logic scheme. A distributed computer study was carried out to analyze the robustness of the biaxial mode under different conditions. Shmoo plots showing the operating window of the biaxial mode for changing biaxial anisotropy, nanomagnet separation, and nanomagnet aspect ratio were computed. The issue of race conditions in the biaxial mode is raised for the standard Majority Logic Gate. A modified two stage "Bgate" is proposed that solves the race condition and can operate correctly given arbitrary input arrival times. Lastly, the issue of a register element compatible with the biaxial mode to allow the creation of finite state machines is discussed.

Chapter 5

Conclusion

Contents

In this dissertation, I discussed several innovations relating to nanomagnetic logic architectures. Many challenges remain before nanomagnetic logic can be considered a viable commercial technology, but the concept shows great promise as a potential device in a post-CMOS world.

5.1 Adiabatic Mode

I first discussed nanomagnetic logic operating in a "slow clocked" adiabatic mode. For nanomagnet chains of more than a few nanomagnets, the relaxation to the ground state was found to take place through defect diffusion. These dynamics were captured in both simulation and experiment. I showed that these dynamics happen at a critical point in the field removal when the energy barriers have been modified by the clock to be near kT. The role of the clock can be thought of as analogous to raising the temperature of a system and cooling it slowly as in the annealing of defects out of a crystal. Next, the robustness of this mode to errors was characterized. Imperfections were modeled as small angular rotations of the easy axis of each nanomagnet in the circuit. The experimental error rates were compared to nanomagnet chains simulated with these imperfections under various conditions, and a good match was shown between the number, frequency, and character of errors that appeared.

5.2 Biaxial Anisotropy and Nanomagnetic Logic

Biaxial anisotropy was investigated as a method of stabilizing the hard axis of the nanomagnets. This changes the dynamics of signal propagation from a stochastic process to a well-defined cascade in which one nanomagnet tips its neighbor one after the other. This mode of operation makes it possible for the clock field to be removed more quickly. The cascade dynamics were demonstrated with both simulation and experiment. The robustness of this mode of operation were investigated through extensive micromagnetic simulation work that explored a large parameter space. Finally I looked at some higher level architectural challenges associated with the biaxial mode.

5.3 Future Work

Many challenges remain before nanomagnetic logic can be considered a viable commercial technology. Below I will briefly discuss some of the future work and challenges that remain.

5.3.1 The Clock Field

Experimentally the clock field is currently implemented through an external field either through a permanent magnet or a large external electromagnet. Neither of these technologies has the capability of removing the clocking field quickly (on the order of 100 ps). This is a key challenge for operating the logic circuits in the biaxial mode and achieving fast operation. Developing a clocking technology that can be fast is an important step in advancing nanomagnetic logic.

This application of the clock is perhaps also the most significant challenge for achieving the ultra-low power promises of this device. Generating magnetic fields is energetically expensive and inherently ”leaky”. There is effort directed toward making the generation of magnet fields with buried Copper wires more efficient, and studies indicate that this approach can be competitive with end-of-the-roadmap CMOS [50]. However, to approach the attojoule regime, magnetoelectric clocking is likely necessary. Magnetoelectric clocking relies on materials that have magnetic and electric properties that couple. Magnet switching could potentially occur through an electric field without the need for a current. Magnetoelectric switching is still being investigated intensively to better understand and control it, but it is a crucial technology for nanomagnetic logic operating at the ultimate limits of energy dissipation [51], [52].

5.3.2 Biaxial Engineering

The experiments conducted in this dissertation implemented biaxial anisotropy in nanomagnets through epitaxially grown single crystal magnetic thin films. The use of single crystal magnetic material presents several integration challenges that need to be overcome. First because the substrate that is grown on has to be chosen carefully to get single crystal growth,

it will be difficult to integrate epitaxial nanomagnets with the different clocking technologies discussed in the previous section. This is true whether the clock is a buried copper wire or a magnetoelectric switching technology. Another integration challenge is using epitaxial nanomagnets in multiple levels. More complex magnetic circuits will require wires to cross over one another. This can be implemented via multiple interacting layers to allow wires to move in and out of the third dimension. This would not be especially difficult for permalloy nanomagnets fabricated with liftoff techniques, but it is not trivial with epitaxial nanomagnets.

Both these issues could be solved with a layer transfer technique, whereby the nanomagnets are patterned first on a donor substrate before being removed and stuck on the desired area of the chip being manufactured. Because the magnets are not used to conduct current, there is no need to worry about creating good electrical contacts between the transferred layers, and this technology is already used for creating Silion-on-Insulator technology (e.g. *SmartCut*^{tm} [53]) in the semiconductor industry.

Another way to solve this issue is to implement biaxial anisotropy through a different means so it is not necessary to use single crystal materials. Biaxial anisotropy has been shown to be possible with shape and strain [39], [54], and developing one of these alternative implementations in a way that is compatible with nanomagnetic logic is a key challenge.

5.4 Conclusions

In this dissertation, I have discussed the stochastic dynamics in the adiabatic mode and showed how these dynamics affect the expected reliability, speed, and energy dissipation of NML systems operating under these conditions.

I showed how the addition of biaxial anisotropy to the magnetic energy landscape creates a metastable state along the hard axis of the nanomagnet. I showed that this metastability can be used to remove the stochastic nature of the computation and discussed the implications that is has for reliability, speed, and energy dissipation.

Lastly, I discussed new challenges arising in the biaxial mode and talk about the architectural changes that are necessary to make a working NML circuit based on nanomagnets with biaxial anisotropy.

These challenges remain formidable, and there is much that has to happen for nanomagnetic logic to be considered a viable replacement for CMOS. I will conclude this dissertation with some thoughts on the two challenges that I consider most significant and discuss what that means for post CMOS-logic in general.

As mentioned previously, a viable clocking field is crucial for this technology to be useful, but currently there isn't one that is practical. Field clocking with buried wires may be competitive with CMOS and useful for experimental studies, but the adaptation of a novel computing architecture probably requires at least an order of magnitude improvement for it to be worth the cost. While nanomagnetic logic itself has the potential to offer architectural improvements that would allow this type of improvement for certain operations (see the discussion of systolic architectures in Chapter 3), it falls short for general purpose computing in the absence of further innovation.

An efficient clock using magnetoelectric clocking would allow nanomagnetic logic to operate closer to the fundamental limits of computing. However, magnetoelectric clocking is not a mature technology and no one knows how viable it will be, if ever. It's possible that in 5 years time this technology will become more mature, but it's also equally possible that basic research will continue and it will remain as a laboratory curiosity for some time. As investigators of room temperature superconductors can attest, in material science it's often difficult to know when and how breakthroughs will occur that will lead to a viable technology. That nanomagnetic logic relies on a completely separate unproven technology to be viable is perhaps its greatest weakness.

I have also shown in this dissertation that errors due to surface roughness are very difficult to control. This is an engineering problem that is likely solvable, but not without a great deal of money, time, and effort. CMOS devices have had decades and billions of dollars to solve the engineering issues such as this that are needed to scale a device from the micron to the nanometer scale. It is perhaps not surprising that trying to create a completely new nanometer-scale device without the same time and financial benefits has been challenging. This is not a unique issue for nanomagnetic logic, however, and it's one of the reasons that coming up with a replacement for CMOS has been so difficult for researchers.

This type of technology "lock-in", characterized by difficulties in innovation due to previous immense investments in time and money in a current but maturing standard, is not unique. A recent article resulting from the *Future Tense* conference discussing innovation in science and technology elegantly explores this same innovation stagnation already occurring in rocket technology [55]. Rocket and information processing technology might not seem to have much in common, but it's easy to see that they might be headed on similar innovation trajectories with similar consequences.

On the other hand, the main issues I have outlined here, while filled with uncertainty and difficulties, don't seem insurmountable. If magnetoelectric clocking can be proven viable, and the materials challenges associated with getting the magnets to behave more reliably can be overcome, then nanomagnetic logic does have the potential to become a practical information processing device in a post-CMOS world.

Bibliography

[1] Gordon E. Moore. Cramming more components onto integrated circuits. *Electronics*, 38(8), 1965.

[2] Image: http://home.fnal.gov/ carrigan/pillars/web_moores_law.htm.

[3] David J. Griffiths. *Introduction to Electrodynamics (3rd Edition)*. Prentice Hall, 1999.

[4] Nicola Spaldin. *Magnetic Materials: Fundamentals and Device Applications*. Cambridge University Press, 2003.

[5] Image: http://www.physicsarchives.com/index.php/courses/464.

[6] Image: https://commons.wikimedia.org/wiki/file:vfpt_dipole_magnetic2.svg.

[7] Image: http://www.ece.neu.edu/faculty/nian/mom/domains.html.

[8] Image: http://www.physik.fu-berlin.de/einrichtungen/ag/ag-kuch/research/techniques/fmr.html.

[9] J. Wu, D. Carlton, J. S. Park, Y. Meng, E. Arenholz, A. Doran, A. T. Young, A. Scholl, C. Hwang, H. W. Zhao, J. Bokor, and Z. Q. Qiu. Direct observation of imprinted antiferromagnetic vortex states in CoO/Fe/Ag(001) discs. *Nature Physics*, 7:303–306, April 2011.

[10] R.P. Feynman. *The Feynman Lectures on Physics*. Redwood City: Addison-Wesley, 1964.

[11] J.H. Cloete. Is B or H the fundamental magnetic field? In *AFRICON, 1996., IEEE AFRICON 4th*, volume 1, pages 354 –361 vol.1, sep 1996.

[12] A. Imre, G. Csaba, L. Ji, A. Orlov, G. H. Bernstein, and W. Porod. Majority logic gate for magnetic quantum-dot cellular automata. *Science*, 311(5758):205–208, 2006.

[13] A. Dingier, M. Garrison, X.S. Hu, M. Niemier, and M.T. Alam. System-level energy and performance projections for nanomagnet-based logic. In *Nanoscale Architectures, 2009. NANOARCH '09. IEEE/ACM International Symposium on*, pages 21 –26, july 2009.

[14] B. Behin-Aein, S. Salahuddin, and S. Datta. Switching energy of ferromagnetic logic bits. *Nanotechnology, IEEE Transactions on*, 8(4):505 –514, july 2009.

[15] M. Niemier, X.S. Hu, A. Dingler, M.T. Alam, G. Bernstein, and W. Porod. Bridging the gap between nanomagnetic devices and circuits. In *Computer Design, 2008. ICCD 2008. IEEE International Conference on*, pages 506 –513, oct. 2008.

[16] U. Hartmann. Magnetic force microscopy. *Annual Review of Materials Science*, 29(1):53–87, 1999.

[17] Andreas Scholl, Hendrik Ohldag, Frithjof Nolting, Joachim Stohr, and Howard A. Padmore. X-ray photoemission electron microscopy, a tool for the investigation of complex magnetic structures (invited). *Review of Scientific Instruments*, 73(3):1362 –1366, mar 2002.

[18] Image: http://ssrl.slac.stanford.edu/stohr/xmcd.htm.

[19] M. J. Donahue, D. G. Porter, National Institute of Standards, and Technology (U.S.). *OOMMF user's guide [microform] / M.J. Donahue, D.G. Porter*. U.S. Dept. of Commerce, Technology Administration, National Institute of Standards and Technology, Gaithersburg, MD, version 1.0. edition, 1999.

[20] Image: http://math.nist.gov/oommf/mmdisp/mmdisp.html.

[21] Werner Scholz, Thomas Schrefl, and Josef Fidler. Micromagnetic simulation of thermally activated switching in fine particles. *Journal of Magnetism and Magnetic Materials*, 233(3):296 – 304, 2001.

[22] Josef Fidler and Thomas Schrefl. Micromagnetic modelling - the current state of the art. *Journal of Physics D: Applied Physics*, 33(15):R135, 2000.

[23] Oommf temperature extension: The spm-group at the institute of applied physics at hamburg. http://www.nanoscience.de/group_r/stm-spstm/projects/temperature/theory.shtml.

[24] M.T. Niemier, X.S. Hu, M. Alam, G. Bernstein, W. Porod, M. Putney, and J. DeAngelis. Clocking structures and power analysis for nanomagnet-based logic devices. In *Low Power Electronics and Design (ISLPED), 2007 ACM/IEEE International Symposium on*, pages 26 –31, aug. 2007.

[25] D.B. Carlton, B. Lambson, A. Scholl, A.T. Young, S.D. Dhuey, P.D. Ashby, E. Tuchfeld, and J. Bokor. Computing in thermal equilibrium with dipole-coupled nanomagnets. *Nanotechnology, IEEE Transactions on*, 10(6):1401 –1404, nov. 2011.

[26] R. P. Cowburn. Probing antiferromagnetic coupling between nanomagnets. *Phys. Rev. B*, 65:092409, Feb 2002.

[27] William Fuller Brown. Thermal fluctuations of a single-domain particle. *Phys. Rev.*, 130:1677–1686, Jun 1963.

[28] T.L. Gilbert. A phenomenological theory of damping in ferromagnetic materials. *Magnetics, IEEE Transactions on*, 40(6):3443 – 3449, nov. 2004.

[29] L. Landau and E. Lifshitz. On the theory of the dispersion of magnetic permeability in ferromagnetic bodies. *Physik. Z. Sowjetunion*, 8, 1935.

[30] R. F. Wang, C. Nisoli, R. S. Freitas, J. Li, W. McConville, B. J. Cooley, M. S. Lund, N. Samarth, C. Leighton, V. H. Crespi, and P. Schiffer. Artificial "spin ice" in a geometrically frustrated lattice of nanoscale ferromagnetic islands. *NATURE*, 439:303, 2006.

[31] R. Landauer. Irreversibility and heat generation in the computing process. *IBM Journal of Research and Development*, 5(3):183 –191, july 1961.

[32] Charles H. Bennett. The thermodynamics of computation, a review. *International Journal of Theoretical Physics*, 21:905–940, 1982. 10.1007/BF02084158.

[33] Charles H. Bennett. Notes on landauer's principle, reversible computation and maxwell's demon. *STUDIES IN HISTORY AND PHILOSOPHY OF MODERN PHYSICS*, 34:501, 2003.

[34] H.T. Kung. Why systolic architectures? *Computer*, 15(1):37 –46, jan. 1982.

[35] Image: http://www.asylumresearch.com/products/vfm2/vfm2.shtml.

[36] David B. Carlton, Nathan C. Emley, Eduard Tuchfeld, and Jeffrey Bokor. Simulation studies of nanomagnet-based logic architecture. *Nano Letters*, 8(12):4173–4178, 2008.

[37] F.M. Spedalieri, A.P. Jacob, D.E. Nikonov, and V.P. Roychowdhury. Performance of magnetic quantum cellular automata and limitations due to thermal noise. *Nanotechnology, IEEE Transactions on*, 10(3):537 –546, may 2011.

[38] W. Doyle. Magnetization reversal in films with biaxial anisotropy. *Magnetics, IEEE Transactions on*, 2(2):68 – 73, jun 1966.

[39] F. Lee. Shape-induced biaxial anisotropy in thin magnetic films. *Magnetics, IEEE Transactions on*, 4(3):502 – 506, sep 1968.

[40] K. Baker and J. von Beers. Shmoo plotting: the black art of ic testing. In *Test Conference, 1996. Proceedings., International*, pages 932 –933, oct 1996.

[41] G. Pelosi. The finite-element method, part i: R. L. courant. *Antennas and Propagation Magazine, IEEE*, 49(2):180 –182, april 2007.

[42] B A Joyce. Molecular beam epitaxy. *Reports on Progress in Physics*, 48(12):1637, 1985.

[43] Image modified with permission: http://commons.wikimedia.org/.

[44] Michael E. Walsh, Yaowu Hao, C. A. Ross, and Henry I. Smith. Optimization of a lithographic and ion beam etching process for nanostructuring magnetoresistive thin film stacks. volume 18, pages 3539–3543. AVS, 2000.

[45] Taehoon Lee, Nam-Ki Min, Hyun Woo Lee, JinNyoung Jang, DongHyuck Lee, MunPyo Hong, and Kwang-Ho Kwon. The deposition of amorphous carbon thin films for hard mask applications by reactive particle beam assisted sputtering process. *Thin Solid Films*, 517(14):3999 – 4002, 2009. The proceedings of the 1st International Conference on Microelectronics and Plasma Technology (ICMAP 2008).

[46] Robert Sherman, Drew Hirt, and Ronald Vane. Surface cleaning with the carbon dioxide snow jet. volume 12, pages 1876–1881. AVS, 1994.

[47] Barbara J. Breen and John F. Lindner. Introduction to Xgrid: Cluster computing for everyone. July 2010.

[48] S. Wolfram. Universality and complexity in cellular automata. *Physica D Nonlinear Phenomena*, 10:1–35, January 1984.

[49] Cristopher Moore. Majority-vote cellular automata, ising dynamics, and p-completeness, 1997.

[50] M.T. Alam, M.J. Siddiq, G.H. Bernstein, M. Niemier, W. Porod, and X.S. Hu. On-chip clocking for nanomagnet logic devices. *Nanotechnology, IEEE Transactions on*, 9(3):348 –351, may 2010.

[51] R Ramesh and Nicola A Spaldin. Multiferroics: progress and prospects in thin films. *Nature Materials*, 6(1):21–29, 2007.

[52] W. Eerenstein, N. D. Mathur, and J. F. Scott. Multiferroic and magnetoelectric materials. *ChemInform*, 37(44), 2006.

[53] Smartcut is a registered trademark of soitec, inc.: http://www.soitec.com/en/technologies/smart-cut/.

[54] M. Tejedor, J. Carrizo, B. Hernando, and A. Fernández. Formation of biaxial anisotropy in nickel by plastic deformation. *Journal of Applied Physics*, 61(1):427–429, 1987.

[55] N. Stephenson. Space stasis: What the strange persistence of rockets can teach us about innovation. *Slate*, 2011.